Synthesis and Properties of Chiral Binaphthyl Dopants for Application to Helical Liquid Crystals

楢﨑, 優

https://doi.org/10.15017/1931945

出版情報：九州大学, 2017, 博士（学術）, 課程博士
バージョン：
権利関係：

Synthesis and Properties of Chiral Binaphthyl Dopants for Application to Helical Liquid Crystals

Yu Narazaki

PhD Thesis

Acknowledgements

First and foremost I would like to thank my supervisor, Professor Hirotsugu Kikuchi, for providing me with the great opportunity to conduct my PhD research, and for all his valuable advice and encouragement. I am also indebted to Professor Jun Yamamoto at Kyoto University, Associate Professor Yasushi Okumura, Dr Kizhakidathazhath Rijeesh, Hiroya Nishikawa and Daisuke Yoshizawa for providing me with the great valuable knowledge throughout my PhD studies.

I would like to thank Keiko Ideta and Taisuke Matsumoto (Kyushu University, Institute for Materials Chemistry and Engineering) for valuable discussion on ^{13}C-NMR spectroscopy and single crystal X-ray diffraction.

Thanks to all staffs and colleagues in Kikuchi Okumura laboratory and Yamamoto Takanishi laboratory at Kyoto University, I have met and worked with over the past three years. In particular, I am grateful to Dr Hiroki Higuchi for a couple of discussion on organic syntheses.

Thanks to all staffs and colleagues in Advanced Graduate Program in Global Strategy for Green Asia at Kyushu University. In particular, I am grateful to Yuki Furutani, my colleagues, for various kinds of valuable discussion on theoretical calculations.

Finally, I would also like to thank everyone in my family and friends for continuing support towards my PhD research.

Dedicated to my family and friends whose has carried me

Achievements

International Conference Presentations

1) Y. Narazaki, H. Higuchi, Y. Okumura and H. Kikuchi (Oral presentation, 5th February 2016)

   'Synthesis of Various 6,6'-substituted Binaphthyl-type Chiral Dopants for Stabilisation of Cholesteric Blue Phases'

   The 2nd Joint Symposium of Kyushu University and Yonsei University

2) Y. Narazaki, H. Nishikawa, H. Higuchi, Y. Okumura and H. Kikuchi (Poster presentation, 5th December 2016)

   'Synthesis and Helical Twisting Power of Various 6,6'-substituted Binaphthyl-type Chiral Dopants'

   International Forum for Green Asia 2016

3) Y. Narazaki, H. Nishikawa, H. Higuchi, Y. Okumura and H. Kikuchi (Poster presentation, 13th February 2017)

   'Synthesis and Properties of Various 6,6'-substituted Binaphthyl-type Chiral Dopants'

   The 3rd Asian Conference on Liquid Crystals

4) Y. Narazaki, H. Nishikawa, H. Higuchi, Y. Okumura and H. Kikuchi (Poster presentation, 29th November 2017)

   'Synthesis and Helical Twisting Power of (*R*)-6,6'-halogenated and -methylated Binaphthy-type Chiral Dopants'

   International Forum for Green Asia 2017

Domestic Conference Presentations

1) Y. Narazaki, H. Higuchi, Y. Okumura and H. Kikuchi (Poster presentation, 5th September 2016)

   'Synthesis and Helical Twisting Power of 6,6'-halogenated Binaphthy-type Chiral Dopants'

   Japanese Liquid Crystal Conference 2016

Journal Papers

1) Y. Narazaki* and T. Watanabe*, 'Social Factors Affection Innovation Cycle of Liquid Crystal Technologies: A Japanese Case Study', *Evergreen – Joint Journal of Novel Carbon Resources & Green Asia Strategy* **2017**, *4*, 8–15.
2) Y. Narazaki, H. Nishikawa, H. Higuchi, Y. Okumura and H. Kikuchi*, 'Substituent Effects on Bridged Binaphthyl-type Chiral Dopants on the Helical Twisting Power in Dopant-Induced Chiral Liquid Crystals', *RSC Advances* **2018**, *8*, 971.

Presentation Awards

1) *Japanese Liquid Crystal Conference 2016*

   JLCS Kosai Poster Award

2) *The 3rd Asian Conference on Liquid Crystals*

   Outstanding Poster Award

Contents

Chapter 1
Introduction

1.1 − Liquid Crystals

1.1.1 – The Mesophase[1–2]

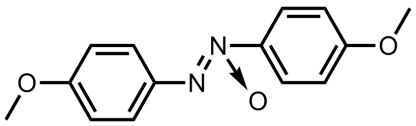

Figure 1.1 The chemical structure of *p*-azoxyanisole.

In general, an anisotropic crystal transitions an isotropic liquid when a crystal reaches a melting point. A unit of a crystal which possesses a three-dimensional regular order, therefore, dissolves into liquid, the loss of three-dimensional order, at a melting point of a crystal; that is, isotopic liquid occurs fluidity. Particular chemical species, for example being *p*-azoxyanisole (**Figure 1.1**), exhibit the mesophase, termed '*the liquid crystal phase*' between the crystalline and isotropic liquid phase (**Figure 1.2**). *p*-azoxyanisole becomes the milky viscous liquid-like state, the liquid crystal (LC) phase, at 116 °C; nevertheless its LC phase possesses anisotropy within the phase. Therefore, as with an isotropic liquid, the LC phase exhibits fluidity, yet it is optically anisotropy; that is remaining the common properties of a crystalline phase within the LC phase. Hence, although LCs lose three-dimensionally positional order, they keep orientational order due to the presence of weak intermolecular interactions between each LC molecule. Due to the combination of them, LC materials are sensitive to several external stimuli such as temperature, electric and magnetic field. These unique properties of LCs have attracted much attention to the scientists in the fields of chemistry and physics.

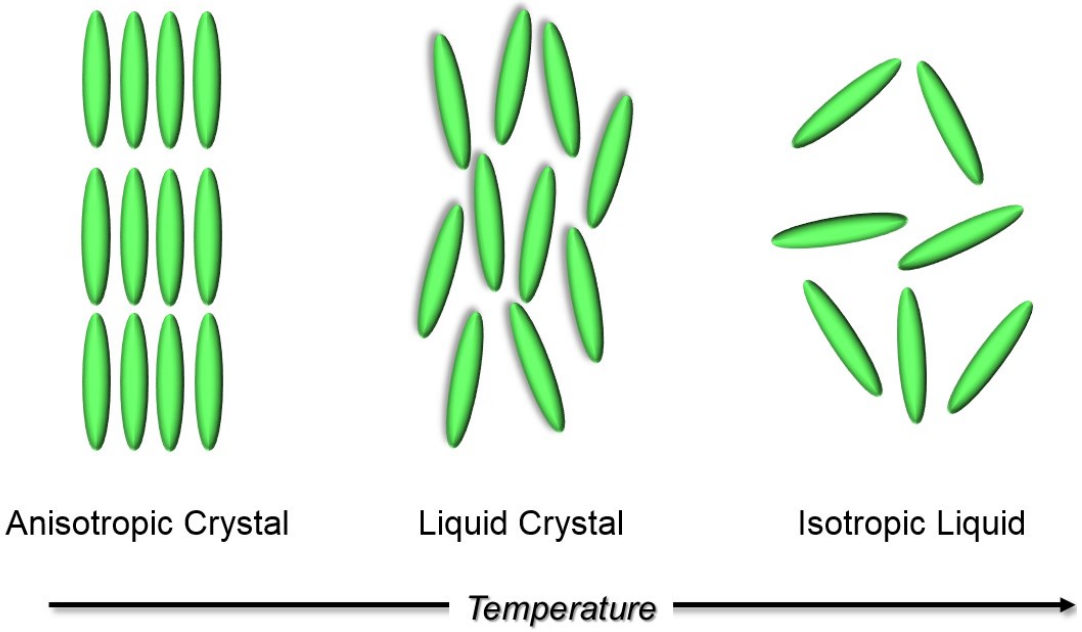

Figure 1.2 States of matter.

1.1.2 – Historical Perspectives[3–6]

In 1888, Friedrich Reinitzer, Professor of botany at the Garman Technical University in Prague, was attempting to research physical properties of several cholesterol derivatives, especially cholesteryl benzoate. Reinitzer observed that cholesteryl benzoate appeared to possess two melting points; its crystalline solid displayed to a milky viscous liquid between 145.5 and 178.5 °C. Above 178.5 °C it began to become isotoropic and clear. Besides, he observed that the phenomenon appeared to be reversible and the violet- blue colour reflections occurred near phase transition temperature under the polarising microscope. This discovery are recognised as 'the discovery of LC' in the present day. On 14 March 1889 he contacted Otto Lehmman, a full professorship at the University of Karlsruhe, to investigate the phenomenon, which Reinitzer observed, since Lehmman had a polarising microscope with a heating stage. Lehmman enabled to specifically investigate cholesteryl benzoate which Reinitzer sent. By the end of August 1889 Lehmman published the results to the technical paper, entitled as '*Über fließende Kristalle*', namely '*On flowing crystals*' in English. Hence, Friedrich Reinitzer is the discoverer of LCs and Otto Lehmman is seen as the founder of LC research, respectively in the present time.

In 1890, Luduwig Gattermann was successful in synthesising *p*-azoxydianisole (**Figure 1.1**), exhibiting the similar phenomenon which Reinitzer and Lehmman observed. He also observed a milky viscous liquid between crystalline and isotoropic liquid. In addition, he realised peculiar streaks within the milky liquid phase, LC phase, of *p*-azoxydianisole under the polarising microscope. He called them '*Schliere*'. Later, it revealed that various kinds of LC materials exhibit '*Schliere*'.

Lehmman found further materials which show the similar properties; that is displaying two melting point. He sometimes called a LC phase '*Fließende Kristalle'* (flowing crystals) or 'Schleimig flüssige *Kristalle*' (slimy liquid crystals). Lehmman's assertion give rise to scepticism from the scientific society, since there rebutted that the phenomena

which Lehmman observed were a result of a binary colloidal system of a liquid in a crystalline solid. Especially, Gustav Heinrich Johann Tammann, being one of a sceptical contributor, strongly opposed to Lehmman's proposals of liquid crystals. Although their argumentations in respect to the properties of LCs were kept for several years, they do not enable to achieve the feasible explanation that LCs exhibit larger anisotropy.

Daniel Vorländer, Professor at University of Halle, synthesised hundreds of a LC molecule with his co-workers to reveal the relationship between the molecular structures of LC materials and their properties for several decades. They observed LC behaviour of their synthesised molecules at various times. Vorländer determined that a *rod-like* chemical structure of LC molecules plays an important role in the appearance of LC phase.

In 1922, Georges Friedel, Professor of Geology at the University of Strasbourg, published an important review paper in respect to LCs in *Annales de Physique*. He utilised '*fliessende krystalle*', 'liquid crystals', for milky anisotropic liquid, observed between a crystal and isotropic liquid in the paper. Further, Friedel classified nematic, smectic and cholesteric phases through their optical textures of milky liquids, which they induce. He was also attempting to explain that phase transitions between crystalline and liquid crystalline phase. Research focusing on LC materials underwent a distinct paradigm shift when Friedel's research work was revealed.

In the 1920s and 1940s, LC research was mainly focusing on physical properties of LC behaviour by Vsevolod Konstantinovich Fréedericksz,[7] Carl Wilhelm Oseen,[8] Wilhelm Kast,[9] Pierre Chatelain,[10] and Mariana Mięsowicz[11]. After the Second World War the first review paper, entitled as 'The Mesomorphic State – Liquid Crystals' in English was published by two American chemists, Glenn H. Brown and Wilfred G. Shaw, in *Chemical Review*.[12] The publication of the review paper led to new LC research style in the United States. Brown established 'Liquid Crystal Institute' at Kent state University in 1965.

Several big breakthrough, utilised LC materials were brought about by James Fergason in the Westinghouse Research Lab[6] and George Heilmeier of the Radio Corporation

America[13]. The first application of LC material was revealed by Fergason. He utilised a cholesteric liquid crystal for a temperature indicator, and obtained a patent application for this in 1958. Moreover, Heilmeier reported a novel LC display application, using the dynamic scattering mode effect of a nematic liquid crystal (NLC) in 1968. LC research focused on the liquid crystal display (LCD) technology. The NLC, possessing stable at room temperature, namely *N*-(4-methoxybenzylidene)-4-butylaniline (MBBA), was synthesised by Hans Kelker at Hoechst AG due to practical applications of LCDs in 1969.[14] MBBA was only stable under the specific conditions, and would strongly be toxic and carcinogenic when it was decomposed. G. W. Gray, Professor of organic chemistry at the University of Hull, provided the cyanobiphenyl (CB) family of NLCs, which exhibited remarkably stable nematic phases at room temperature, and were relatively harmless (**Figure 1.3**).[15] Wolfgang Helfrich and Martin Schadt developed the twisted nematic (TN) mode, which is LCD fundamental technology at Hoffmann-La Roche in 1971.[16] Further, a proto-type LCD from Hoffmann-La Roche was demonstrated. The first pocket calculator which utilised these LC technology was put on the market by Sharp Corporation in 1973.[17] Besides, Sharp produced a colour television, namely 'Crystaltone', in 1987.[18] In 1996, there began to be produced large screen full-colour LCDs. Eventually, the world's LCD shipment volume exceeded that of cathode-ray tube (CRT) display in 2007.[19]

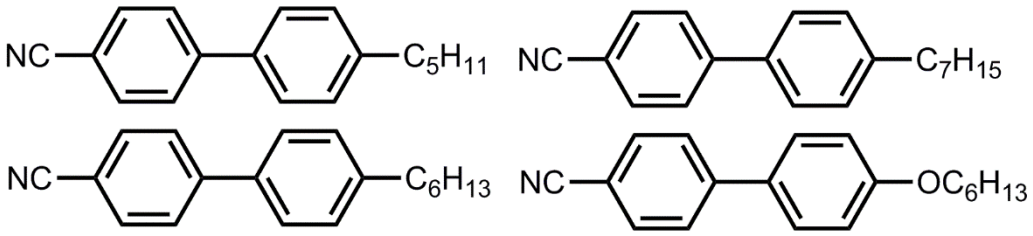

Figure 1.3 The chemical structures of CB type NLCs.[15]

1.1.3 – Classes of Liquid Crystals[1–2, 20–22]

LCs can be divided into two classes: thermotropic and lyotropic LCs (**Figure 1.4**). Pure thermotropic LC molecules exhibit its LC phase over a specific temperature range. About 1% of all of the organic molecules melt from crystalline solids to form a thermotropic LC phase before phase transition of an isotropic liquid phase. Thermotropic LCs are divided into two sub-classes: calamitic and discotic LCs (**Figure 1.4**). Calamitic and discotic LCs are a *rod*-like and *disc*-like mesogens, respectively. The features of calamitic mesogens possess a rigid aromatic core, bearing more than one flexible alkyl chain. Their mesogen core is formed from liquid 1,4-phenyl group such as cyanobiphenyl-type LC molecules. The discotic mesogens are composed of a disc's rigid aromatic core such as triphenilene and several flexible alkyl chains. LC phase stability of thermotoropic LCs is encouraged by an intermolecular interaction, for example being 'van der Waals interaction', between each thermotropic LC molecules. By contrast, lyotropic LCs need solvent to possess their liquid crystallinity. Lyotropic LCs are, therefore, controlled by concentration and also temperature. Lyotropic LCs are encountered biomolecules, including brains, nerves and muscles. In this thesis, calamitic thermotropic LCs are explained in more details.

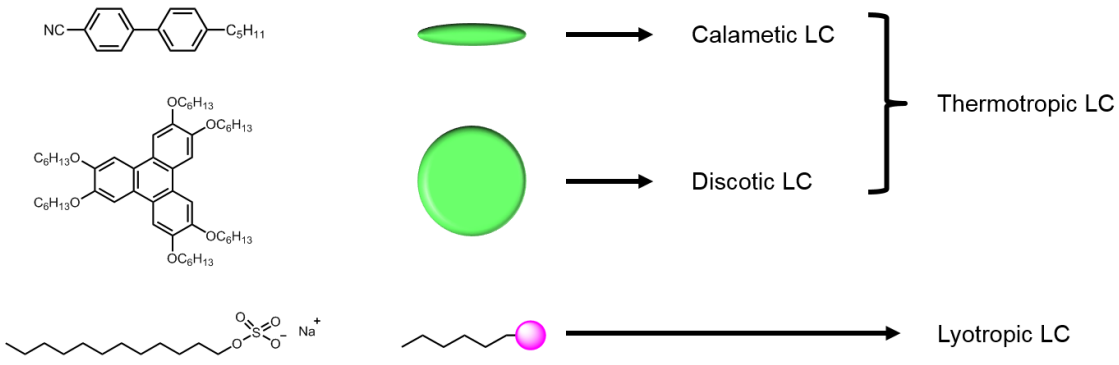

Figure 1.4 Classes of liquid crystals.

Calamitic thermotropic LCs usually occur the nematic, smetic phase or both whilst heating them. The nematic (N) phase is the least order and highest symmetry (**Figure 1.5a**). Its phase exhibits long-range orientational order of the axis of elongated molecules, called the director **n**. The smetic (Sm) phases possess also the orentational order like the N phase and they simultaneously possess one-dimensional positional order, forming a layered arrangement. The direction of the smectic A (SmA) phase can averagely be perpendicular to the smectic layers (**Figure 1.5b**). The smectic C (SmC) phase's director is tilted to the layers (**Figure 1.5c**). Generally, the increased order of the Sm phases forms their phases at lower temperature than the N phase with following on an increase of viscosity. A large number of the Sm phases exist with a higher degree of order than that of SmA and SmC, for example; that is Smectic B (SmB), which packed hexagonally.

If the calamitic thermotropic LCs have '*Chirality*'; that is a geometric property of chemical structures that indicates a lack of mirror symmetry, they inevitably occur chiral LC phases, the cholesteric phase also known as the chiral nematic (N*) phase (**Figure 1.5d**) and chiral smectic C (SmC*) phase. Herein, typical example of the former is discussed without that of the SmC* phase. The director, meaning average direction of LC molecules in the N* phase, twists around in a helix. The structure of the N* phase, therefore, has a helical axis and structure.

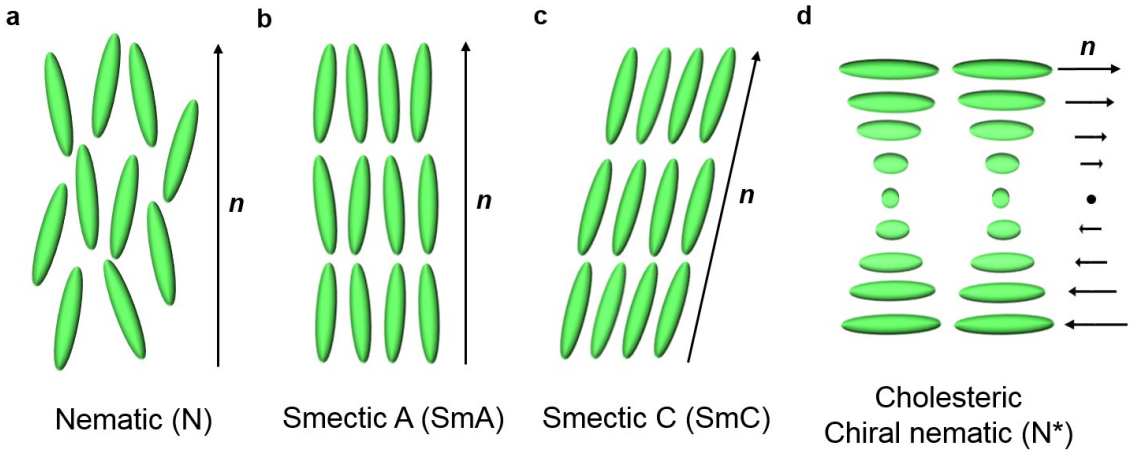

Figure 1.5 Schematic representation of the (a) nematic, (b) smectic A, (c) smectic C and (d) chiral nematic (N*) phase.

1.1.4 – Liquid Crystal Phases[2, 20–23]

1.1.4.1 – The Nematic Phase

The nematic (N) phase is the simplest LC phase. It is formed by calamitic and discotic thermotropic LCs. As the molecules possess no long-range translational order an isotropic liquid, they also lose its order in the N phase. Unlike an isotorpic liquid, the molecules, however, have long-range orientational order of the axis of elongated molecules in the N phase. Therefore, the N phase can refer to an anisotropic liquid. The director **n** is the average local director of the long LC molecular axis, and also indicates to the direction of the optical axis of the system. In general, the formation of the N phase is allowed to be stable by dependence of LC molecular features. Furthermore, its formation plays an important role in an anisotropic chemical structure; that is bearing polar substituents such as fluorine (-F), trifluoromethyl (-CF_3), trifluoromethoxy (-OCF_3) cyano (-CN) and methoxy group (-OMe) in a terminal and lateral position. The essential features, required to exhibit the N phase are a rigid aromatic core and flexible alkyl chain, respectively. The former, an aromatic core with the polar substituents, corresponds to biphenyl (**Figure 1.6a**), azomethine (**Figure 1.6b**), azoxy (**Figure 1.6c**), biphenyl cyclohexane (**Figure 1.6d**), phenyl bicyclohexane (**Figure 1.6e**) and aromatic ester (**Figure 1.6f**) core. By contrast, the latter, a flexible alkyl chain, pertains to *n*-alkyl and *n*-alkyloxy groups. It should be noted that the N phase shall be stable when a flexible alkyl chain is shorter, whereas the smectic phase shall be found with a longer alkyl chain.

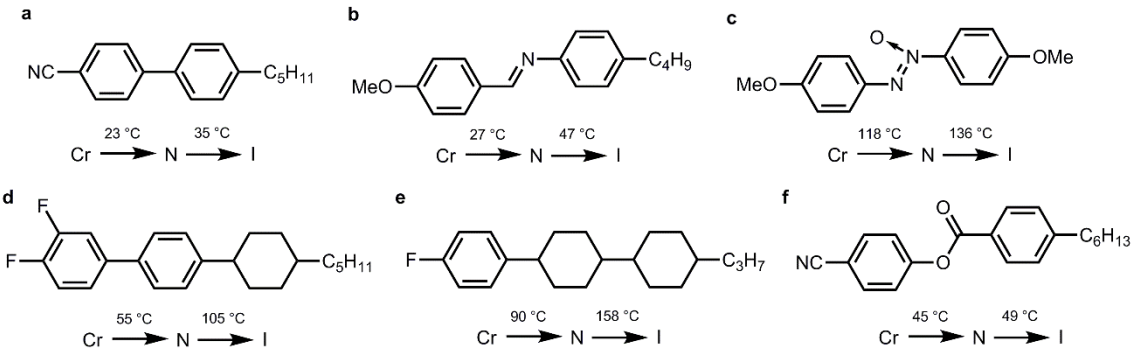

Figure 1.6 The chemical structures of the (a) biphenyl-, (b) azomethine-, (c) azoxy-, (d) biphenyl cyclohexane-, (e) phenyl bicyclohexane- and (f) aromatic ester-type[23] NLC molecules. Cr, N and I denote the crystalline, nematic and isotropic phase, respectively.

The elastic properties of the N phase can be modelled utilising the continuum theory. If a NLC is deformed by external forces, the free energy density F is increased by occurring a deformation of a director **n** in the N phase. An increase of F due to a deformation of a NLC, termed F_d, is described by the continuum theory. This theory in respect to LCs was built by Carl Wilhelm Oseen[8], Hans Ernst Werner Zocher[24] and Frederick Charles Frank[25]. In the present time, the theory of a NLC was formulated as:

$$F_d = (1/2)K_{11}(\mathrm{div}\mathbf{n})^2 + (1/2)K_{22}(\mathbf{n}\cdot\mathrm{curl}\mathbf{n})^2 + (1/2)K_{33}(\mathbf{n}\times\mathrm{curl}\mathbf{n})^2 \quad (1.1)$$

where div**n** and curl**n** are defined as:

$$\mathrm{div}\mathbf{n} = \nabla\cdot\mathbf{n} \quad (1.2)$$

$$\mathrm{curl}\mathbf{n} = \nabla\times\mathbf{n} \quad (1.3)$$

∇ is differential operator, called nabla, as:

$$\nabla = (\partial/\partial x, \partial/\partial y, \partial/\partial z) \quad (1.4)$$

The K_{11}, K_{22} and K_{33} are elastic constants of a NLC, especially termed 'the Frank elastic constant'; that is K_{11} for a splay deformation (**Figure 1.7a**), K_{22} for a twist deformation (**Figure 1.7b**) and K_{33} for a bend deformation (**Figure 1.7c**).

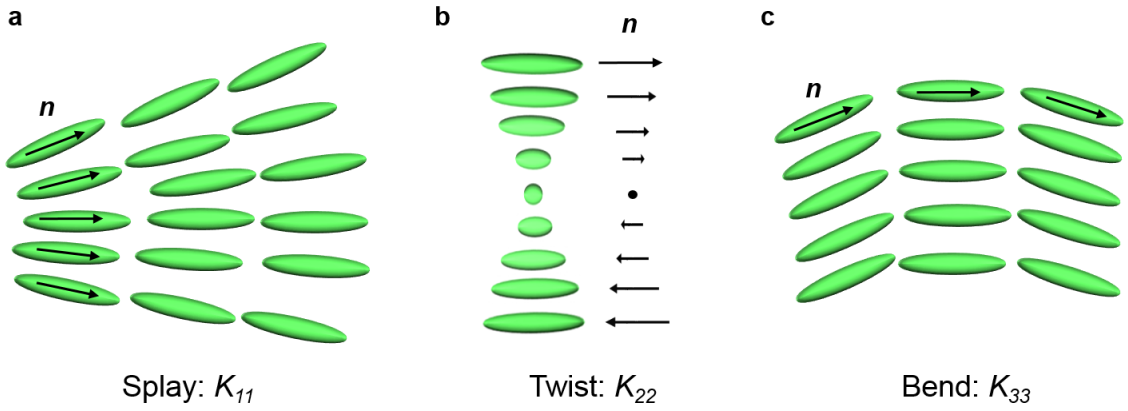

Figure 1.7 Schematic representation of the three fundamental deformations of a NLC: (a) splay, (b) twist and (c) bend.

Therefore, all bulk deformations of the N phase include the three fundamental deformations. The continuum theory of the N phase has been applied to a threshold electric field in terms of the LCD application, utilising a NLC. In general, NLC molecules respond by external stimuli, such as electric and magnetic fields. These applied field can be utilised to change the average orientation of NLC molecules. This is the fundamental technology for nematic LCDs. Indeed, V. K. Fréedericksz[7] led to the above-mentioned external response of NLC molecules, i.e. the so-called 'Fréedericksz transition' (**Figure 1.8b**), in the 1930s. NLC molecules are orientated parallel towards the glass with a thin layer of rubbed polymer (**Figure 1.8a**) when these molecules are sandwiched between two pieces of glass substrates, coated thin rubbed polymer on surface of NLC molecules. When an electric (E) or magnetic (B) field are applied to its sandwich cell on the surface, NLC molecules tend to reorientate in the direction of the applied field around centre of the its cell without neighbour NLC molecules nearby the glass substrates due to working on strong anchoring around glass substrates (**Figure 1.8b**). Hence, the directors of NLC

molecules change by applying an E or B field, and deformations of a NLC is brought about by Fréedericksz transition.

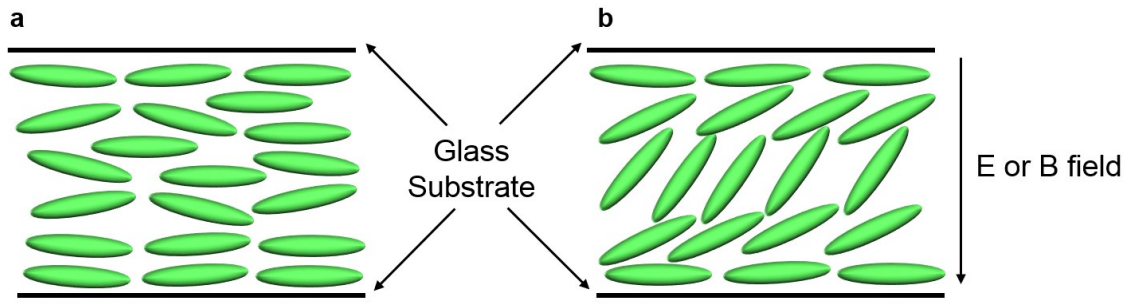

Figure 1.8 Schematic representation of (a) the planer orientation of the NLC and (b) Fréedericksz transition.

It is natural that there is the threshold electric field of Fréedericksz transition. The threshold electric field, namely E_{th}, was defined as:

$$E_{th} = \pi / d\sqrt{K/\varepsilon_0 \Delta\varepsilon} \tag{1.5}$$

where d is the thickness of the LC cell, K is either K_{11}, K_{22} or K_{33}, ε_0 is the permittivity of vacuum electric constant and $\Delta\varepsilon$ ($= \varepsilon_{\perp} - \varepsilon_{\parallel}$) is the dielectric anisotropy of a NLC.

Further,

$$V_{th} = E_{th} d \tag{1.6}$$

Therefore, the threshold voltage, termed the V_{th}, can be rewritten by:

$$V_{th} = \pi\sqrt{K/\varepsilon_0 \Delta\varepsilon} \tag{1.7}$$

If V_{th} is low, low-voltage LCDs can accomplish. A NLC, possessing low elastic constants and large $\Delta\varepsilon$ are required for the sake of accomplishment of low-voltage LCDs from the equation (1.7). Fluorinated NLCs tend to have a lower dielectric anisotropy $\Delta\varepsilon$, elastic constants K and viscosity than those of cyanobiphenyl-type NLCs. V_{th} of fluorinated ones is lower than that of cyanobiphenyl ones, since they possess lower elastic constants.

Moreover, the fluorinated NLCs are unlikely to include ionic impurities. It is the biggest advantage for production of thin-film-transistor (TFT) LCDs. In present time, development of the novel fluorinated LCDs, possessing larger $\Delta\varepsilon$ have attracted much attention for even more low-voltage TFT LCDs.

1.1.4.2 – The Chiral Nematic Phase

The property of chirality indicates that it is a mirror image of each other which cannot overlap like our hands (**Figure 1.9a**). Chirality in molecules, therefore, refers to a geometric property of chemical structures that lack mirror symmetry, such as binapthyl derivatives (**Figure 1.9b**).

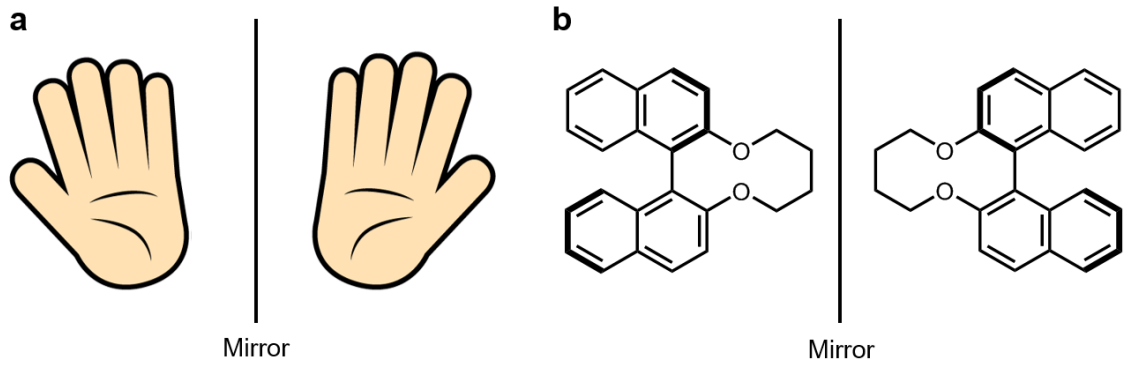

Figure 1.9 Schematic representation of (a) the mirror image of hands and (b) chirality of (*R*)-binaphthyl derivatives.

In stereochemistry, the chemical structure, possessing chirality corresponds to 'chiral compound'. On the other hand, the structure which does not have chirality is 'achiral compound'. A human body is composed of a large number of chiral compounds, such as amino acids, DNA and proteins. Molecular chirality is classified by central, axial, planer and helical chirality. Above Schematic illustration of b, i.e. (*R*)-binaphthyl structures, corresponds to axial chirality.

The chiral nematic (N*) phase can occur by its LC molecule with chirality or the addition of a chiral dopant, i.e. chiral compound, to an achiral NLCs. The N* phase has a helical

axis and superstructure, since the director **n** of its phase rotates by 360° (**Figure 1.10a**). There is, hence, the helical pitch (*p*) in the N* phase (**Figure 1.10a**). Its phase exhibit unusual physical properties such as periodic helical structures and selective reflections of circularly polarised light (CPL), based on Bragg's law, since the pitch length in the N* phase usually corresponds to visible wavelength (**Figure 1.10b**).[26–27] Furthermore, the pitch is utilised plus (+) and minus (−) for representation of helical senses. Its plus and minus corresponds to the right- and left-handed helical structure in the N* phase, respectively. The right-handed helical structure in the N* phase reflects right CPL. Similarly, the left-handed reflects the same direction of CPL (**Figure 1.10b**). A helical sense is determined by absolute configurations of chiral compounds; that is a (*S*)- or (*R*)-chiral isomer.

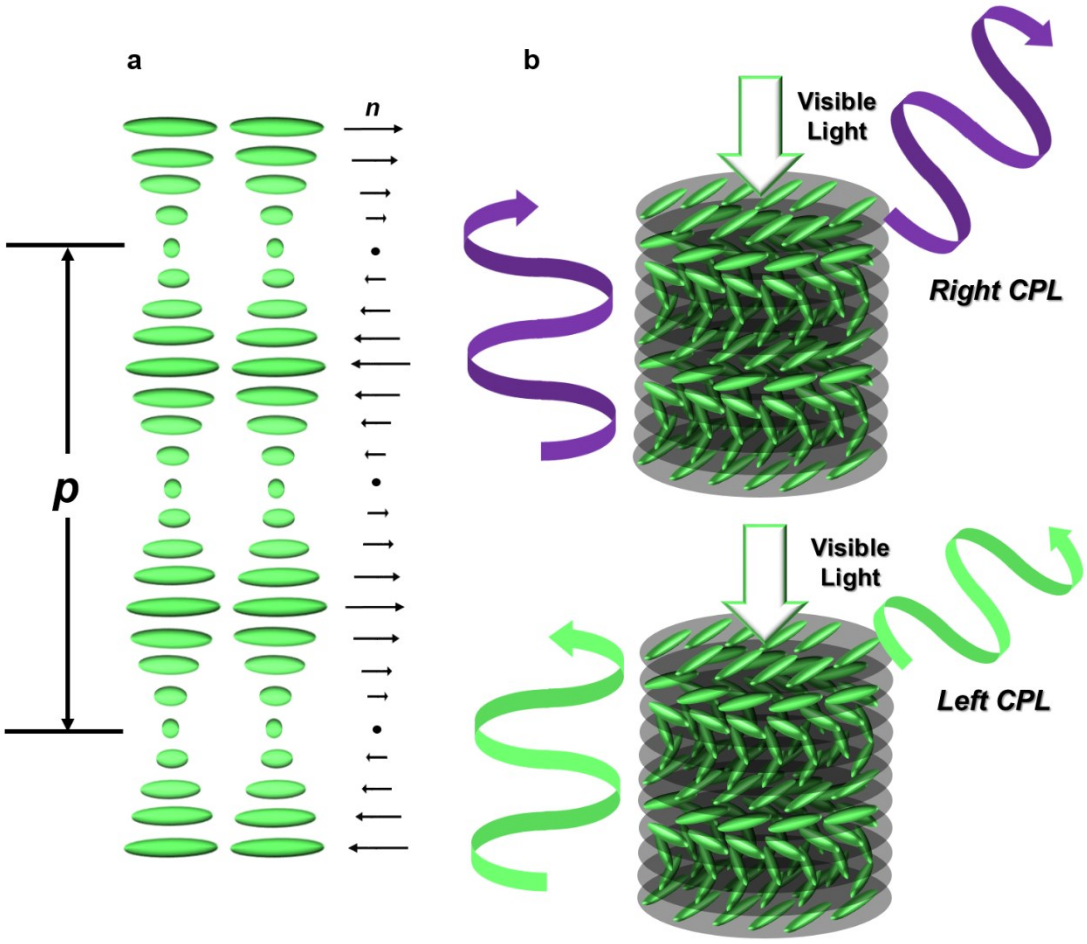

Figure 1.10 Schematic representation of (a) the N* phase representing the helical pitch and (b) selective reflections in the N* phase. Top and down representations denote right- and left-helix.

The free energy density of the N* phase, namely F_d*, can be expressed by the inclusion of the helical wavevector, termed q_0, based on the Eq 1.1.

$$q_0 = 2\pi/p \tag{1.8}$$

to afford

$$F_d^* = (1/2)K_{11}(\mathrm{div}\mathbf{n})^2 + (1/2)K_{22}(\mathbf{n}\cdot\mathrm{curl}\mathbf{n} + q_0)^2 + (1/2)K_{33}(\mathbf{n}\times\mathrm{curl}\mathbf{n})^2 \tag{1.9}$$

It should be noted that q_0 is positive for a right-handed and negative for a left-handed helix.

Interestingly, the N* phase can be identified the structure of N*LCs on glass surface from its characteristic optical textures. There are two types of LC alignment; that is *planar* alignment with a director parallel on glass surface, and *homeotropic* alignment in case of a director with perpendicular against glass surface by rubbing treatment. In case of the N* phase, the planar texture occurs as planar alignment of a director; that is the perpendicular helical axis (**Figure 1.11a**); whereas homeotropic alignment of a director which means that its helical axis is parallel to glass surface produces the fingerprint texture (**Figure 1.11b**). Besides, random alignment results the focal conic texture (**Figure 1.11c**).

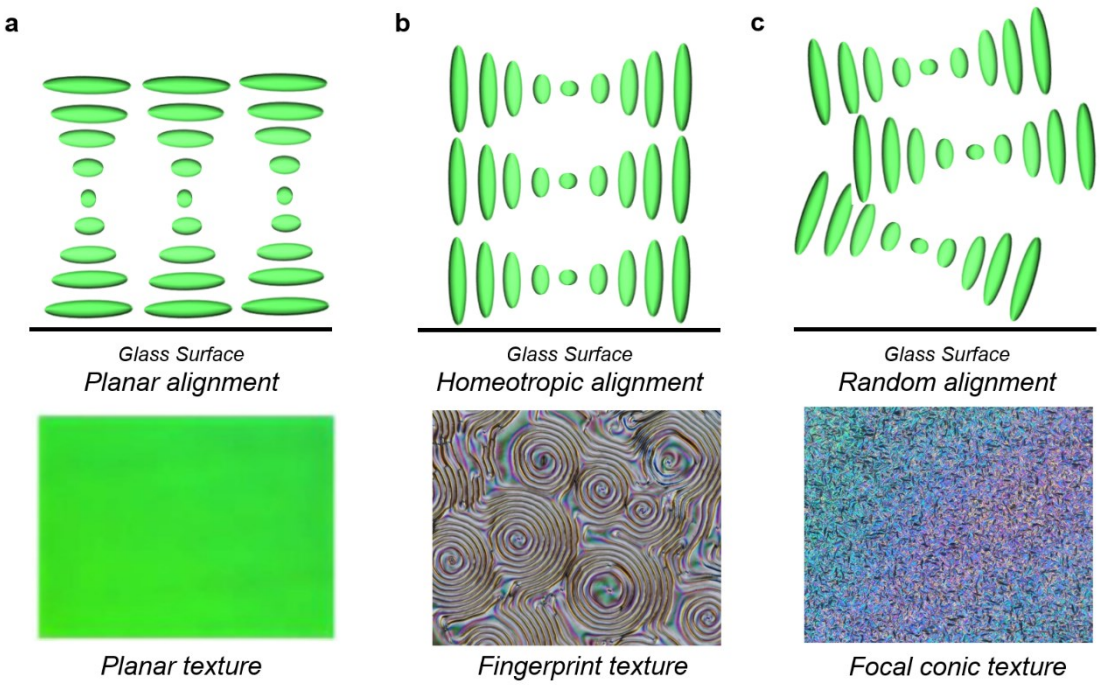

Figure 1.11 Schematic representation of (a) planar alignment of N*LC and the planar texture, (b) homeotropic alignment of N*LCs and the fingerprint texture and (c) random alignment of N*LCs and the focal conic texture.

The planar texture, Figure 1.11a, is observed the brilliant coloured selective reflections. The reflection wavelength (λ) is felt the simple equation to explain the phenomena as:

$$\lambda = np \tag{1.10}$$

Where n is the average refractive index and p is the pitch length of the N* phase. When the average refractive index n is fixed, the reflection wavelength is depended on the cholesteric pitch length p. Therefore, the blue colour reflection is observed when the pitch is shorter. In case of the longer pitch of the N* phase, the reflections tend to exhibit red shift. The N*LCs has been applied to reflective colour LCDs, based on the selective reflections of the N* phase.[28] Moreover, the pitch p is sensitive towards thermal. For this feature, the N*LCs has also been applied to thermochromic devices.

1.1.4.3 – The Blue Phases

Indeed, there are the independent chiral LC phases, i.e. the blue phases (BPs), between the isotropic and N* phase. The BPs occur when the helical pitch of the N* phase is less than 500 nm. In addition, the BPs possess the very narrow temperature range (typically < 3 ^{o}C), and do not show a birefringence.[29] In 1973, Gray *et al*. reported the present of the independent liquid crystal phase, which has coloured textures (**Figure 1.12b-d**) of eight cholesterol derivatives. They identified the independent liquid crystal phase as the 'Blue phase'.[30] In 1980s, Much effort was devoted to revealing the structure of the BPs both experimentally and theoretically.[29, 31–36] The BPs are composed of double-twist cylinders (**Figure 1.12a**) which have double twist structure. These cylinders cannot be filled whole of cubic lattices. There are disorder regions that LC molecules cannot be orientated continuously at contact points of three double-twist cylinders. The disorder regions are called disclination lines. The BPs are the frustrated phases with the coexistence of double-twist cylinders and disclination lines and unstable thermodynamically (**Figure 1.13**). Hence, BPs appear in the very narrow temperature range. The structures of the BPs are three types such as Blue phase I (BP I), Blue phase II (BP II), and Blue phase III (BP III). The structure of the BP I is body-centred cubic lattice $\{O^8, (I4_132)\}$ (Figure **1.12b**), that of the BP II is simple cubic lattice $\{O^2, (P4_232)\}$ (**Figure 1.12c**) and that of the BP III is amorphous or liquid-like state which are known as "the blue fog" (**Figure 1.12d**), respectively.[36–37] Moreover, BP I, II, and III regularly occurs on the heating process from the N* to isotropic phase. The cubic lattices of BP I and II have the huge three-dimensional periodic structure of a visible light wavelength order.

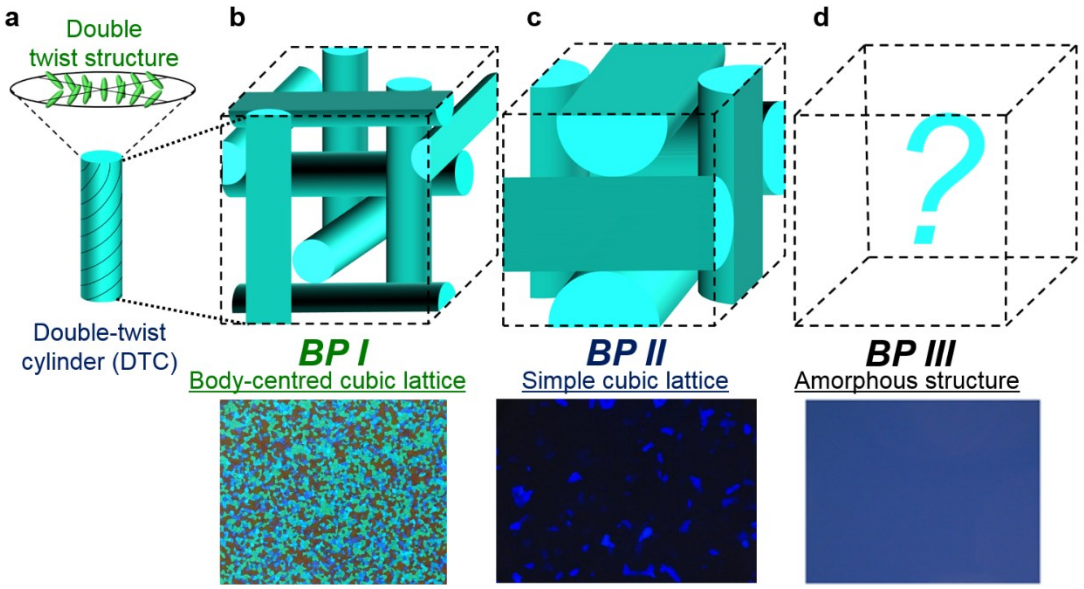

Figure 1.12 Schematic representation of (a) the double-twist cylinder structure and the structures and corresponding typical coloured platelet textures of (b) the BP I and (c) BP II. It should be noted that the structures of (d) the BP III remain unclear due to its amorphous structure and corresponding texture, called 'the blue fog'.

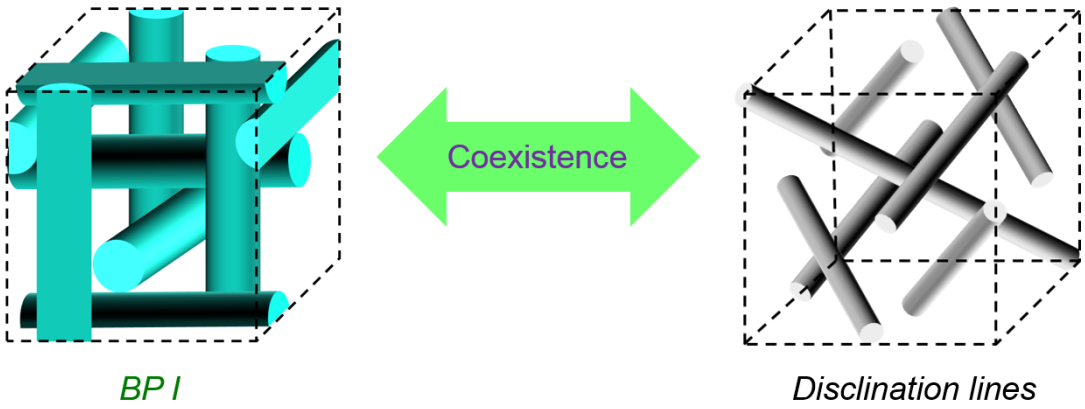

Figure 1.13 Schematic representation of disclination lines of the BP I.

The BPs had the biggest issue of a narrow available temperature range for their application. Studies of the BPs as a LC material was gradually disappearing from LC research. In 2002, applied research was revived by H. Kikuchi *et al*., who reported polymer-stabilised cholesteric BPLC (PSChBPLC, **Figure 1.14**).[38] The immobilised BPLC by *in situ* photo-polymerisation of the chiral and non-chiral diacrylate LC monomers had already been reported by H. S. Kitzerow *et al.* in 1993 before the PSChBPLC.[39] This method maintained the structure of BPs, however, the dynamics of LC molecules in the BPs have lost due to polymerisation of whole LC molecules in the BP cubic lattice. By contrast, PSChBPLCs do not lose the dynamics of LC molecules due to concentrating polymer network formed by small amount of monomers in disclination lines. Besides, the concentrating polymer network in disclination lines contributes to stabilise BPs (**Figure 1.14**). The attractive features of PSChBPLCs results the large temperature range, more than 60 °C, and, response towards electric applied field due to retention of dynamics of LC molecules, which form PSChBPLCs. In 2008, a prototype BP-mode LCD, utilising a PSChBPLC had been demonstrated by Samsung.[6]

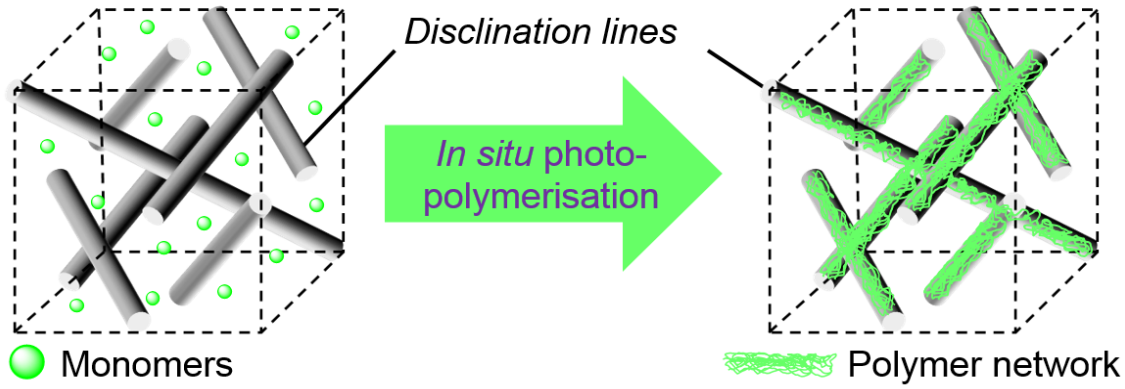

Figure 1.14 Schematic representation of PSBPLCs.

1.1.5 – Chiral Dopants[40–42]

Chiral LCs (CLCs), i.e. especially N*LCs and BPLCs, is obtained by two chemical methodology; that is i) synthesis of LC molecules with more than one chiral moiety and ii) the addition of chiral molecules as chiral dopants to achiral host NLCs. The methodology ii) is focused on this thesis. Chiral dopants are chiral molecules, and their molecular structures can be classified into four types: central, axial, planar, and helical chirality. In this thesis, chiral dopants with central, helical and axial chirality is explained. The ability of a chiral dopant to generate a helical structure in a given host NLC is evaluated using helical twisting power (HTP, $\beta_{wt\%}$)[27], as expressed below:

$$\beta_{wt\%} = (pc_w)^{-1} \tag{1.11}$$

where p is the helical pitch of the N* phase, and c_w is the concentration of the chiral dopant in weight percentage. If the concentration of the chiral dopant is replaced mole fraction c, the equation 1.11 is represented as:

$$\beta_M = (pc)^{-1} \tag{1.12}$$

Chiral dopants with large HTP values are required for the practical applications, since excess doping of chiral molecule in a host NLC negatively affects the physical properties of induced CLCs. The handedness of the dopant-induced N*phase as *P* for a right-handled and *M* for a left-handed helical sense, respectively. These can be measured by the contact methods, utilising cholesteryl oleyl carbonate (COC) as the reference material.

Three types of the host NLCs, namely 5CB, E7 and MBBA, are often utilised as in the Figure 1.15.

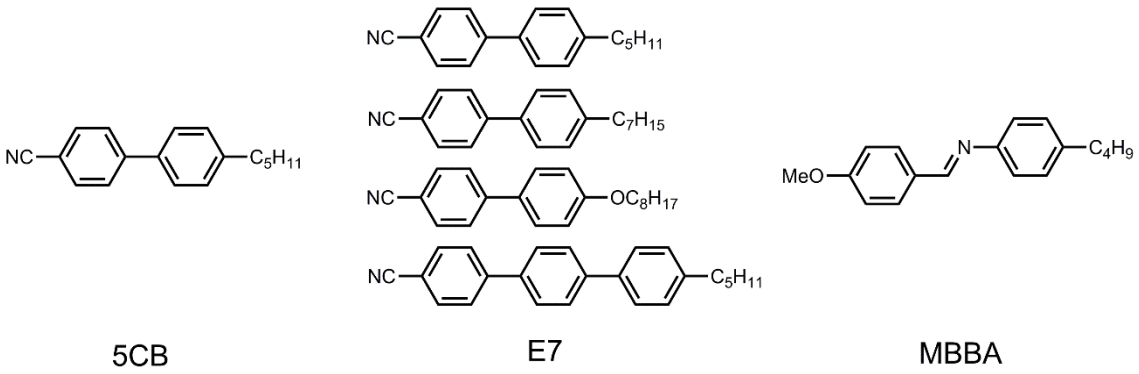

Figure 1.15 The chemical structures of typical host NLCs.

1.1.5.1 – Chiral Dopants with Central Chirality

When a small amount of a chiral dopant was dissolved in host NLCs, an intermolecular interaction between a chiral dopants and host NLC molecules works on anisotropy of host nematics and symmetry system. Chirality transfer occurs from a chiral dopant to host NLCs to form the N* phase from the achiral N phase (**Figure 1.16**). The intermolecular interaction between a chiral dopant and host NLC molecule is mostly the arene-arene interactions between them. There are four types of the arene-arene interactions, such as 'van der Waals', 'electrostatics', 'inductive' and 'charge-transfer' interactions of each an aromatic ring.[43] Therefore, the arene-arene interactions should be the dominant intermolecular interaction that could regulate the alignment of the molecular axes, by which the twisted molecular alignment of the LC molecules is induced.

The molecules, having central chirality include more than one asymmetric carbon centre. Indeed, these types of chiral dopants exhibits quite low HTP value without adequate chemical treatment. As a rule of thumb, the chiral dopants with central chirality must undergo adequate treatment; that is i) substitution of an aromatic ring to a neighbour asymmetric carbon and ii) inclusion of an asymmetric carbon into the small cycles, especially five-membered cycles, to exhibit a large HTP value. Therefore, chiral aryl alkyl carbinols[44] have the lowest HTP value in MBBA (**Figure 1.17**). By contrast, TADDOL

(α, α, α, α-tetraaryl-1,3-dioxolane-4,5-dimethanol)[45], 1,2-diphenylethane-1,2-diol[46] and tartaric imide derivatives[47] tend to exhibit large HTP values in cyano biphenyl-type NLCs, such as E7 and 5CB, compared with that of chiral carbinols (**Figure 1.17**).

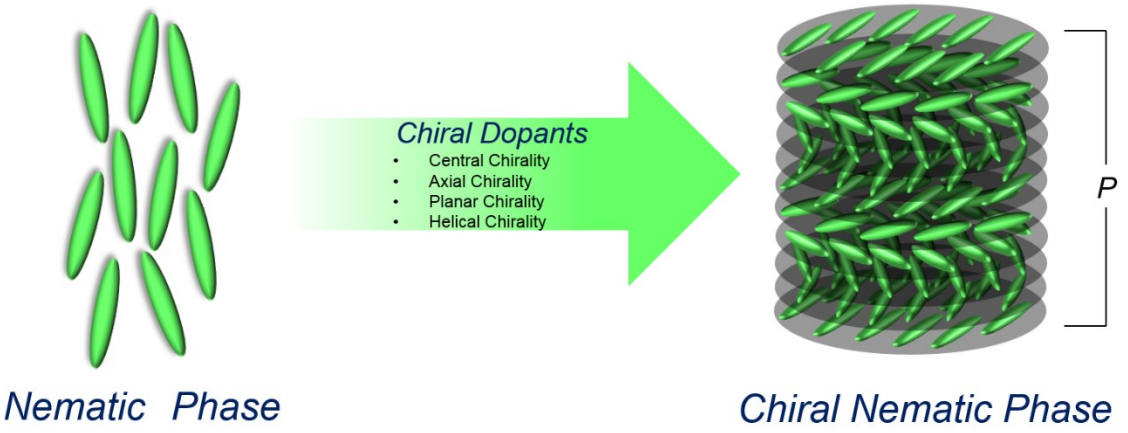

Figure 1.16 Schematic representation of the dopant-induced N* phase by adding a chiral dopant to host NLCs.

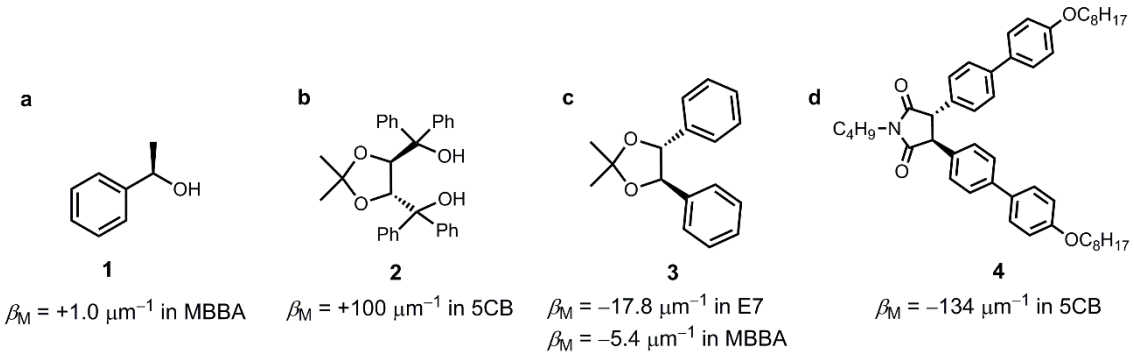

Figure 1.17 The chemical structures and the HTP values of (a) chiral aryl alkyl carbinol **1**, (b) TADDOL **2**, (c) 1,2-diphenylethane-1,2-diol **3** and (d) tartaric imide derivatives **4**. The sign of + and – denotes *P* and *M* helicity.

Interestingly, molecular structural similarity between the chiral dopants and host nematics can affect chirality transfer between them in case of 1,2-diphenylethane-1,2-diol derivatives, **3**, **5**–**8** (**Figure 1.18** and **Figure 1.19**).[46] The 1,2-diphenylethane-1,2-diol derivative **3** displays larger HTP value in E7 than that of MBBA (**Figure 1.18**). Structural similarity between this derivative and E7 is quite similar, i.e. the same molecular length

(l = 7.1 Å). On the other hand, the molecular length of MBBA core is longer than that of E7. Thus, the arene-arene interaction, especially the van der Waals interaction, between the 1,2-diphenylethane-1,2-diol derivative **3** and E7 core is more favourable than that between the derivatives and MBBA core. Similarly, this effect can been seen the other 1,2-diphenylethane-1,2-diol derivatives **5**–**8** (**Figure 1.19**).

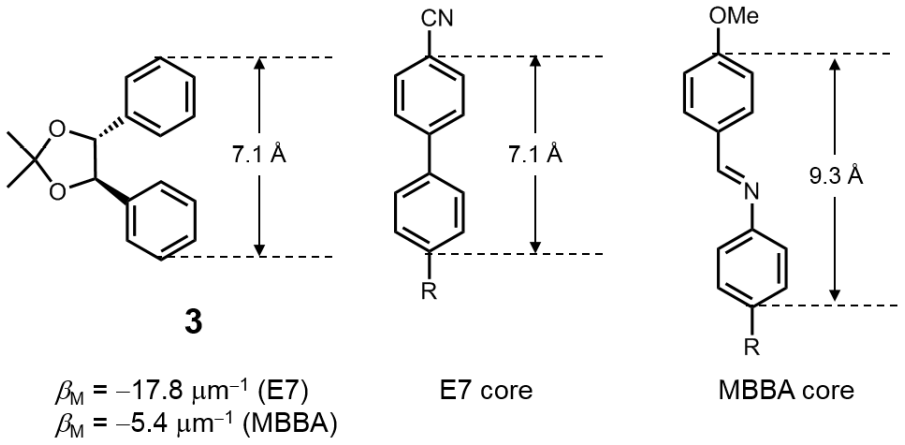

Figure 1.18 The molecular length of the 1,2-diphenylethane-1,2-diol-type chiral dopant **3** and aromatic core of host NLCs such as E7 and MBBA.

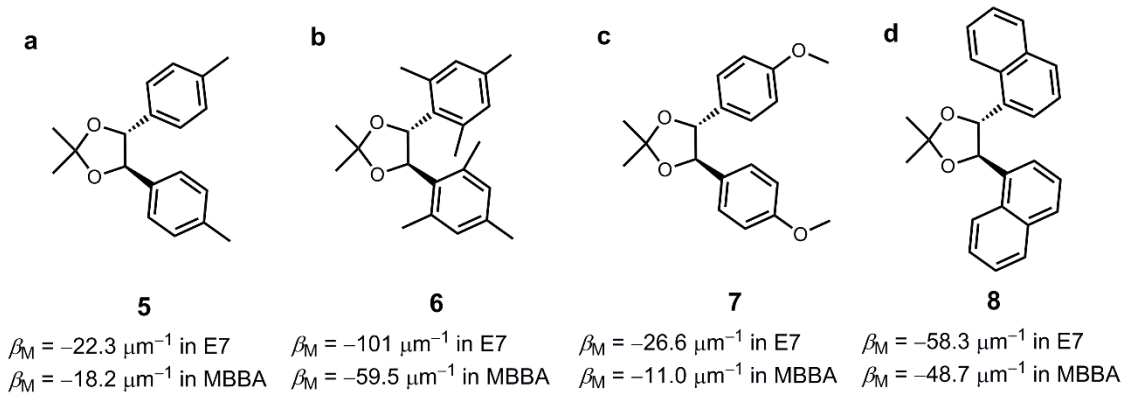

Figure 1.19 The chemical structures and corresponding HTP values in E7 and MBBA of (a) the 1,2-di(4-tolyl)ethane-1,2-diol **5**, (b) 1,2-dimesitylethane-1,2-diol **6**, (c) 1,2-di(4-methoxyphenyl)ethane-1,2-diol **7** and (d) 1,2-di(1-naphthyl)ethane-1,2-diol chiral dopants **8**.

The next interest research results are stabilisation of the BPs by the chiral dopant. The tartaric imide derivative **9** in *N*-(4-ethoxybenzylidene)-4-butylaniline (EBBA) as the host

nemtics exhibits the slightly wider temperature range of the BPs (**Figure 1.20**).[48] The HTP value of **9** in EBBA is –67 μm^{-1}. Further, EBBA, doping with 7.0 mol% of **9**, results that its temperature range is 7.2 °C on heating and 11.3 °C on cooling, respectively.

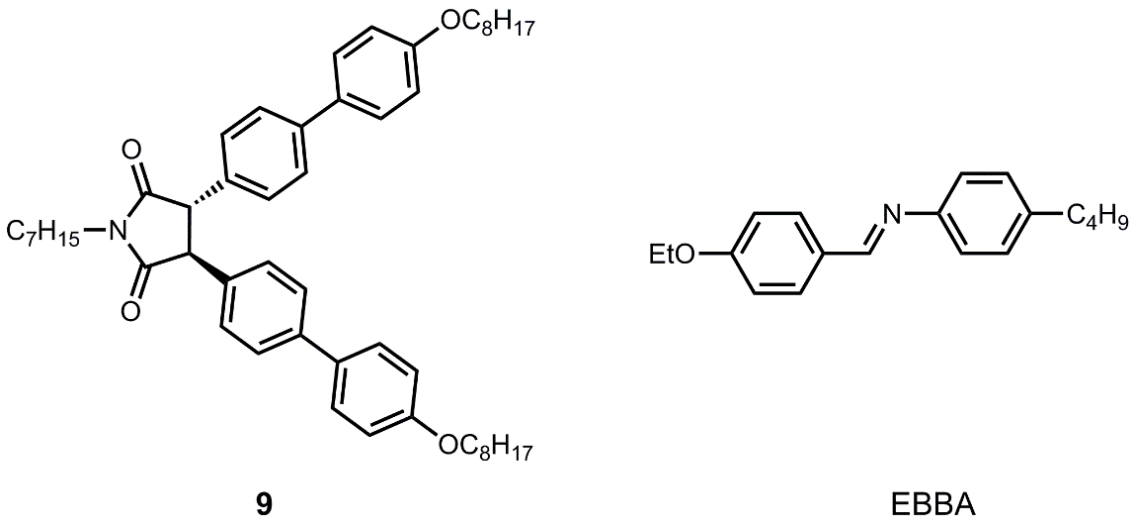

Figure 1.20 The chemical structures of the tartaric imide type chiral dopant **9** and EBBA.

1.1.5.2 – Chiral Dopants with Helical Chirality

The chiral dopants with helical chirality is employed helicenes.[49] Helicenes do not include an asymmetric carbon centre. They, thus, induce chirality, deriving from their chiral configurations: helical structures. The helicene-type chiral dopants **10**–**12** tend to show the moderated or large HTP values in E7 and MBBA (**Figure 1.21**). In addition, the absolute configuration of helical chirality represents plus (*P*) and minus (*M*). The dopants **10**–**12** possess *M* helicity. The sign of the induced N* phase corresponds to helicene-type chiral dopants' absolute configurations.

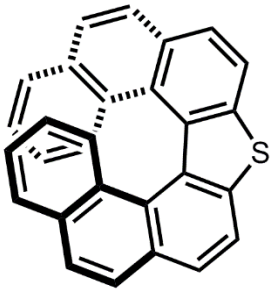

10

β_M = –20.0 μm^{-1} (E7)

β_M = –20.0 μm^{-1} (MBBA)

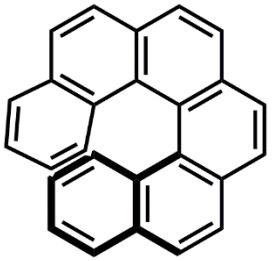

11

β_M = –20.0 μm^{-1} (E7)

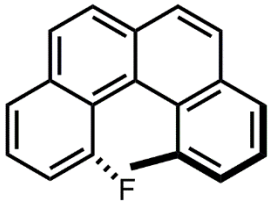

12

β_M = –9.0 μm^{-1} (E7)

Figure 1.21 The chemical structures and corresponding HTP values in E7 and MBBA of helicene-type chiral dopants **10**–**12**.

1.1.5.3 – Chiral Dopants with Axial Chirality

Molecules, possessing axial chirality represent biphenyl and binaphthyl derivatives. In particular, the 1,1'-binaphthyl structure is bonded two naphthyl ring at each 1-position of them. If the binaphthyl structure is substituted relative large substituent groups, for example being di-hydroxyl groups, at the 2,2'-position, it induces axial chirality due to preventing interconversion of enantiomers by its steric hindrance (**Figure 1.22**). Therefore, the 2,2'-dihydroxyl-1,1'-binaphthyl structure possess a chiral axis, although they do not include an asymmetric carbon centre. Moreover, binaphthyl derivatives possess C_2 molecular symmetry.

The biphenyl[50–52] and binaphthyl[52–59] derivatives are mainly utilised as chiral dopants with axial chirality for several decades. In comparison of HTP values of the biphenyl- and binaphthyl-type chiral dopants, the binaphthyl ones tend to exhibit larger HTP values without the unbridged binaphthyl chiral dopants **28**–**32** than those of biphenyl ones (**Figure 1.23** and **Figure 1.24**). Therefore, binapthyl-type chiral dopants bridged by an alkyl chain in the 2,2′-position have attracted a great deal of attention both experimentally[52–59, 60–62] and theoretically,[63] since they exhibit a relatively large HTP value in several host NLCs.

The binaphthyl-chiral dopants can exist in two conformations, called the '*cisoid*' and '*transoid*' conformations in host NLCs (**Figure 1.25**). These conformations are dependent on a dihedral angle of the binaphthyl derivatives (**Figure 1.25**). Moreover, a dihedral angle between two naphthyl planes of a binaphthyl-type chiral dopant in a host NLCs are estimated by comparing differences in a helical sense of its chiral dopant (**Figure 1.25**). The *cisoid* ($0° < \theta < 90°$) and *transoid* ($90° < \theta < 180°$) conformations of (*R*)-binaphthyl-type chiral dopants induce the left-handed and the right-handed senses, respectively (**Figure 1.25**). Further, in case of (*S*)-binaphthyl type chiral dopants, the left-handed and the right-handed helical senses correspond to the *transoid* and *cisoid* conformation, respectively.It should be noted that when a dihedral angle of the binaphthyl-type chiral dopants is 0°, 90° and 180°, the helical twisting ability of the binaphthyl-type chiral dopants disappear.

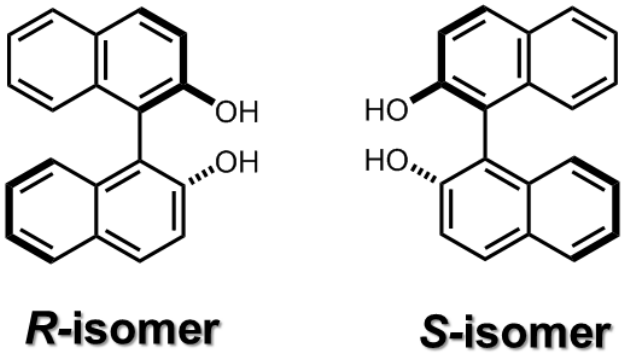

Figure 1.22 The enantiomer relationship between (*R*)- 2,2'-dihydroxyl-1,1'-binaphthyl.

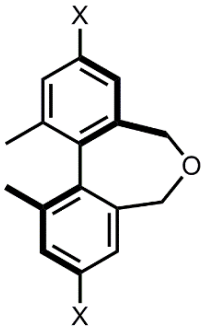

13:X = NO_2 $|\beta_M|$ = 20.3 μm^{-1} in 5CB
14:X = Br $|\beta_M|$ = 19.3 μm^{-1} in 5CB
15:X = Cl $|\beta_M|$ = 17.2 μm^{-1} in 5CB
16:X = NMe_2 $|\beta_M|$ = 4.2 μm^{-1} in 5CB
17:X = H $|\beta_M|$ = 0.3 μm^{-1} in 5CB

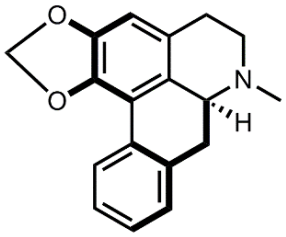

18
β_M = +24.0 μm^{-1} in E7

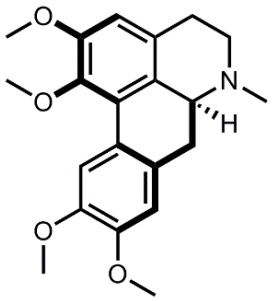

19
β_M = +8.0 μm^{-1} in E7

Figure 1.23 The chemical structures and corresponding HTP values in E7 and 5CB of the biphenyl-type chiral dopants **13**–**19**. $|\beta_M|$ denotes the absolute HTP values.

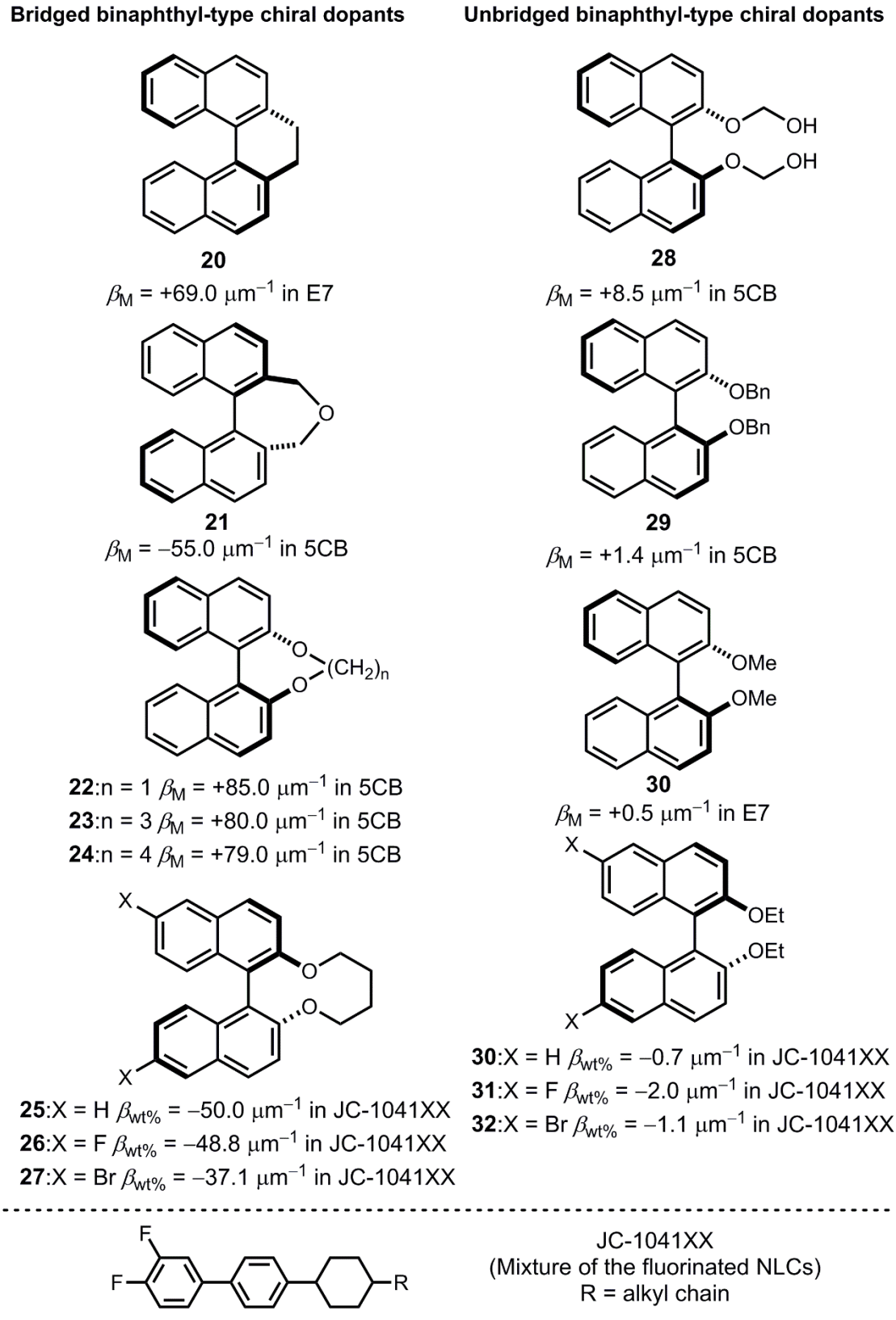

Figure 1.24 The chemical structures and corresponding HTP values in cyanobiphenyl- or biphenyl cyclohexane-type host NLCs of the typical binaphthyl-type chiral dopants **20**–**32**.

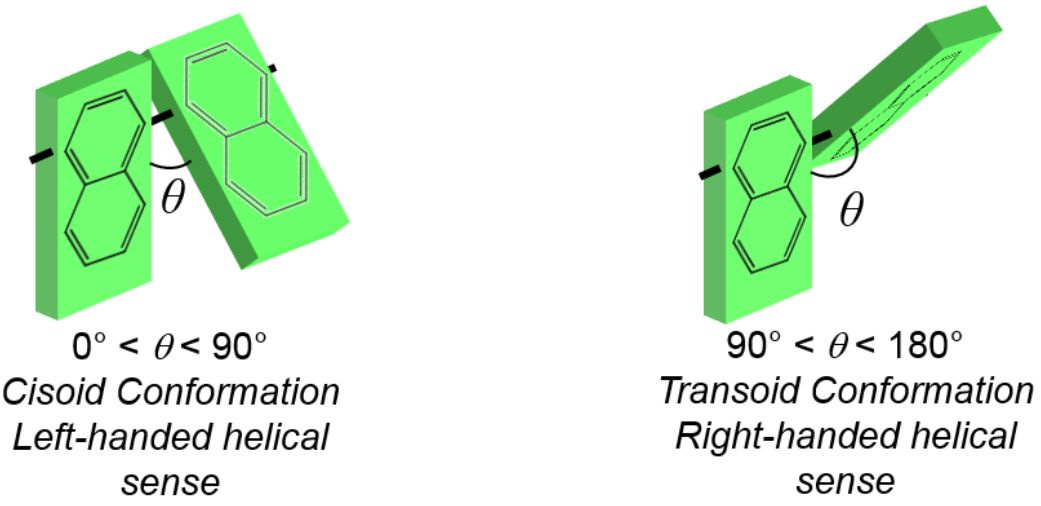

Figure 1.25 Schematic representation of the *cisoid* and *transoid* configurations as the (*R*)-binaphthyl structure.

The effect of molecular structural similarity is observed, in case of the binaphthyl-type chiral dopants (**Table 1.1**). Besides, Gottarelli *et al.* proposed the model for the chiral solute-solvent interaction between the binaphthyl-type chiral solute and the host nematic solvent (**Figure 1.26**).[52–54] The cyanobiphenyl-type NLC molecules, e.g. 5CB, usually show rapid interconversion. The host nematics is slanted the same conformation of the chiral solutes by the addition of the binaphthyl-type chiral dopants. Thus, the binaphthyl-type chiral dopants and cyanobiphenyl, based NLCs are associated though the arene-arene interaction. Additionally, the strong solute-solvent molecular interaction between the chiral dopants and the nematic solvents is known to enhance the HTP value.[41]

Table 1.1 Influence of molecular structural similarity the HTP values of the binaphthyl-type chiral dopants

Binaphthyl derivatives	β_M/μm^{-1} (5CB)	β_M/μm^{-1} (MBBA)
23	+80	+56
24	+79	+65

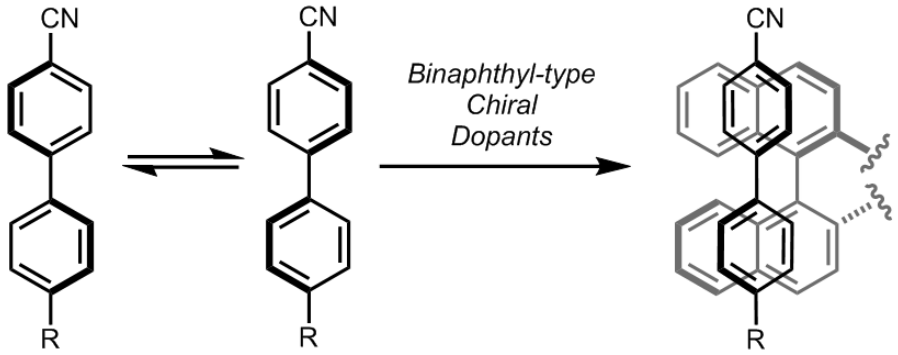

Figure 1.26 The model for the chiral solute-solvent interaction between the binaphthyl-type chiral dopant and cyanobiphenyl-type host NLC molecule.

The theoretical HTP value can forecast for the chiral dopants, possessing C_2 molecular symmetry, such as the binaphthyl-, biphenyl- and heptalene-type chiral dopants. This physical model has been called 'the surface chirality model'.

The theoretical HTP equation[63–67] is expressed as:

$$\beta = RT\xi Q / 2\pi K_{22} \nu_{\mathrm{m}} \tag{1.13}$$

where R is the gas constant, T is the temperature, ξ is the orienting strength, which is proportional to the order parameter of the nematic solvent and inversely proportional to temperature,[64] K_{22} is the twist elastic constant of the host nematic solvent, ν_{m} is the molar volume of the solution and Q is the chirality order parameter, which is a scalar quantity of a helicity tensor ($\boldsymbol{Q}_{\mathrm{ii}}$), based on molecular helix and an ordering matrix ($\boldsymbol{S}_{\mathrm{ii}}$) of the solute. The $\boldsymbol{S}_{\mathrm{ii}}$'s subscript of ii denotes the principal ordering axis of the solute. The chirality order parameter Q is defined as:

$$Q = -(2/3)^{1/2}\left(\boldsymbol{Q}_{\mathrm{xx}}\boldsymbol{S}_{\mathrm{xx}} + \boldsymbol{Q}_{\mathrm{yy}}\boldsymbol{S}_{\mathrm{yy}} + \boldsymbol{Q}_{\mathrm{zz}}\boldsymbol{S}_{\mathrm{zz}}\right) \tag{1.14}$$

The $\boldsymbol{S}_{\mathrm{ii}}$ corresponds to the order parameter tensor. This tensor is the local molecular order of a host NLC molecule, which interacts with a chiral solute's chiral surface. Consider

chiral surface of the binaphthyl-type chiral dopant **22** with the projection of them (**Figure 1.27**). The chirality tensor $\boldsymbol{Q}_{ii}$ represents the helicity of chiral dopant's molecular surface along the *i*-th axis.

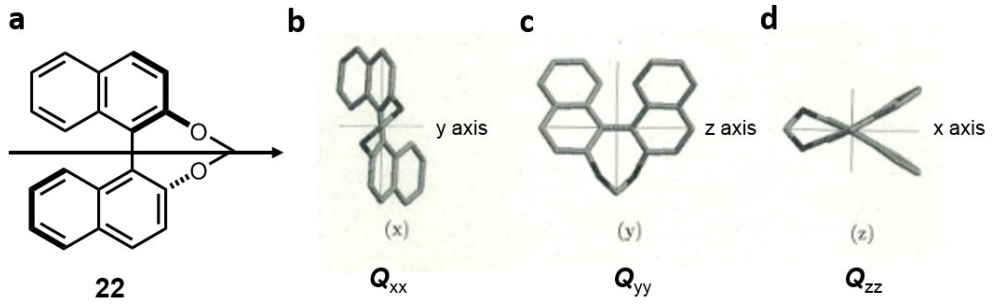

Figure 1.27 (a) The chemical structure of the bridged-type chiral dopant **22**, (b) the projection of **22**, viewed along x axis, (c) that of **22**, viewed along y axis and (d) that of **22**, viewed along z axis.[63] The arrow denotes the C_2 symmetry axis. The C_2 symmetry axis corresponds to the x axis.

This surface chirality model, is derived from (i) a continuous representation of the twist distortions of the nematic solvent and (ii) a representation of the solute interactions with a type of anchoring energy in the nematic solvents with macroscopic surface.

A theoretical HTP value and the parameter Q for binaphthyl-type chiral dopants strongly depend on the dihedral angles (θ) between their two naphthyl planes (**Figure 1.28**).[63, 65] When a bridged binaphthyl derivative forms a *cisoid* conformation ($0° < \theta < 90°$), the theoretical HTP should display a maximum value at $\theta = 45°$ (Q is the maximum). By contrast, the HTP value of chiral dopants disappears when θ is 0° and 90° ($Q \approx 0$). The same is true of a maximum value at $\theta = 135°$ (Q is the maximum) when binaphthyl-type chiral dopants form a *transoid* conformation. Similarly, the theoretical ones vanish at $\theta =$ 90° and 180° in their *transoid* conformations.

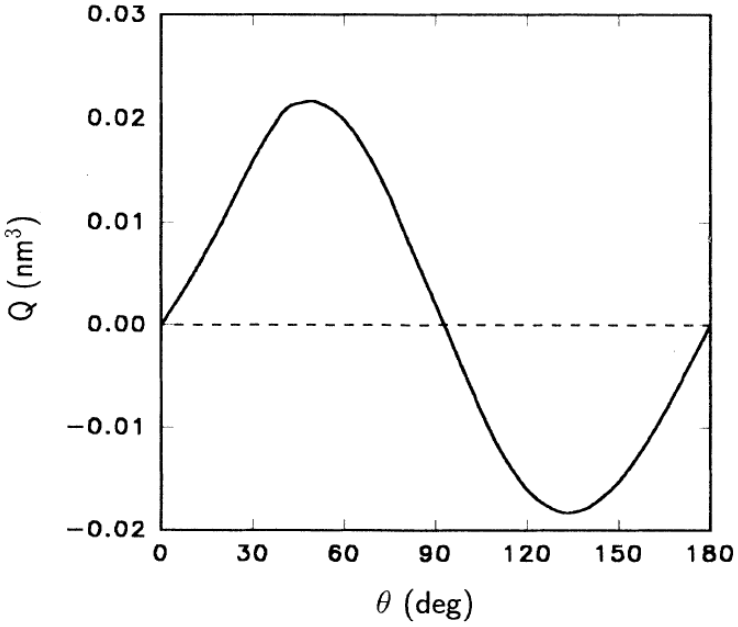

Figure 1.28 The relationship between the chiral order parameter Q and dihedral angle θ of a binaphthyl-type chiral dopant.[65]

1.2 – Aims and Outline of This Thesis

The 6,6'-fluorinated bridged binaphthyl-type chiral **26** is known to possess a relatively large HTP value[58] and slightly wide temperature range of the BPs[37] in the mixture of fluorinated host NLC, namely JC-1041XX. However, these studies do not take into account a role of substituents, molecular shapes and theoretical perspectives of a HTP value to interpret their phenomena. In order to address these issues, I have undertaken a systematic study of substituent effects and linker flexibility on the dopant-induced N* phase by the 6,6'-substituted bridged binaphthyl chiral dopants and 2,2'-unbridged, -alkyl and -alkynyl bridged binaphthyl-type chiral dopants (**Figure 1.29**). If these effects of their chiral dopants on a dopant-induced N* phase are revealed in a molecular level, the research field of LC science and technology will greatly advance on chemical structure modelling and material design for high performance LCs. Detailed research results and discussion can be found in *Chapter 2* and *3*.

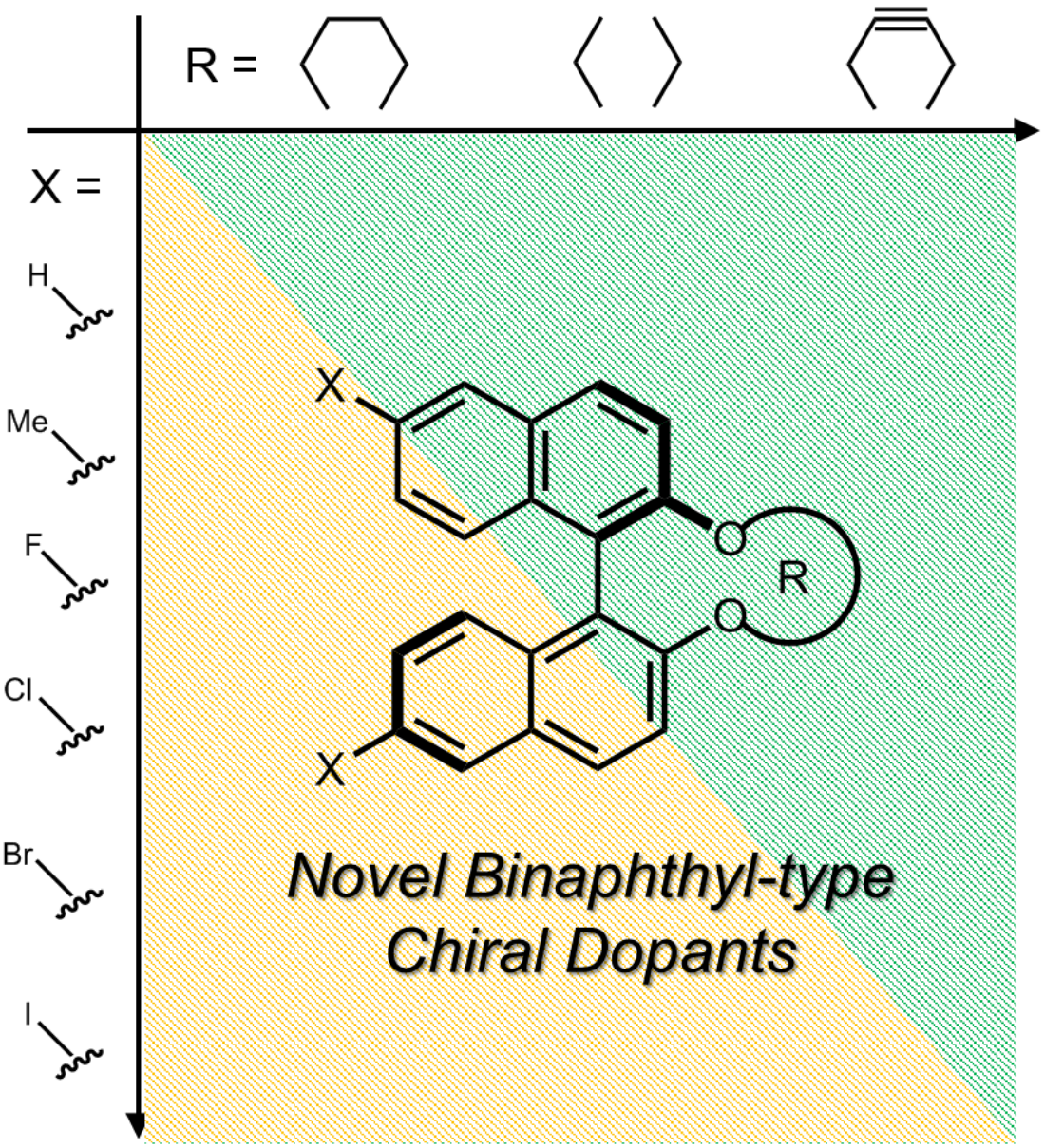

Figure 1.29 The molecular design of binaphthyl-type chiral dopants.

In Chapter 1, a review of LC science is presented. The CLCs, the N* and cholesteric blue phases, –chemical and physical perspectives–, is especially focused. Further, the current issue that 'why the 6,6'-fluorinated bridged binaphthyl-type chiral **26** give the larger HTP value and phase stabilisation of the BPs in the dopant-induced CLCs, such as the N* and blue phases, and research approach have been described.

The research results and discussion, described in Chapter 2, focuses on the 6,6'-substituents effects of the synthesised binaphthyl-type chiral dopants on induced helical

twisting properties in the induced N* phase in terms of intermolecular interactions between host NLC molecules and chiral dopants.

In Chapter 3, effects of linker flexibility of the synthesised chiral dopants at the 2,2' positions are discussed in respect to induced helical twisting properties from the viewpoint of the dihedral angle and theoretical vibration of the synthesised chiral dopants.

The detail experimental procedures have been described in Chapter 4. Syntheses, methodology of measurement of HTP values and helical senses and computational calculation, utilising the Gaussian can be found.

In Chapter 5, the general conclusion which my research reaches have been described.

1.3 – References and Notes

1. T. Yamamoto, *Jpn. J. Appl. Phy.* **1937**, *6*, 237.
2. *Introduction to Soft Matter – Revised Edition: Synthetic and Biological Self-Assembling Materials*, ed. by I. W. Hamley, John Wiley & Sons, **2007**. DOI: 10.1002/9780470517338.
3. H. Kawamoto, *Proc. I.E.E.E.* **2002**, *90*, 460.
4. *CRYSTALS THAT FLOW*, ed. by T. J. Sluckin, D. A. Dunmur, H. Stegemeyer, Taylor & Francis, London, **2004**.
5. T. Geelhaar, K. Griesar, B. Reckmann, *Angew. Chem. Int. Ed.* **2013**, *52*, 8798.
6. *Soap, science, and flat-screen TVs –A history of liquid crystals–*, ed. by D. Dumur, T. Sluckin, OXFORD UNIVERSITY PRESS, Oxford, **2014**.
7. V. Fréedericksz, V. Zolina, *Trans. Am. Electrochem. Soc.* **1929**, *55*, 85.
8. C. W. Oseen, *Trans. Faraday Soc.* **1933**, *29*, 883.
9. L. S. Ornstein, W. Kast, *Trans. Faraday Soc.* **1933**, *29*, 930.
10. P. Chatelain, *Bull. Soc. Fr. Mineral* **1944**, *66*, 105.
11. M. Mięsowicz, *Nature* **1946**, *158*, 27.
12. G. H. Brown, W. G. Shaw, *Chem. Rev.* **1957**, *57*, 1049.
13. G. H. Heilmeier, L. A. Zanoni, L. A. Barton, *Proc. I.E.E.E.* **1968**, *56*, 1162.

14. H. Kelker, B. Scheurle, *Angew. Chem. Int. Ed.* **1969**, *8*, 884.

15. G. W. Gray, K. J. Harrison, J. A. Nash, *Electron. Lett.* **1973**, *9*, 130.

16. W. Helfrich, M. Schadt, *Appl. Phy. Lett.* **1971**, *18*, 127.

17. https://www.icom.co.jp/beacon/electronics/001407.html, (accessed on 04 December 2017)

18. http://www.sharp.co.jp/aquos/history/, (accessed on 04 December 2017)

19. T. Nagai, *management sensor* **2008**, *108*, 36.

20. *Textures of Liquid crystals*, ed. by I. Dierking, John Wiley & Sons, **2003**. DOI: 10.1002/3527602054.fmatter.

21. I. Dierking, *Symmetry* **2014**, *6*, 444.

22. M. Hird, *Chem. Soc. Rev.* **2007**, *36*, 2070.

23. S. Frunza, A. Schönhals, L. Frunza, T. Beica, I. Zgura, P. Ganea, D. Stoenescu, *Chem*. *Phys*. **2010**, *327*, 51.

24. H. Zocher, *Trans. Faraday Soc.* **1933**, *29*, 930.

25. F. C. Frank, *Discuss. Faraday Soc.* **1958**, *25*, 19.

26. H. K. Bisoyi, Q. Li, *Acc. Chem. Res.* **2014**, *47*, 3184.

27. H. Nishikawa, D. Mochizuki, H. Higuchi, Y. Okumura, H. Kikuchi, *ChemistryOpen* **2017**, *6*, 710.

28. K. Hashimoto, M. Okada, K. Nishiguchi, N. Masazumi, E. Yamakawa, T. Taniguchi, *J. Soc*. *Inf. Display* **1998**, *6*, 239.

29. H. Onisseit, H. Stegemeyer, *J. Cryst*. *Growth* **1983**, *61*, 409.

30. D. Coates, G. W. Gray, *Phys*. *Lett*. **1973**, *45*A, 115.

31. S. Meiboom, M. Sammon, *Phys*. *Rev*. *Lett*. **1980**, *44*, 882.

32. D. L. Johnson, J. H. Flack, P. P. Crooker, *Phys*. *Rev*. *Lett*. **1980**, *45*, 641.

33. J. H. Flack, P. P. Crooker, *Phys. Lett.*, **1981**, *82A*, 247.

34. S. Meiboom, J. P. Sethna, P. W. Anderson, W. F. Brinkman, *Phys*. *Rev*. *Lett*. **1981**, *46*, 1216.

35. T. Blümel, H. Stegemeyer, *J. Cryst. Growth* **1984**, *66*, 163.

36. P. E. Cladis, T. Garel, P. Pieranski, *Phys. Rev. Lett*., **1986**, *57*, 2841.

37. K. Kakisaka, H. Higuchi, Y. Okumura, H. Kikuchi, *J*. *Mater*. *Chem*. *C* **2014**, *2*, 6467.

38. H. Kikuchi, M. Yokota, Y. Hisakado, H. Yang, T. Kajiyama, *Nat*. *Mater*. **2002**, *1*, 64.

39. H. S. Kitzerow, H. Schmid, A. Ranft, G. Heppke, R. A. M. Hikmet, J. Lub, *Liq*. *Cryst*. **1993**, *3*, 911.

40. R. Eelkema, B. L. Feringa, *Org*. *Biomol*. *Chem*. **2006**, *4*, 3729.

41. S. Pieraccini, A. Ferrarini, G. P. Spada, *Chirality* **2008**, *20*, 749.

42. S. Pieraccini, S. Masiero, A. Ferrarini, G. P. Spada, *Chem*. *Soc*. *Rev*. **2011**, *40*, 258.

43. C. A. Hunter, K. R. Lawson, J. Perkins, C. J. Urch, *J*. *Chem*. *Soc*. *Perkin Trans*. 2 **2001**, 651.

44. G. Gottarelli, B. Samori, C. Stremmenos, G. Torre, *Tetrahedron* **1981**, *37*, 395.

45. H. G. Kuball, B. Weiß, A. K. Beck, D. Seebach, *Helv*. *Chim*. *Acta*. **1997**, *80*, 2507.

46. S. Superchi, M. I. Donnoli, G. Proni, G. P. Spada, C. Rosini, *J*. *Org*. *Chem*. **1999**, *64*, 4762.

47. K. Kishikawa, Y. Furukawa, T. Watanabe, M. Kohri, T. Taniguchi, S. Kohmoto, *Liq*. *Cryst*. **2017**, *44*, 969.

48. K. Kishikawa, T. Sugiyama, T. Watanabe, S. Aoyagi, M. Kohri, T. Taniguchi, M. Takahashi, S. Kohmoto, *J*. *Phys*. *Chem*. *B* **2014**, *118*, 10319.

49. G. Gottarelli, G. Proni, G. P. Spada, D. Fabbri, S. Gladiali, C. Rosini, *J*. *Org*. *Chem*. **1996**, *61*, 2013.

50. V. E. Williams, R. P. Lemieux, *Chem*. *Commun*. **1996**, 2259.

51. A. di Matteo, S.M Todd, G. Gottarelli, G. Solladié, V. E. Williams, R. P. Lemieux, A. Ferrarini, G. P. Spada, *J*. *Am*. *Chem*. *Soc*. **2001**, *123*, 7842.

52. G. Gottarelli, M. Hobert, B. Samori, G. Solladié, G. P. Spada, R. Zimmermann, *J*. *Am*. *Chem*. *Soc*. **1983**, *105*, 7318.

53. G. Gottarelli, G. P. Spada, *J*. *Org*. *Chem*. **1986**, *51*, 589.

54. G. Gottarelli, M. A. Osopov, G. P. Spada, *J*. *Phys*. *Chem*. **1991**, *95*, 3879.

55. M. Zhang, G. B. Schuster, *J*. *Phys*. *Chem*. **1992**, *96*, 3603.

56. H-J. Deuβen, P. V. Shibaev , R. Vinokur , T. Bjørnholm , K. Schaumburg , K. Bechgaard, V. P. Shibaev, *Liq. Cryst.* **1996**, *21*, 327.

57. G. Proni, G. P. Spada, *J. Org. Chem.* **2000**, *65*, 5522.

58. K. Kakisaka, H. Higuchi, Y. Okumura, H. Kikuchi, *Chem*. *Lett*. **2014**, 43, 624.

59. K. Kakisaka, Doctoral thesis, Kyushu University, **2014**.

60. K. Akagi, S. Guo, T. Mori, M. Goh, G. Piao, M. Kyotani, *J*. *Am*. *Chem*. *Soc*. **2005**, *127*, 14647.

61. S. Pieraccini, A. Ferrarini, K. Fuji, G. Gottarelli, S. Lena, K. Tsubaki, G. P. Spada, *Chem*. *Eur*. *J*. **2006**, *12*, 1121.

62. T. Mori, M. Kyotani, K. Akagi, *Macromolecules* **2008**, *41*, 607.

63. A. Ferrarini, P. L. Nordio, P. V. Shibaev, V. P. Shibaev, *Liq*. *Cryst*., **1998**, *24*, 219.

64. A. Ferrarini, G. J. Moro, P. L. Nordio, *Mol*. *Phys*. **1996**, *87*, 485.

65. A. Ferrarini, G. J. Moro, P. L. Nordio, *Phys*. *Rev*. *E* **1996**, *53*, 681.

66. D. J. Earl, M. R. Wilson, *J*. *Chem*. *Phys*. **2003**, *19*, 10280.

67. A. Ferrarini, S. Pieraccini, S. Masiero, G. P. Spada, *Beillstein J*. *Org*. *Chem*. **2009**, *5*, 50.

Chapter 2
Substituents Effects on the Dopant-induced Chiral Nematic Phase

2.1 − Introduction

Chirality is a geometric property of chemical structures that indicates a lack of mirror symmetry, and it often induces intriguing physical properties in materials.[1] For example, chiral liquid crystals (CLCs), especially chiral nematic liquid crystals (N*LCs)[2] and blue phase liquid crystals (BPLCs),[3] including polymer-stabilised cholesteric BPLCs (PSChBPLCs),[4] exhibit unusual physical properties, such as periodic helical structures, selective reflections of circularly polarised light based on Bragg's law,[5–6] and a fast electric response[4, 7–9]. These CLCs have potential applications in low energy consumption displays[10–11] and tuneable optical or laser devices[12–14] due to their unique properties. The development of CLCs or chiral dopants that enable the formation of a N*LC from a nematic liquid crystal (NLC), therefore, has attracted considerable attention. Chiral dopants are asymmetric molecules, and their molecular structures can be classified into four types; that is central, axial, planar, and helical chirality. The ability of a chiral dopant to generate a helical structure in a given host NLC is evaluated, using helical twisting power (HTP), as expressed below:

$$\beta_{\mathrm{wt\%}} = (pc_w)^{-1} \tag{2.1}$$

where p is the helical pitch of the chiral nematic (N*) phase, and c_w is the concentration of the chiral dopant in weight percentage. Chiral dopants with large HTP values are required for the above-mentioned applications since excess doping of chiral molecule in a host NLC negatively affects the physical properties of induced CLCs.

To date, significant efforts have been devoted to revealing an interrelation between the molecular structure of chiral dopants and the HTP value. In particular, binapthyl-type chiral dopants bridged by an alkyl chain in the 2,2′-positions have attracted a great deal of attention both experimentally and theoretically, since they exhibit a relatively large HTP value in several host NLCs for several decades (see *Chapter 1*, **1.1.5.3**). This means their effective chirality makes them act as solutes to nematic solvent. However, the

mechanism of chirality transfer from chiral dopants to host nematics remains unclear. If the mechanism was to be understood on a molecular level, the field of LC science and technology would greatly advance in chemical structure modelling and material design to produce high performance LCs.

In our laboratory's previous research, the 6,6'-fluorinated binaphthyl-type chiral dopant **26** exhibited a large HTP value, high solubility[15], and availability of slightly wider blue phase (BP) temperature range[16] in the fluorinated NLC. The effects of fluorine substituents on the HTP value in the induced N*LC phase and the BP temperature range have not yet been well understood. Herein, non-substituted (**25**), 6,6'-halogenated (X = F: **26**, X = Cl: **33**, X = Br: **27**, X = I: **34**) and -methylated (**35**) binaphthyl-type chiral dopants were synthesised to examine dominant molecular factors like the steric hindrance, polarity, and polarisability of their substituents that affect the chirality transfer between the chiral dopant and the host nematics. The binaphthyl-type dopants possessing smaller volumes, larger polarisabilities, and good molecular structural similarities to that of the two different host NLCs, MBBA and JC-1041XX, exhibited excellent HTP values. Moreover, the electronic states of the aromatic rings of the dopants and the host nematics have a great impact on the HTP values. The chemical structures of the synthesised chiral dopants are represented (**Figure 2.1**). Besides, the chemical structures and phase transition temperatures of host NLCs are also shown in Figure 2.2.

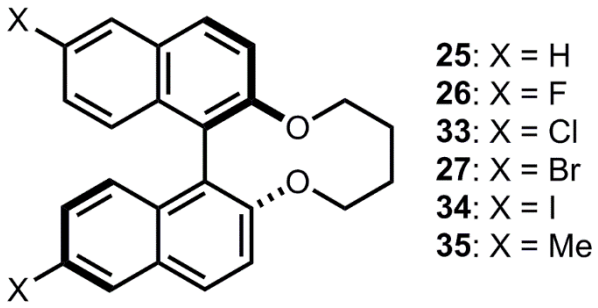

Figure 2.1 The chemical structures of the synthesised chiral dopants.

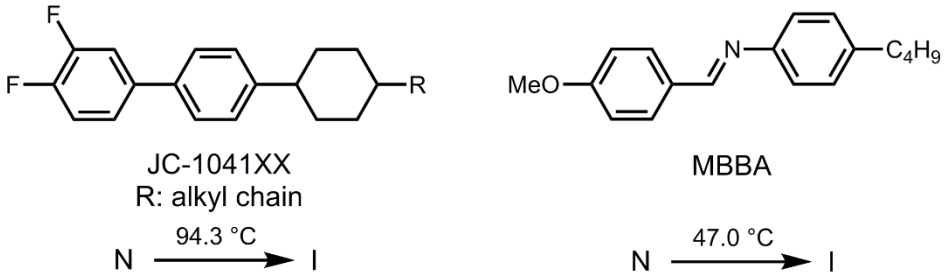

Figure 2.2 The chemical structures and phase transition temperatures of host NLCs. N and I denote the namatic and isotropic phase, respectively.

2.2 – Substituent Effects of Binaphthyl-type Chiral Dopants on Induced Helical Twisting Powers

2.2.1 – Effects of Substituents on Dihedral Angle of Synthesised Binaphtyl-type Chiral Dopants

The dihedral angle of **25**–**27** and **33**–**35** was calculated by means of density functional theory (DFT) under the conditions, described in *Chapter 4*, **3.1**, and the optimised structure of **25**–**27** and **33**–**35** is represented (**Figure 2.3**). According to the DFT calculations, the calculated dihedral angle, θ(C8-C1-C1′-C8′, see **Figure 2.3**), of **25**, **26**, **33**, **27**, **34**, and **35** was −67.7°, −67.6°, −67.6°, −67.7°, −67.4°, and −67.3°, respectively. The variation in the dihedral angle caused by the different substituents was small even though the sizes of the substituents were different. Furthermore, the crystal structures of **25**, **26**, **33**, **27**, and **35** were successfully determined without **34**[17] (**Figure 2.4**–**2.8**). The crystal structure of **26** showed one independent molecule. Those of **25** and **35** displayed two independent molecules. Those of **33** and **27** exhibited six independent molecules. The dihedral angle θ(C8-C1-C1′-C8′) of **25**, **26**, **33**, **27**, and **35** was finalised in Table 2.1.

Table 2.1 The dihedral angle θ of **25**, **26**, **33**, **27**, and **35** in their crystal structures

Substituents	**25**: X = H	**26**: X = F	**33**: X = Cl	**27**: X = Br	**35**: X = Me
	−67.3	−80.0	−77.1	−73.5	−67.5
	−75.7		−77.3	−75.6	−69.8
Dihedral			−77.3	−76.5	
angles/°			−79.1	−76.7	
			−79.6	−78.9	
			−85.5	−82.4	

All dihedral angles of **25**, **26**, **33**, **27**, and **35** in their crystal were less than −90° ($\theta < 90°$). It is known that the determination method of helical senses of a dopant-induced N* phase is carried out by the contact method (**Figure 2.9a**). The helical senses of a dopant-induced N* phase were determined by well-known contact method (**Figure 2.9a**). In the method, N*LC sample, induced by doping a chiral dopant, contacted with the referential N* phase of cholesteryl oleyl carbonate (COC, **Figure 2.9b**) possessing the left-handed helical sense in the wedged cell. If a defect line is not appeared between both the N* phases, both helical senses of the chiral dopant and COC are left-handed. By contrast, if a defect line is appeared, a helical sense of each the N* phases are opposite, and the helical sense of the chiral dopant is determined to be right-handed. Here, the defect line is a linear area of the N phase, induced by cancelling between the right- and left-handed helical senses.

By utilising the contact method, the helical sense of the N*LC induced by the chiral dopant was confirmed to be left-handed for all of the synthesised chiral dopants **25**–**27** and **33**–**35** in the two host NLCs, JC-1041XX and MBBA, whose dielectric anisotropies were positive and negative, respectively (**Figure 2.10**).

It is known that the *cisoid* ($0° < \theta < 90°$) and *transoid* ($90° < \theta < 180°$) conformations of (*R*)-binaphthyl-type chiral dopants induce the left-handed and the right-handed senses, respectively (**Figure 2.9c**).[18] Therefore, the results of the contact method indicate that the

conformations of **25**–**27** and **33**–**35** adopt a *cisoid* conformation in the host NLCs (**Figure 2.10**). These experimental results agree well with the DFT calculations ($\theta = 67°–68°$) and their crystal structures ($\theta < 90°$).

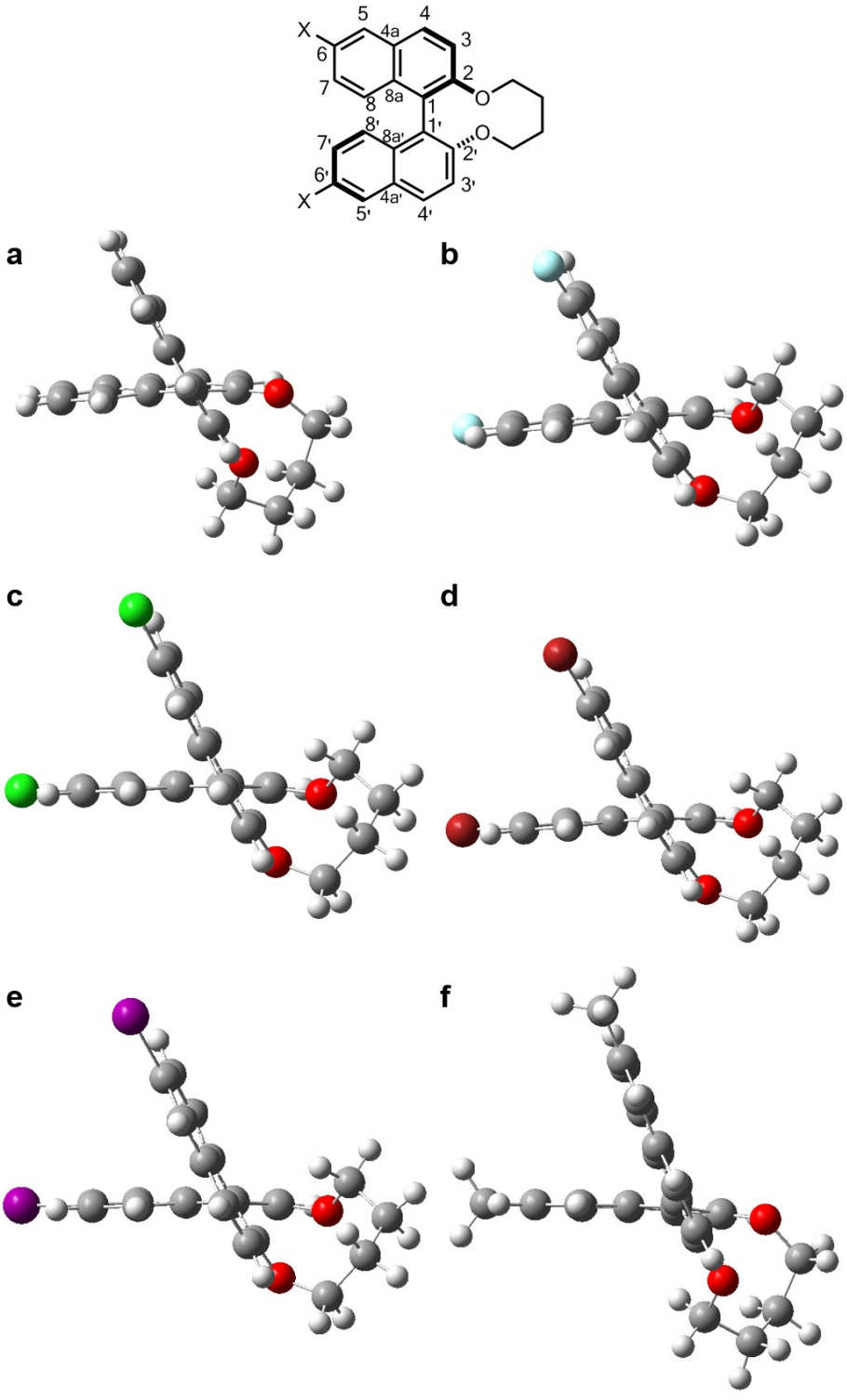

Figure 2.3 The optimised structures of (a) **25**, (b) **26**, (c) **33**, (d) **27**, (e) **34** and (f) **35**.

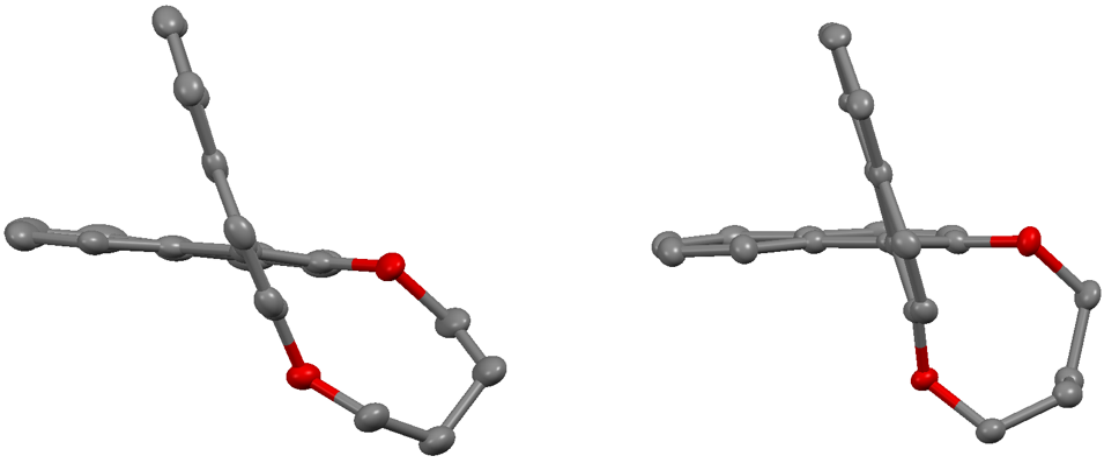

Figure 2.4 The crystal structure of **25** at 123 K. Hydrogen atoms have been omitted for clarity. Thermal ellipsoids are displayed at the 50% probability level.

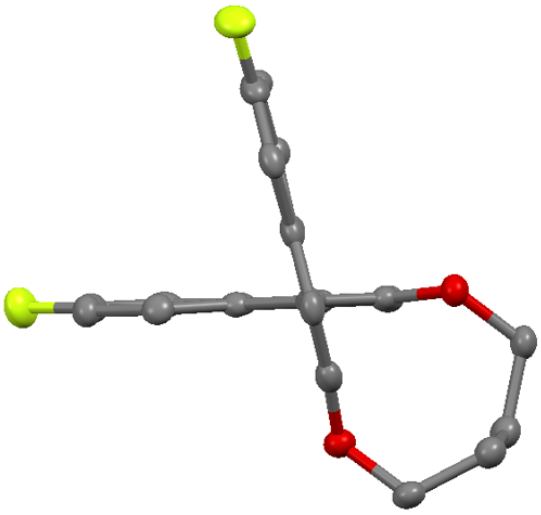

Figure 2.5 The crystal structure of **26** at 123 K. Hydrogen atoms have been omitted for clarity. Thermal ellipsoids are displayed at the 50% probability level.

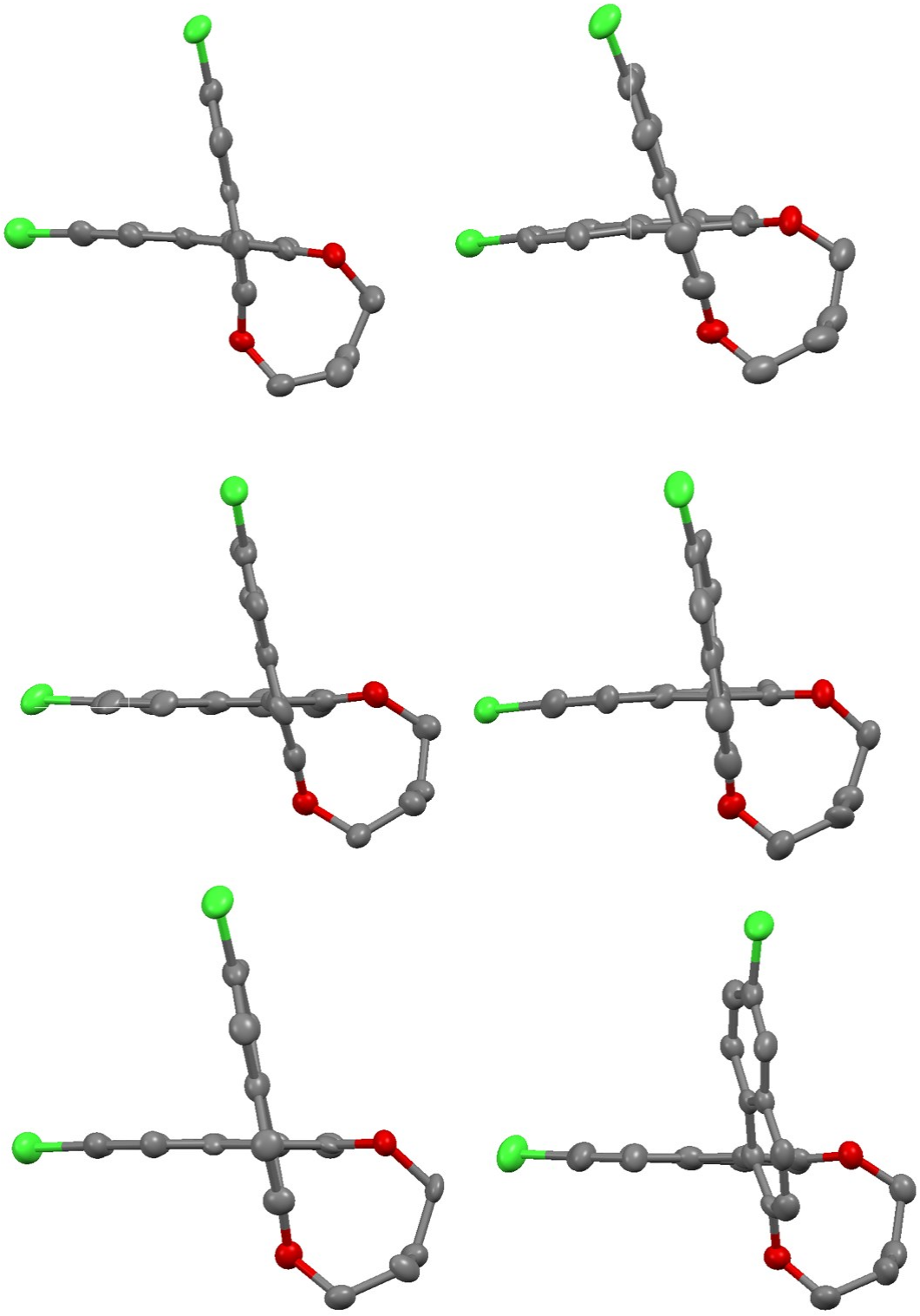

Figure 2.6 The crystal structure of **33** at 123 K. Hydrogen atoms have been omitted for clarity. Thermal ellipsoids are displayed at the 50% probability level.

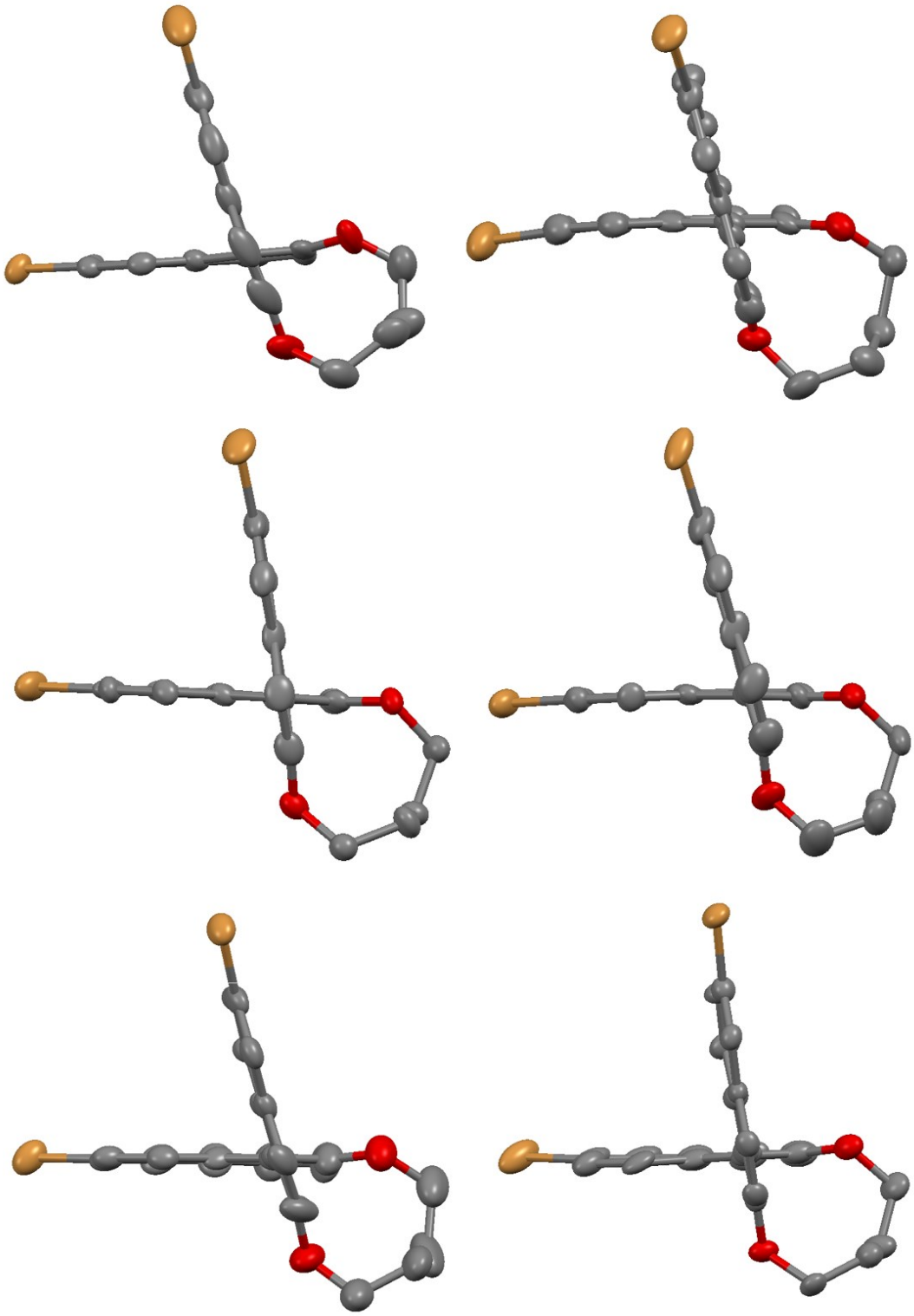

Figure 2.7 The crystal structure of **27** at 123 K. Hydrogen atoms have been omitted for clarity. Thermal ellipsoids are displayed at the 50% probability level.

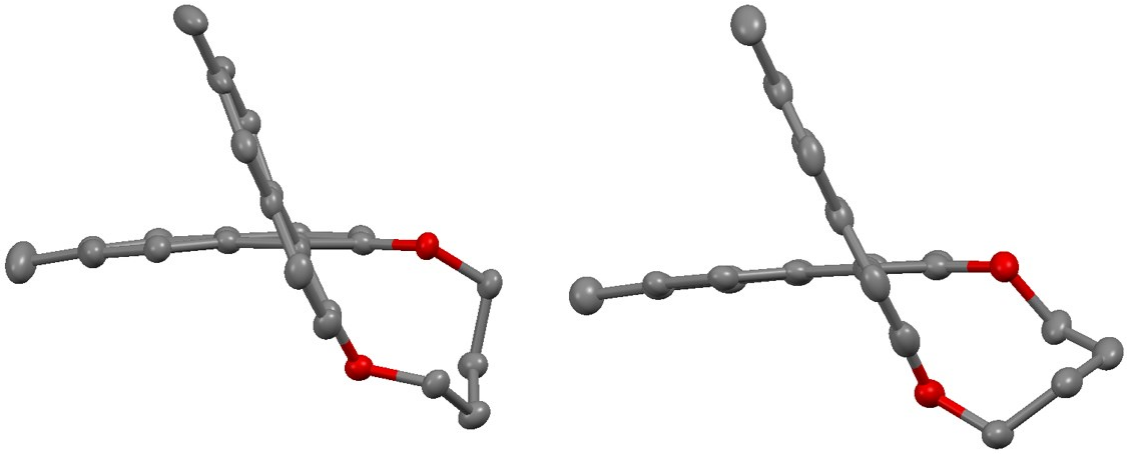

Figure 2.8 The crystal structure of **35** at 123 K. Hydrogen atoms have been omitted for clarity. Thermal ellipsoids are displayed at the 50% probability level.

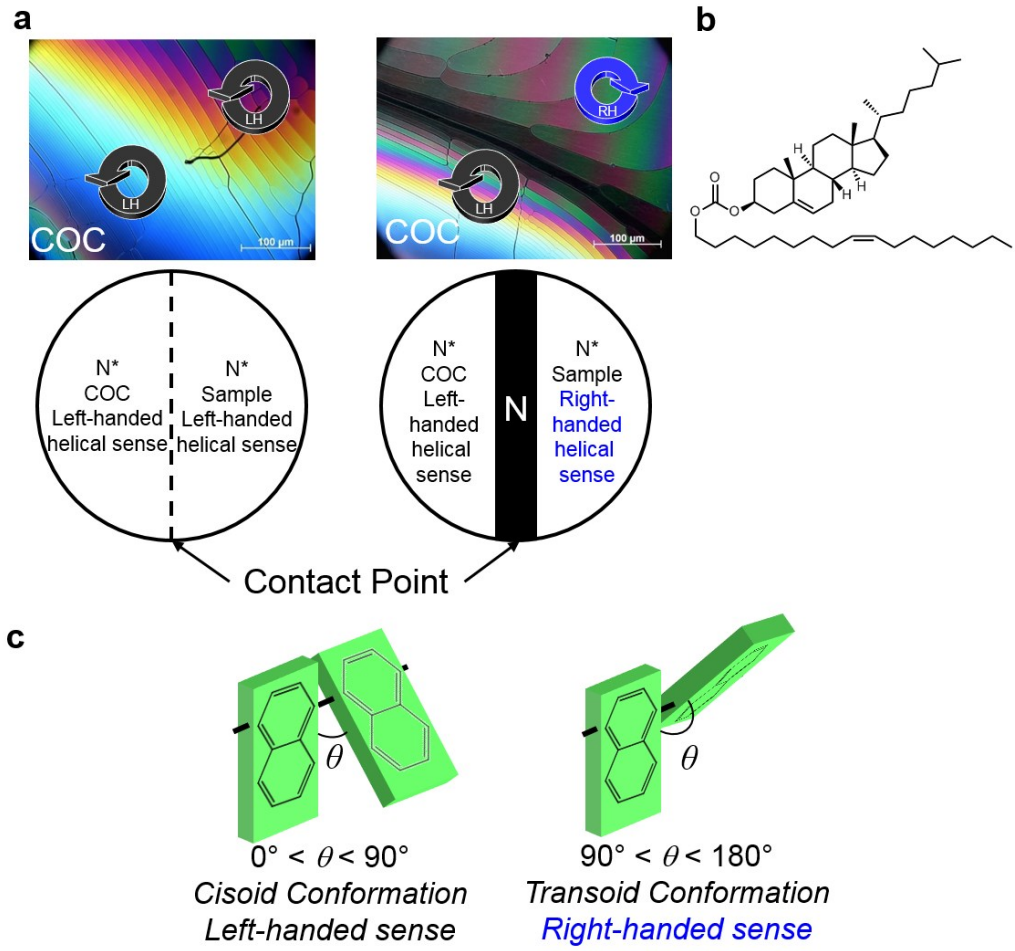

Figure 2.9 (a) The contact method, (b) The chemical structure of cholesteryl oleyl carbonate (COC), possessing a left-handed (LH) helical sense and (c) relationship between binaphthyl's conformations and their induced helical senses.

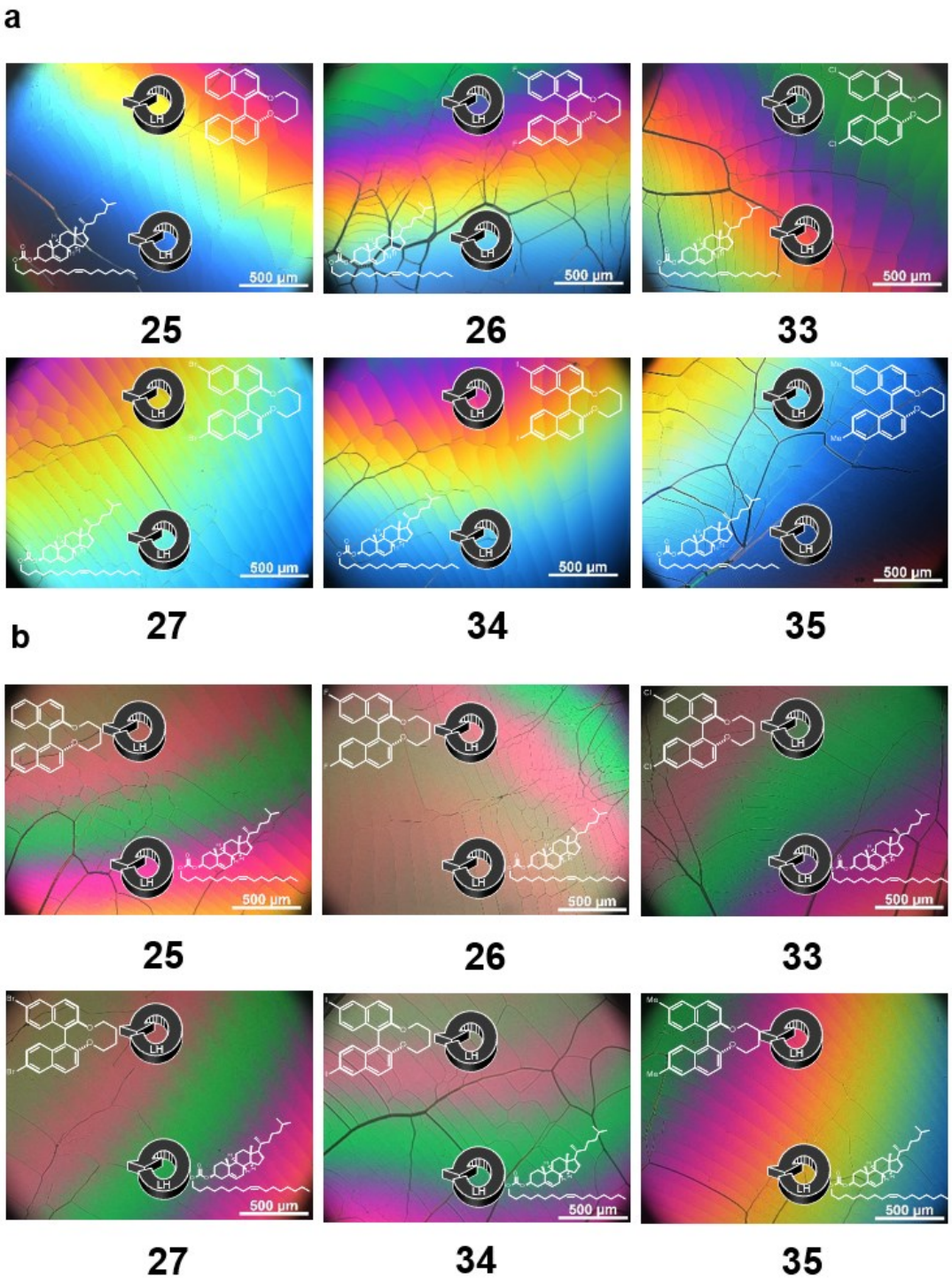

Figure 2.10 Optical textures of (a) 0.5wt% mixtures of **25–27** and **33–35** in JC-1041XX and (b) 0.5wt% mixtures of **25–27** and **33–35** in MBBA.

2.2.2 – Effects of the Substituents on Induced Helical Twisting Powers

The absolute $\beta_{wt\%}$ values, $|\beta_{wt\%}|$, obtained at the clearing point (T_c) below 5 °C, termed T_c−5 °C, in JC-1041XX and MBBA and three types of substituent parameters that are expected to affect the intermolecular interaction between the chiral dopants and the LC molecules are shown in Table 2.2. The van der Waals volume parameter (V_{vdw}) corresponds to the steric size of the substituent group.[19] The Hammett constant at the para position (σ_p) indicates an electron-withdrawing or -donating inductive effect of the substituent group.[20] The polarisability (α) is a relative tendency of electric charge distribution of the substituent group, which is calculated as per an equation given in Ref. 21. The equation of the α, called the Lorentz–Lorenz equation, is expressed as below:

$$\alpha = (3/4\pi N_A)(n^2 - 1/n^2 + 2)(M_w/\rho) \quad (2.2)$$

where α is the polarisability, N_A is the Avogadro constant, n is the refractive index, M_w is the molecular weight and ρ is the density value. The α was determined to utilise the refractive indexes and density values of benzene, fluorobenzene, chlorobenzene, bromobenzene, iodobenzene and toluene.[22]

Table 2.2 The $|\beta_{wt\%}|$ values of **25**–**27** and **33**–**35** at T_c−5°C in JC-1041XX and MBBA and their substituents parameters. The concentration of the chiral dopant was 0.5 wt%.

Entry	X	$\lvert\beta_{wt\%}\rvert/\mu m^{-1}$		Substituent parameters		
		JC-1041XX	MBBA	V_{vdw}/ cm·mol^{-1}	σ_p	$\alpha/10^{-23}$cm^3
25	H	49.9	37.1	3.5	0	1.04
26	F	51.7	46.5	5.8	0.06	1.03
33	Cl	56.1	48.4	12.0	0.24	1.24
27	Br	44.9	39.3	15.1	0.27	1.35
34	I	35.3	30.1	19.6	0.30	1.55
35	Me	61.7	46.2	13.7	−0.13	1.23

The $|\beta_{wt\%}|$ values of **25**–**27** and **33**–**35** in JC-1041XX and MBBA are plotted for substituents of α and V_{vdw} to indicate a relationship between the polarisability and steric effect of their substituents and their $|\beta_{wt\%}|$ values (**Figures 2.11–2.12**).

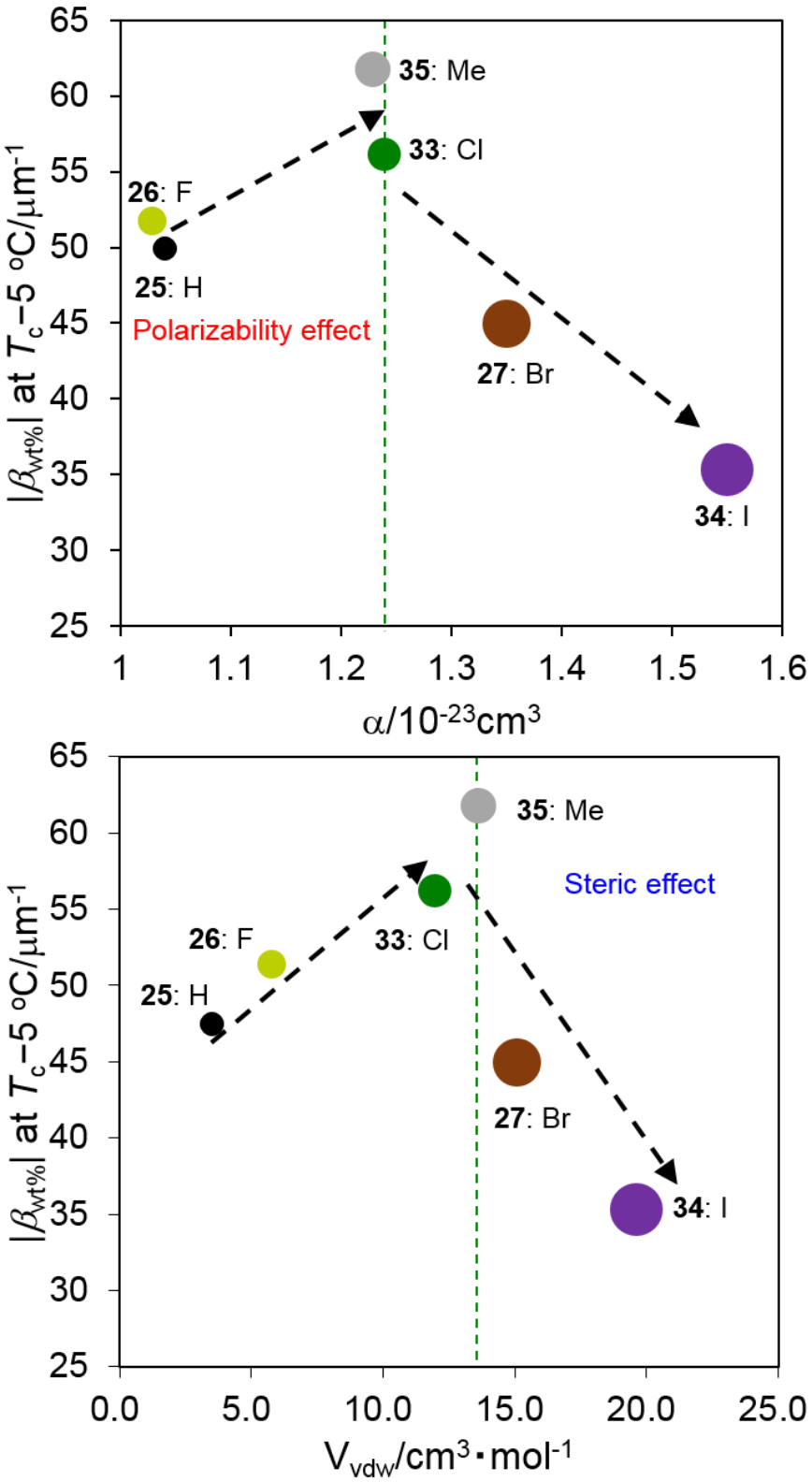

Figure 2.11 Plots of the $|\beta_{wt\%}|$ values of **25**–**27** and **33**–**35** in JC-1041XX vs. the α and V_{vdw} of their substituents.

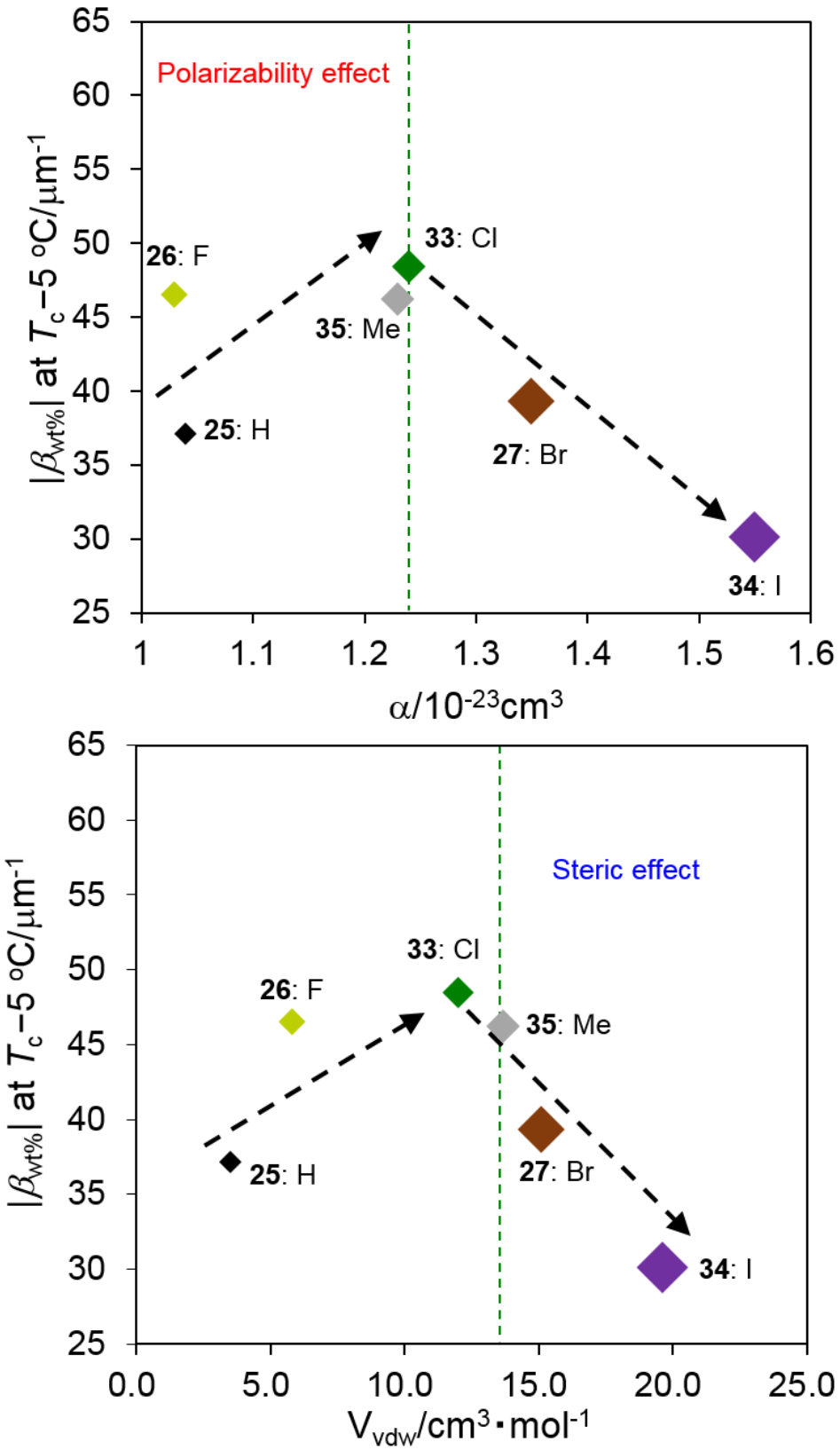

Figure 2.12 Plots of the $|\beta_{wt\%}|$ values of **25**–**27** and **33**–**35** in MBBA vs. the α and V_{vdw} of their substituents.

Three trends were found to stand out in the Figures 2.11–2.12. First, as the substituents parameters α and V_{vdw} increased from their values of non-substituents (**25**: X = H) to chlorine substituents (**33**: X = Cl), the $|\beta_{wt\%}|$ values tended to increase; however, upon a further increase in the substituent parameters α and V_{vdw} to the values of bromine substituents (**27**: X = Br) and iodo substituents (**35**: X = I), the $|\beta_{wt\%}|$ values decreased. Second, the overall values of **25**–**27** and **33**–**35** in JC-1041XX were larger than those in the MBBA. Third, comparing the $|\beta_{wt\%}|$ values of the two host nematics, it was found that the maximum values were for **35** in JC-1041XX in Figure 2.11 and for **33** in MBBA in Figure 2.12, meaning that the substituents with the highest value was swapped in these two NLCs. In order to understand the causes of those three tendencies, the material parameters affecting the HTPs had to be taken into account. According to Ref. 23, the theoretical HTP equation is expressed as follows:

$$\beta = RT\xi Q / 2\pi K_{22} v_m \tag{2.3}$$

where R is the gas constant, T is the temperature, ξ is the orienting strength, which is proportional to the order parameter of the nematic solvent and inversely proportional to temperature,[24] K_{22} is the twist elastic constant of the host nematic solvent, v_m is the molar volume of the solution and Q is the chirality order parameter, which is a scalar quantity of a helicity tensor ($\boldsymbol{Q}_{ii}$), based on molecular helix and an ordering matrix ($\boldsymbol{S}_{ii}$) of the solute.

This theoretical model, the so-called surface chirality model, is derived from (i) a continuous representation of the twist distortions of the nematic solvent and (ii) a representation of the solute interactions with a type of anchoring energy in the nematic solvents with macroscopic surface.[25] The main chiral intermolecular interaction focused in this study is included in the chirality order parameter Q. A theoretical HTP value and the parameter Q for the binaphthyl-type chiral dopants strongly depend on the dihedral angles (θ) between their two naphthyl planes.[25, 26] When a bridged binaphthyl derivative

forms a *cisoid* conformation ($0° < \theta < 90°$), the theoretical HTP should show a maximum value at $\theta = 45°$ (Q is the maximum). By contrast, the helical twisting ability of chiral dopants disappears when θ is 0° and 90° ($Q \approx 0$). In my study, since the dihedral angles of the chiral dopants are almost equivalent to the theoretical DFT calculations as mentioned above, the differences in the observed HTP values for different chiral dopants dissolved in the same nematic LC should be attributed to the influence of the substituents. When comparing the HTP data in different nematic solvent, such as in Figures 2.11–2.12, the HTP should be normalised by the material parameters depending on the kind of NLC, such as the order parameter included in ξ, K_{22} and v_m. In the data shown in Figures 2.11–2.12, the measurements were performed at a low temperature, T_c−5°C, and the effect of the order parameter of the host nematics was small. The influence of v_m would also be negligible in this study because the dimensions of the JC-1041XX and MBBA molecules are comparable. However, there is a significant difference in K_{22} between the two LCs, 8.3[27] and 4.2[28] pN for JC-1041XX and MBBA, respectively. Therefore, a normalised |HTP| was calculated, using K_{22}, termed $|HTP|K_{22}$. The values of $|HTP|K_{22}$ are summarised in Table 2.3.

Table 2.3 The values of $|HTP|K_{22}$ for **25**–**27** and **33**–**35** at T_c−5°C in JC-1041XX and MBBA

Entry	X	$\lvert HTP\rvert K_{22}/10^{-9}\mu m^{-1}\cdot N$	
		JC-1041XX	MBBA
25	H	4.1	1.6
26	F	4.3	2.0
33	Cl	4.7	2.0
27	Br	3.7	1.7
34	I	2.9	1.3
35	Me	5.1	1.9

The values of $|HTP|\cdot K_{22}$ for **25**–**27** and **33**–**35** in JC-1041XX were approximately twice as large as the values in MBBA. Therefore, it is an intrinsic property that the HTPs of **25**–**27** and **33**–**35** in JC-1041XX are larger than those in the MBBA, as mentioned in trend 2 above.

The possible intermolecular interactions for the three tendencies, observed in Figures 2.11–2.12 should be discussed. First, the substituents parameters, α and V_{vdw}, dependences of the $|\beta_{wt\%}|$ values showed a maximum of around 1.2×10^{-23}cm^3 for the polarisability parameter and 13–14 cm$^3\cdot$mol^{-1} for the steric parameter in both JC-1041XX and MBBA. We assume that the steric volume and polarisability effects of the substituents are involved in this phenomenon. Since both the chiral solute and the host LC solvent have phenyl or naphthyl groups, the arene-arene interaction[29] should be a dominant intermolecular interaction that could regulate the alignment of the molecular axes, by which the twisted molecular alignment of the LC molecules is induced. The intermolecular interactions are mainly governed by a van der Waals interaction in which the polarisability and/or a dipole moment is involved. This means that the interaction should be stronger if a molecule possesses a larger polarisability and/or dipole moment. If the 6,6' positions of **25** are replaced by the small-sized halogens, F and Cl, the polarisability and/or the dipole moment of the chiral dopant would be increased. This was seen in the data, where the induced $|\beta_{wt\%}|$ values of the chiral dopants possessing smaller substituents increased from non-substituents (**25**: X = H) to chlorine (**33**: X = Cl) groups. The substituents steric hindrance should have an influence on the intermolecular interaction between the chiral dopants and the host NLC molecules since the arene-arene interactions between them are short-range. Hence, it is reasonable that the weakened intermolecular interactions lead to decrease in the $|\beta_{wt\%}|$ values for chiral dopants with large substituents (**Figure 2.13**). Furthermore, similar results had been already reported with biphenyl[21] and 1,2-diphenylethane-1,2-diol.[30] These studies suggested that lower steric hindrance in the substituents on the phenyl ring plays an important role in inducing

a larger HTP value because of the presence of arene-arene interactions between the chiral dopants and the host NLC molecules.

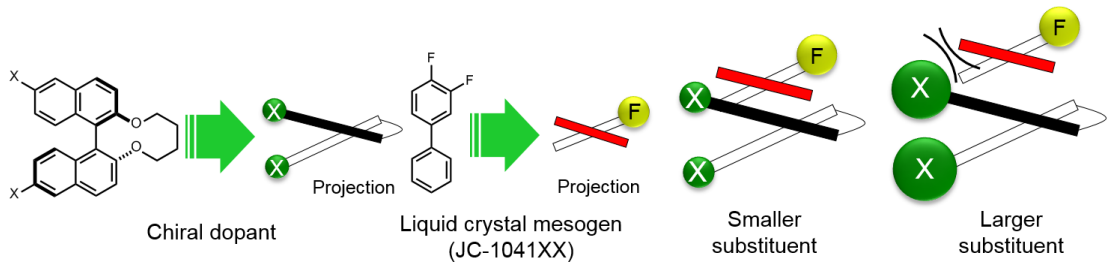

Figure 2.13 Schematic representation of the steric effect of the substituents on arene-arene interactions between the chiral dopant and host NLCs, JC-1041XX's mesogen core.

Second, it is important to discuss that the $|\beta_{wt\%}|$ values of **25**–**27** and **33**–**35** are larger in the JC-1041XX (**Figure 2.11**) than in the MBBA (**Figure 2.12**). The mesogen core of JC-1041XX is biphenyl cyclohexane (**Figure 2.14b**); by contrast, the mesogen core of MBBA is azomethine (**Figure 2.14c**). The length of the aromatic unit at the core of JC-1041XX corresponds to the surface of a bridged binaphthyl-type chiral dopant (**Figure 2.14a**), particularly in comparison with the core of the MBBA. JC-1041XX, which has a higher molecular structural similarity to its dopant than MBBA, should interact well with the chiral dopants. This is seen in the larger $|\beta_{wt\%}|$ values for **25**–**27** and **33**–**35** in JC-1041XX than that for in the MBBA. Gottarelli *et al.* proposed the model for the solute-solvent interaction between the bridged binaphthyl-type chiral solute and the host NLC solvent in 1983 (**Figure 2.14d**). The model indicates that the structural similarity between the chiral solutes and the host NLC solvents leads to a larger HTP value. The HTP values for bridged binaphthyl-type chiral dopants tend to be larger in the biphenyl-type NLC, such as 5CB and E7, than that in the MBBA, because both the dopant and the NLC have a biphenyl core.[30] Therefore, it is reasonable that such a strong intermolecular interaction between chiral dopants and host NLC molecules contribute to chiral transfer.

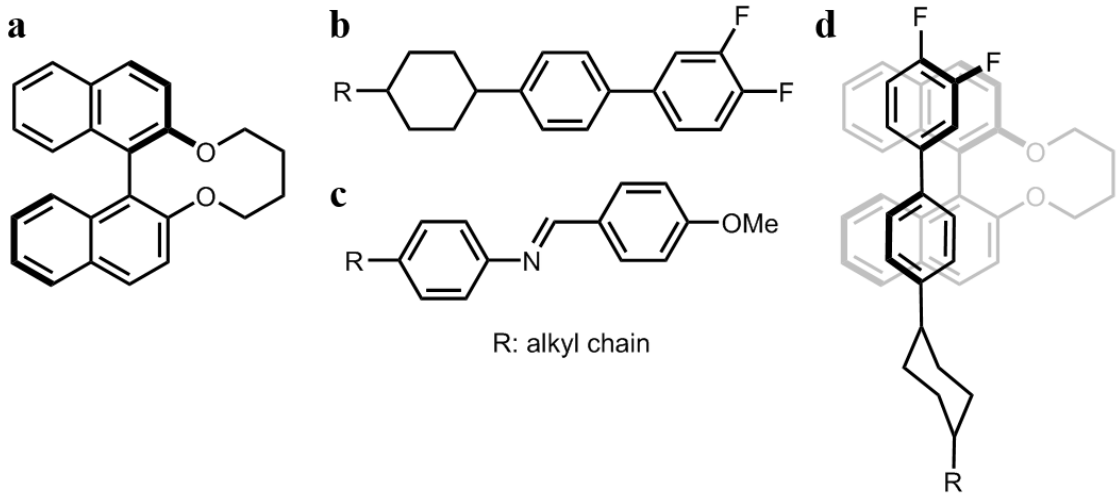

Figure 2.14 The chemical structure of (a) a bridged, binaphthyl-type chiral dopant and the mesogenic chemical structures of (b) JC-1041XX and (c) MBBA. (d) The model for the solute-solvent interaction between a and b.

Third, the relationship between the $|\beta_{wt\%}|$ values for **33** (X = Cl) and **35** (X = Me) was reversed between JC-1041XX (**Figure 2.11**) and MBBA (**Figure 2.12**). The steric and polarisability parameters (V_{vdw} and α) are almost similar between **33** and **35**. Conversely, the signs of the Hammett constant at the para position, σ_p, of **33** and **35** are the opposite, i.e., positive for **33** and negative for **35**. This means that the electron of the aromatic ring is withdrawn by the Cl substituent for **33** and donated by the Me substituent for **35**. JC-1041XX and MBBA bear one part of an electron withdrawing and donating aromatic ring, respectively. The electronic states of the aromatic rings of **33** and JC-1041XX are electron rich and electron deficient, respectively. In contrast, those of **35** and MBBA are electron deficient and electron rich, respectively. The combination of the electron-rich and -deficient aromatic rings can lead to favourable arene-arene interactions (**Figure 2.15**).[31] Additionally, the strong solute-solvent molecular interaction between the chiral dopants and the nematic solvents is known to enhance the HTP value.[32] This explains why the

$|\beta_{wt\%}|$ values were maximised for **35** in JC-1041XX (**Figure 2.11**) and **33** in MBBA (**Figure 2.12**).

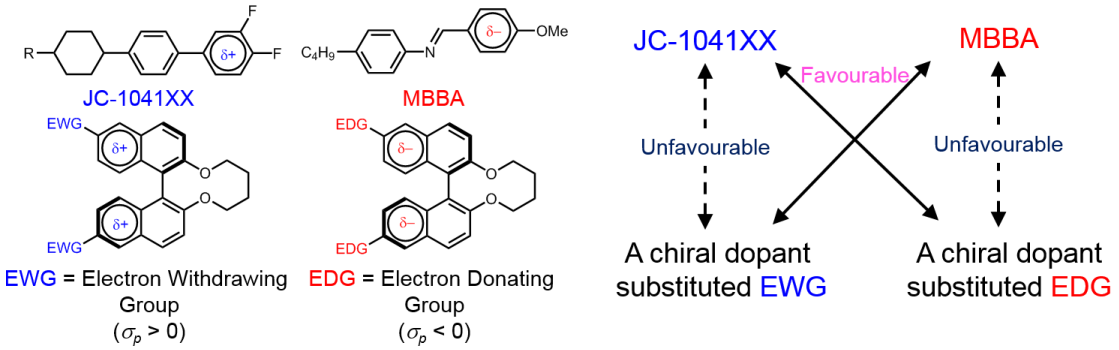

Figure 2.15 The electrostatic arene-arene interactions between the binaphthyl-type chiral dopants and host NLC molecules.

2.2.3 – Substituents Effects on Temperature Dependence of Helical Twisting Powers

Unlike pure cholesterol materials, the pitch of induced N* doped with **25**–**27** and **33**–**35** increases as a function of temperature, i.e., the $|\beta_{wt\%}|$ values decrease with increase in the temperature. The $HTP_{t.d.}$ was defined as below:

$$HTP_{t.d.} = (\Delta HTP / \overline{HTP}) / \Delta T \times 100 \quad (2.4)$$

where ΔHTP is the difference between the maximum and minimum $|\beta_{wt\%}|$ values, and $\overline{HTP}$ is the arithmetic mean of the $|\beta_{wt\%}|$ values in the temperature range from $T - T_c$ = −5 to 25°C.[15, 33] The index indicates the percentage change in the $|\beta_{wt\%}|$ values per 1°C.[15, 33] The $HTP_{t.d.}$ values for **25**–**27** and **33**–**35** and their substituents parameters are shown in Table 2.4.

Table 2.4 The $HTP_{t.d.}$ values for **25**–**27** and **33**–**35** in JC-1041XX and MBBA and their substituents parameters

Entry	X	$HTP_{t.d.}/\%\cdot T^{-1}$		Substituent parameters		
		JC-1041XX	MBBA	$V_{vdw}/cm\cdot mol^{-1}$	σ_p	$\alpha/10^{-23}cm^3$
25	H	0.46	0.49	3.5	0	1.04
26	F	0.43	0.73	5.8	0.06	1.03
33	Cl	0.59	0.85	12.0	0.24	1.24
27	Br	0.60	0.87	15.1	0.27	1.35
34	I	0.69	0.87	19.6	0.30	1.55
35	Me	0.64	0.82	13.7	−0.13	1.23

The $HTP_{t.d.}$ values for **25**–**27** and **33**–**35** in JC-1041XX and MBBA are plotted against their steric (V_{vdw}) and polarisability (α) substituent parameters in Figures 2.16–2.17 to evaluate the effect of the substituents on their subsequent $HTP_{t.d.}$ values.

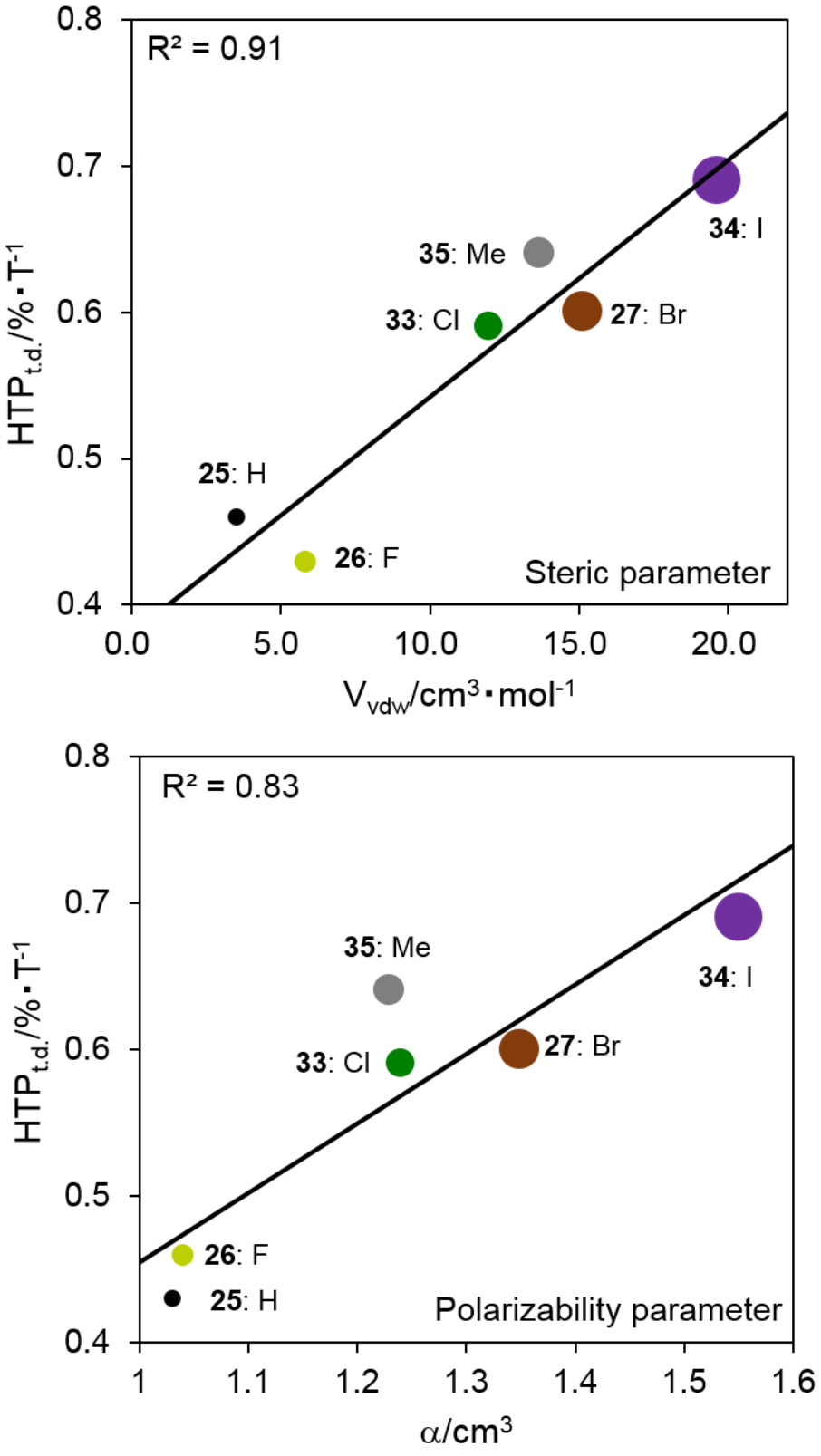

Figure 2.16 Plots of the $HTP_{t.d.}$ values for **25**–**27** and **33**–**35** against the V_{vdw} and α of their substituents in JC-1041XX. R^2 denotes the correlation coefficient.

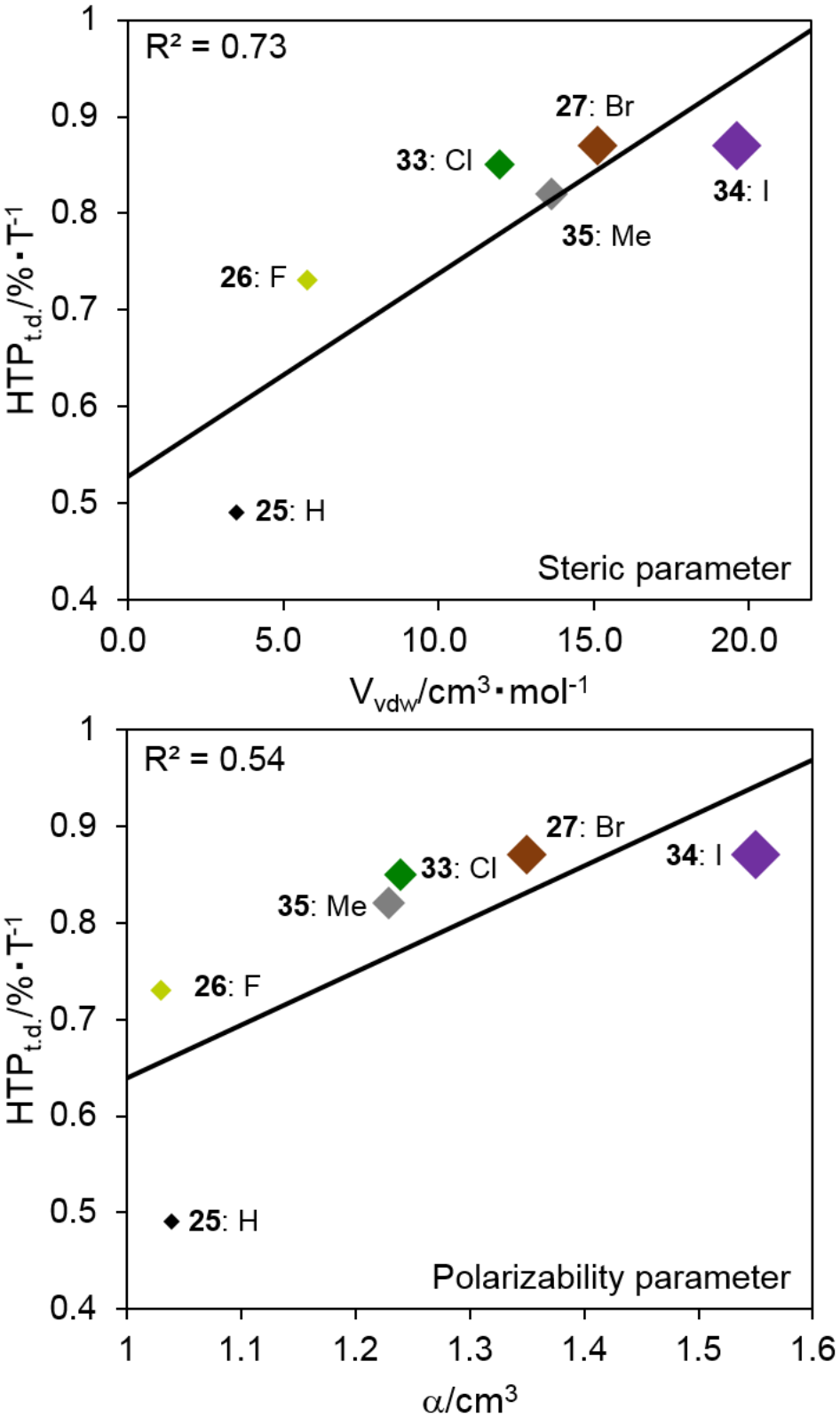

Figure 2.17 Plots of the $HTP_{t.d.}$ values for **25**–**27** and **33**–**35** against the V_{vdw} and α of their substituents in MBBA. R^2 denotes the correlation coefficient.

As shown in Figures 2.16–2.17, the $HTP_{t.d.}$ values increased with increasing V_{vdw} and α. This trend was especially clear in JC-1041XX, more so than in MBBA. In addition, the $HTP_{t.d.}$ values in MBBA were larger than those in JC-1041XX. When the host NLC was JC-1041XX, the correlation coefficients (R^2) for the steric and polarisability parameters were 0.91 and 0.83, respectively. Those same in parameters had correlations of 0.73 and 0.54, respectively, in MBBA. From these results, it is clear that the $HTP_{t.d.}$ values and R^2 values in JC-1041XX were better than those in MBBA. It is appropriate that molecular structural similarity of a solute-solvent interaction between a bridged chiral solute and host nematic solvent can affect the $HTP_{t.d.}$ and R^2 values. It is assumed that the structural similarity between the chiral solutes and MBBA might cause the resultant LCs to thermally disintegrate faster than in JC-1041XX.

In comparison with the $HTP_{t.d.}$ values in the two host nematics with their steric and polarisability substituents parameters, it became clear that the $HTP_{t.d.}$ values correlated well with their substituents parameters. Our understanding is that a van der Waals interaction involving polarisability can impact the $HTP_{t.d.}$ values of the smaller substituents of synthesised chiral dopants, such as **25** (X = H), **26** (X = F), **33** (X = Cl) and **35** (X = Me), because these $HTP_{t.d.}$ values gradually increase as their polarisability increased. Moreover, the steric substituent effects of the relevant chiral dopants on $HTP_{t.d.}$ values were observed; chiral dopants possessing a larger substituent, such as the bromo (**27**) and iodo (**34**) groups, promoted a disaggregation of the arene-arene interactions between these chiral dopants and the host NLC molecules. This could be because the steric hindrance between them should affect their short-range interactions. This effect should be reflected the $HTP_{t.d.}$ values of **27** (X = Br) and **34** (X = I), since these values were comparatively larger than those of **25** (X = H), **26** (X = F), **33** (X = Cl) and **35** (X = Me) in the two host NLCs. Therefore, the 6,6’ substituents of synthesised chiral dopants also affect their $HTP_{t.d.}$ values.

2.3 – Conclusions

Systematic studies of the 6,6'-substituted bridged binaphthyl-type chiral dopants suggested that the induced $|\beta_{wt\%}|$ and $HTP_{t.d.}$ values were significantly dependent on the arene-arene interactions between the chiral dopants and the host nematic NLCs. Furthermore, their interactions were affected by the steric hindrance, aromatic ring polarity, and polarisability of the substituents. The bridged binaphthyl-type chiral dopant with the least steric hindrance and a largest substituent polarisability, the 6,6'-chlorinated chiral dopant, exhibited large $|\beta_{wt\%}|$ values in both host NLCs since the chlorine group has an adequate substituent volume and large polarisability that contribute to a strong arene-arene interaction between the dopants and the host NLC molecules. Moreover, the aromatic polarity of the chiral dopants and host NLCs exerted a beneficial impact on the induced $|\beta_{wt\%}|$ values to give a strong electrostatic arene-arene interaction between them. In $HTP_{t.d.}$ investigations, the $HTP_{t.d.}$ values depended upon the structural similarity of a solute-solvent interaction between the chiral solutes and host nematic solvents. Structural similarity between the synthesised chiral dopants and biphenyl cyclohexane type NLC, JC-1041XX, lead to smaller $HTP_{t.d.}$ values, indicating a better thermal property for a chiral dopant. By contrast, the values between the chiral dopants and azomethine-type NLC, MBBA, exhibited larger $HTP_{t.d.}$ values, meaning they displayed a lesser stability towards heat. Furthermore, the $HTP_{t.d.}$ values were affected by the steric and polarisability substituent parameters since the $HTP_{t.d.}$ values in the two host NLCs had a good correlation with their substituent parameters. My understanding is that when a substituent polarisability is larger, which is relevant for a van der Waals interaction between the chiral dopants and the NLC molecules, the $HTP_{t.d.}$ values for the smaller substituents increase. In the case of larger substituents, such as bromo and iodo groups, the $HTP_{t.d.}$ values are considerably larger because of a disaggregation of the arene-arene interactions between these chiral dopants and the host NLCs via steric hindrance.

2.4 – References and Notes

1. I. Dierking, *Symmetry* **2014**, *6*, 444.
2. G. Solladié, R. G. Zimmermann, *Angew. Chem. Int. Ed. Engl.* **1984**, *23*, 348.
3. D. C. Wright, N. D. Mermin, *Rev. Mod. Phys.* **1989**, *61*, 385.
4. H. Kikuchi, M. Yokota, Y. Hisakado, H. Yang, T. Kajiyama, *Nat. Mater.* **2002**, *1*, 64.
5. S. Shibayama, H. Higuchi, Y. Okumura, H. Kikuchi, *Adv. Funct. Mater.* **2013**, *23*, 2387.
6. H. K. Bisoyi, Q. Li, *Acc. Chem. Res.* **2014**, *47*, 3184.
7. Y. Hisakado, H. Kikuchi, T. Nagamura, T. Kajiyama, *Adv. Mater.* **2005**, *17*, 96.
8. S. Yabu, H. Yoshida, G. Lim, K. Kaneko, Y. Okumura, N. Uehara, H. Kikuchi, M. Ozaki, *Opt. Mater. Expr.* **2011**, *1*, 1577.
9. H. Choi, H. Higuchi, H. Kikuchi, *Soft Matter* **2011**, *7*, 4252.
10. Y. Hirakata, D. Kubota, A. Yamashita, H. Miyake, M. Hayakawa, J. Koyama, S. Yamazaki, K. Okazaki, R. Sato, T. Cho, K. Tochibayashi, M. Sakakura, *SID'11 Digest*, **2011**, *42*, 32.
11. J. Chen, C.T. Liu, *IEEE Access* **2013** *1*, 150.
12. M. Ozaki, Y. Matsuhisa, H. Yoshida, R. Ozaki, A. Fujii, *Phys. Stat. Sol. (a)* **2007**, *204*, 3777.
13. W. Cao, A. Muñoz, P. Palffy-Muhoray, B. Taheri, *Nat. Mater.* **2002**, *1*, 111−113.
14. S. Yokoyama, S. Mashiko, H. Higuchi, K. Uchida, T. Nagamura, *Adv. Mater.* **2006**, *18*, 48.
15. K. Kakisaka, H. Higuchi, Y. Okumura, H. Kikuchi, *Chem. Lett.* **2014**, 43, 624.
16. K. Kakisaka, H. Higuchi, Y. Okumura, H. Kikuchi, *J. Mater. Chem. C* **2014**, *2*, 6467.
17. I attempted to measure the crystal structure of **34**. However, this crystal structure could not be determined due to its amorphous crystal.
18. G. Proni, G. P. Spada, *J. Org. Chem.* **2000**, *65*, 5522.
19. A. Bondi, *J. Phys. Chem.* **1964**, *68*, 441.
20. P. R. Wells, *Chem. Rev.* **1963**, *63*, 171.
21. V. E. Williams, R. P. Lemieux, *Chem. Commun.* **1996**, 2259.
22. *Lange's handbooks of chemistry 15th edn.*, ed. by J. A. Dean, John McGraw-Hill, New York, **1999**.

23. A. Ferrarini, S. Pieraccini, S. Masiero, G. P. Spada, *Beillstein J. Org. Chem*. **2009**, *5*, 50.

24. A. Ferrarini, G. J. Moro, P. L. Nordio, *Mol. Phys*. **1996**, *87*, 485.

25. A. Ferrarini, G. J. Moro, P. L. Nordio, *Phys. Rev. E* **1996**, *53*, 681.

26. A. Ferrarini, P. L. Nordio, P. V. Shibaev, V. P. Shibaev, *Liq. Cryst*. **1998**, *24*, 219.

27. The K_{22} of JC-1041XX was provided by JNC Co.

28. A. Krekhov, W. Pesch, *Phys. Rev. E*, **2011**, *83*, 051706-1.

29. C. A. Hunter, K. R. Lawson, J. Perkins, C. J. Urch, *J. Chem. Soc. Perkin Trans*. 2 **2001**, 651.

30. G. Gottarelli, M. Hobert, B. Samori, G. Solladié, G. P. Spada, R. Zimmermann, *J. Am. Chem. Soc*. **1983**, *105*, 7318.

31. F. Cozzi, M. Cinquini, R. Annunziata, T. Dwyer, J. S. Siegel, *J. Am. Chem. Soc*. **1992**, *144*, 5729.

32. S. Pieraccini, A. Ferrarini, K. Fuji, G. P. Spada, *Chirality*, **2008**, *20*, 749.

33. H. Nishikawa, D. Mochizuki, H. Higuchi, Y. Okumura, H. Kikuchi, *ChemistryOpen* **2017**, *6*, 710.

Chapter 3
Effects of Linker Flexibility on the Dopant-induced Chiral Nematic Phase

3.1 − Introduction

A chiral nematic liquid crystals (N*LCs) behaves as thermochromic liquid crystals, since selective reflections of N*LCs are changed by thermal changes.[1–3] The helical structure of N*LCs possesses ability to selectively reflect circularly polarised light with wavelength equal to its pitch length, in incident light. The pitch length in the helical structure depends upon temperature variation, and therefore the wavelength of selectively reflected light also depends on the temperature variation. N*LCs have potential applications as thermal indicators in medical thermography[4] and microfluidic devices[5] due to their thermal-optical properties. Thus, a greater understanding of chiral dopants' helical twisting properties should lead to application of dopant-induced N*LCs to thermal indicators.

Thus far, much effort was devoted to revealing a relationship between chemical structures of the linker at the 2,2' position in binapthyl-type chiral dopants and their thermal properties of helical twisting power (HTP) values.[6–8] It has been considered that temperature dependences of HTP ($HTP_{t.d.}$) values are caused by thermal vibrations of the dihedral angle of two naphthyl plains, since the alkyl bridged binapthyl-type chiral dopant (**25**) exhibited smaller $HTP_{t.d.}$ value than that of unbridged one (**30**).[7] However, a critical mechanism of a correlation between their linker structures and $HTP_{t.d.}$ values remains unclear. If the mechanism is to be disclosed in molecular level, a binaphthyl-type chiral dopant, possessing specified HTP and $HTP_{t.d.}$ values will be developed by a combination with the 6,6' substituents effects.

Here, I attempted to reveal the effect of linker flexibility of the alkyl (**25**) and alkynyl (**36**) bridged and unbridged (**30**) binaphthyl-type chiral dopants (**Figure 3.1**) on their induced HTP and $HTP_{t.d.}$ values in the mixture of JC-1041XX/5CB (= 1/1 wt/wt%, **Figure 3.2**) as the host NLC. Linker flexibility of the dihedral angle is regularly **30**, **25** and **36**, respectively (**Figure 3.1**). The CH···π interaction in host NLC molecules and acetylene moiety of **36** might affect the HTP value for **36**. Moreover, the variation in

the dihedral angle of the synthesised chiral dopants have an impact on the $HTP_{t.d.}$ value based on the theoretical studies for the chiral dopants.

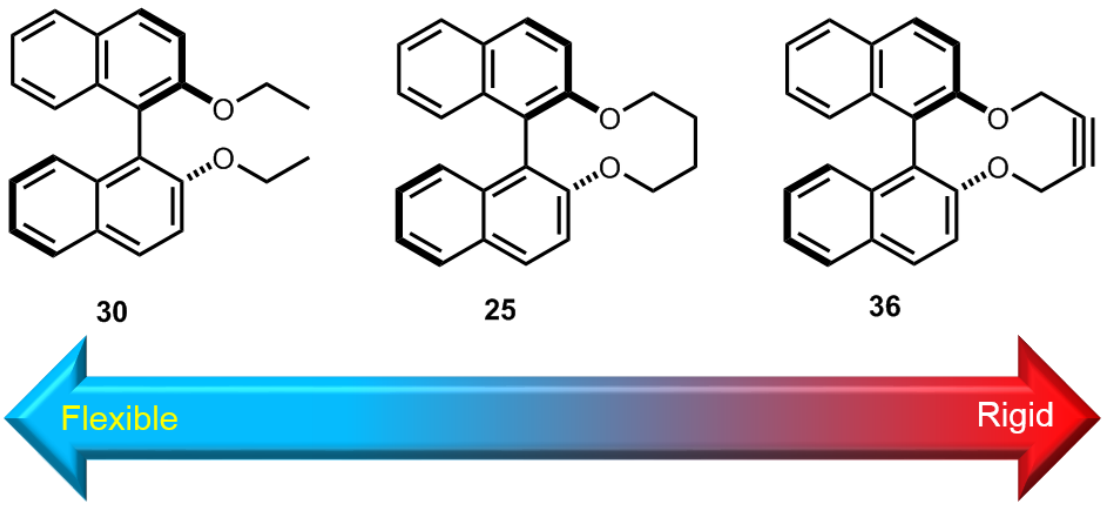

Figure 3.1 The flexibility of the dihedral angle of **25**, **30** and **36**.

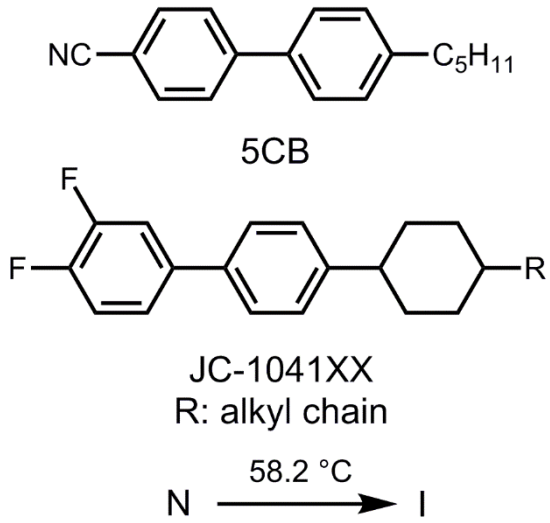

Figure 3.2 The chemical structures and phase transition temperatures of the host NLC. N and I denote the namatic and isotropic phases, respectively.

3.2 – Effects of Linker Flexibility of Binaphthyl-type Chiral Dopants on Induced Helical Twisting Powers

3.2.1 – Effects of Linker Flexibility on Dihedral Angle of Synthesised Binaphthyl-type Chiral Dopants

Consider the theoretical and crystal conformations of the binapthyl derivatives **25**, **30** and **36** into *cisoid* ($0° < \theta < 90°$) and *transiod* ($90° < \theta < 180°$) conformations. The dihedral angle θ of **36** was calculated, using DFT under the conditions, described in *Chapter 4*, **4.1**. The optimised structure of **36** is represented in the Figure 3.3b. The potential energy vs. the dihedral angle of **30** was scanned to explore its optimised structure from $\theta = -45°$ to $-135°$, since the dihedral angle of **30** can rotate more freely than that of bridged binaphathyl-type chiral dopants. From the results of DFT calculations, the most stable dihedral angles (θ, C8-C1-C1′-C8′, see **Figure 3.3**) of **25** and **36** were obtained to be $-67.7°$ and $-103.5°$, respectively (**Figure 3.3**). The theoretical conformations of **25** and **36**, thus, were the *cisoid* and *transoid* conformations, respectively. By scanning the dihedral angle of **30** in DFT calculations, its optimised angle θ(C8a-C1-C1'-C8a')[9] was $-95°$ (**Figure 3.4** and **Table 3.1**).

Table 3.1 The dihedral angle (C8a-C1-C1'-C8a') of **30** vs. potential energy

	Dihedral angle/°	Potential energy[10]/Hartree
	−45	−1078.257482
	−50	−1078.259736
	−55	−1078.261533
	−60	−1078.262933
	−65	−1078.263926
	−70	−1078.264568
	−75	−1078.264975
	−80	−1078.265218
	−85	−1078.265316
30	−90	−1078.265381
	−95	−1078.265417
	−100	−1078.265334
	−105	−1078.265223
	−110	−1078.265018
	−115	−1078.264567
	−120	−1078.263809
	−125	−1078.262718
	−130	−1078.261261
	−135	−1078.259369

The potential curve of **30** was asymmetric, since the unfavourable π-π electrostatic repulsion between two naphthyl plains would exist from $\theta = -90°$ to −45°. Therefore, the conformation of **30** can be more stable from $\theta = -90°$ to −135° than that from $\theta = -90°$ to −45°. Moreover, the crystal structure of **30** and **36** was successful determined (**Figures 3.5**–**3.6**). The dihedral angle θ (C8-C1-C1′-C8′) of **25**, **30** and **36** in their

crystal structures was finalised in the Table 3.2.

Table 3.2 The dihedral angle θ of **25**, **30** and **36** in their crystal structures.

	25[11]	**30**	**36**
Dihedral angle/°	−67.3	−113.2	−102.0
	−75.7		−105.3
			−108.0

The dihedral angle θ (C8-C1-C1′-C8′) of **30** and **36** was more than 90° in their crystals. By contrast, that of **25** was less than 90° in its crystal. Therefore, the conformation of **30** and **36** corresponded to the *transoid* conformation in their crystal due to $\theta > 90°$. That of **25** corresponded to the *cisoid* conformation in its crystal.

By using the contact method, the helical sense of the induced N* phase by **25**, **30** and **36** was confirmed in the mixture of JC-1041XX and 5CB in the Figure 3.7. The N* phase, doped with **30** and **36** displayed the right-helical sense. On the other hand, **25** had a potential of induction of left-handed in the induced N* phase. Hence, the conformation of **30** and **36** adopt the *transoid* conformation in the host nematics. That of **25** also was the *cisoid* conformation in the host NLC. These experimental results were in agreement with their theoretical and crystal conformations. It should be interestingly noted that the chemical structure of **36** included the strained alkyne in its bridged carbon chain from the evidence of its optimised and crystal structure (**Figures 3.3c** and **3.6**). Thermal stability of **36** have been discussed thought the ^{1}H-NMR spectroscopic study for it in **3.2.2**.

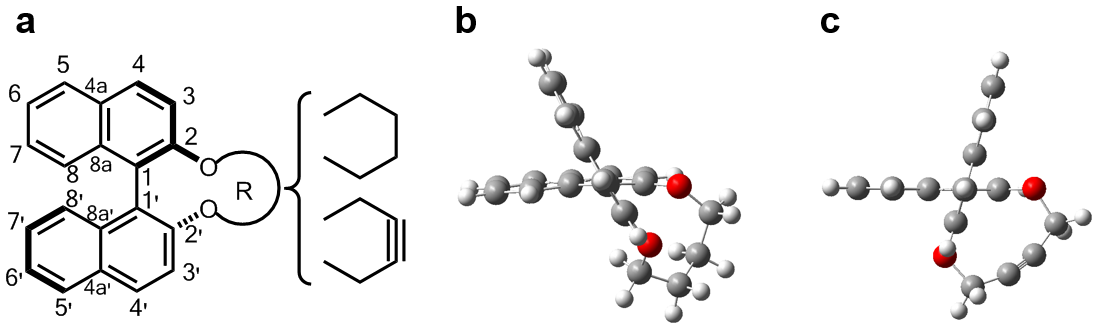

Figure 3.3 (a) The chemical structure of **25** and **36** and the optimised structures of (b) **25** and (c) **36**.

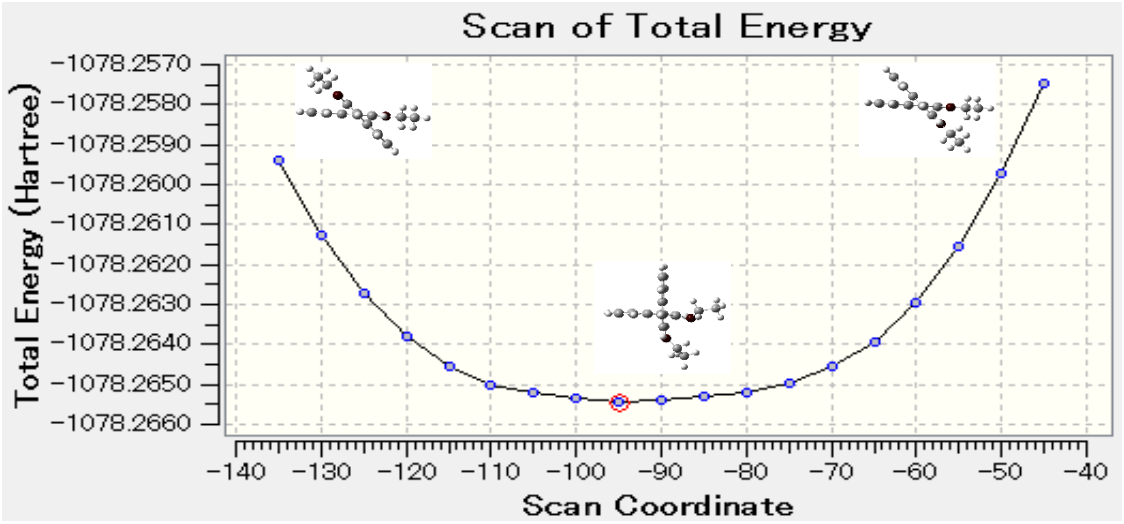

Figure 3.4 Plots of calculated potential energy vs. the dihedral angle (C8a-C1-C1′-C8a′) for **30**.

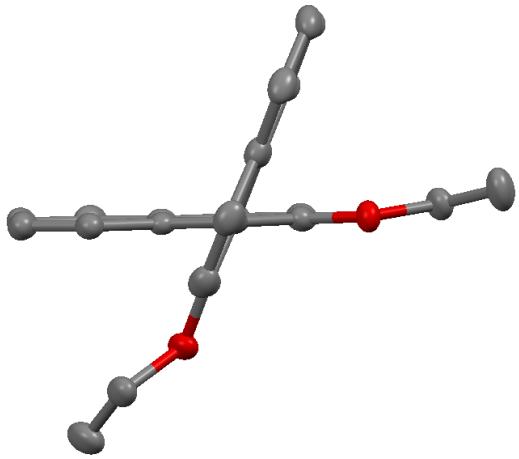

Figure 3.5 The crystal structure of **30** at 123 K. Hydrogen atoms have been omitted for clarity. Thermal ellipsoids are displayed at the 50% probability level.

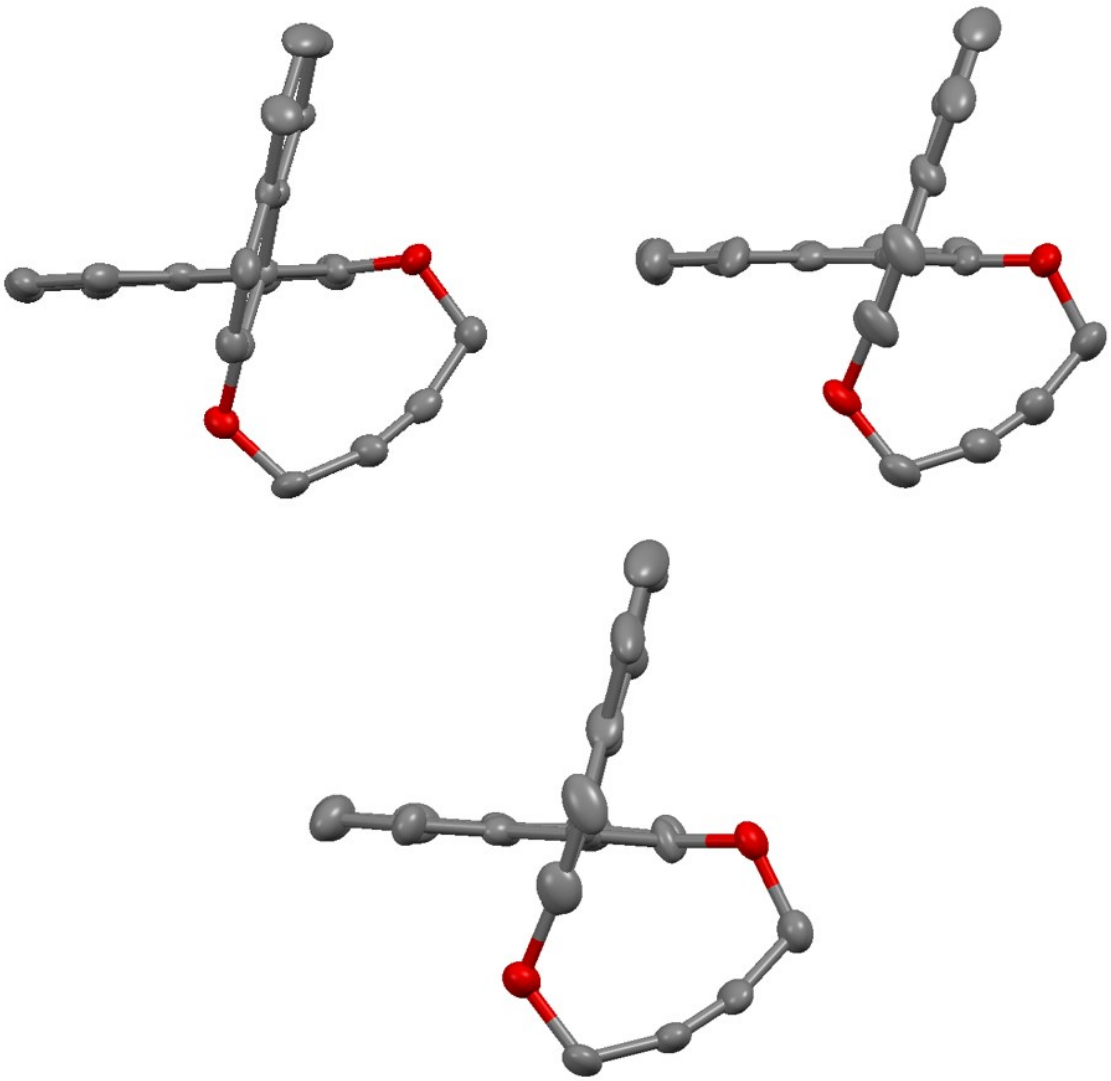

Figure 3.6 The crystal structure of **36** at 123 K. Hydrogen atoms have been omitted for clarity. Thermal ellipsoids are displayed at the 50% probability level.

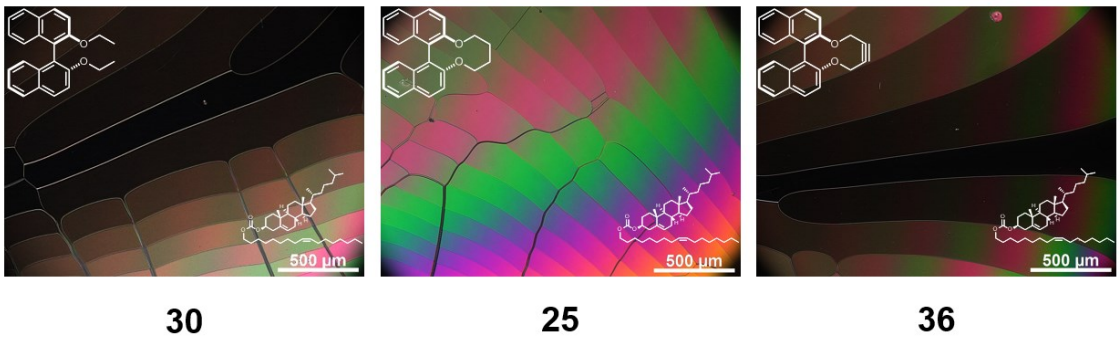

Figure 3.7 Optical textures of the 1.0wt% sample, doped with **30** and 0.2wt% samples, doped with **25** and **36** in the mixture of JC-1041XX/5CB as the host NLC.

3.2.2 – ^{1}H-NMR Spectroscopic Study for the Strained Alkynyl Bridged Binaphthyl-type Chiral Dopants

36 was linked the strained alkyne at the 2,2' positions of the synthesised binaphthyl derivative (**Figures 3.3c** and **3.6**). Strained alkynes are known to have high reactivity, since they possess high strain-energy.[12] Strained alkynes, therefore, tend to occur thermal decomposition themselves. Thermal stability of **36** was recorded by ^{1}H-NMR spectroscopy with the experimental procedure (see *Chapter 4*). The ^{1}H-NMR spectra of **36** are shown in the Figure 3.8.

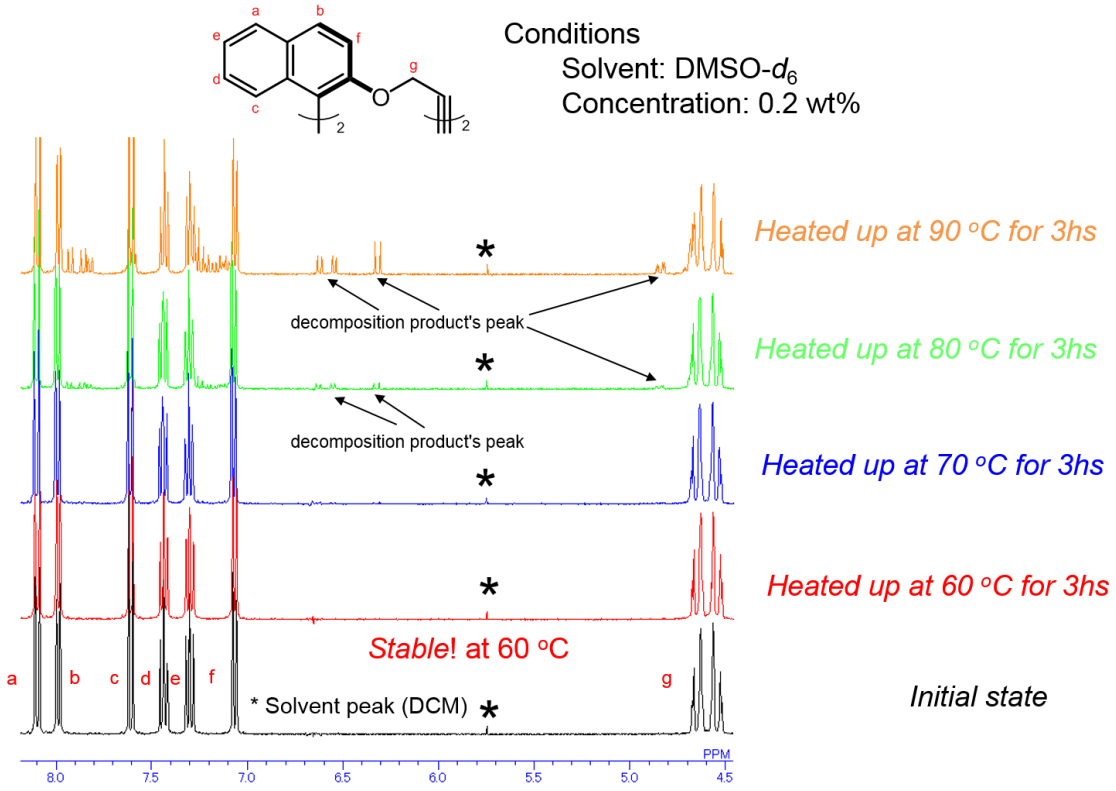

Figure 3.8 The ^{1}H-NMR spectra of **36** as a function of temperature.

It is clearly that there began to decompose **36** itself from 80 °C, since decomposed product's peaks came out around 4.7 and 6.0–6.5 ppm. Hence, **36** was stable at 60 or 70 °C. In order to prevent thermal decomposition of **36**, the host NLCs is suitable to have low T_c (60–70 °C) for measurement of its HTP value. The mixture of JC-1041XX and 5CB was utilised as the host NLC for HTP measurement, since its mixture

possesses adequate T_c (58.4 °C, **Figure 3.2**) and higher solubility for **36** than that of MBBA.

3.2.3 – Effects of Linker flexibility on Temperature Dependence of Helical Twisting Powers

The ability of a chiral dopant to generate a helical structure in a given host NLC is evaluated, using helical twisting power (HTP), as expressed below:

$$\beta_{wt\%} = (pc_w)^{-1} \quad (3.1)$$

where p is the helical pitch of the N* phase, and c_w is the concentration of the chiral dopant in weight percentage. Further, The $HTP_{t.d.}$ was defined as below:

$$HTP_{t.d.} = (\Delta HTP / \overline{HTP}) / \Delta T \times 100 \quad (3.2)$$

where ΔHTP is the difference between the maximum and minimum $|\beta_{wt\%}|$ values, and $\overline{HTP}$ is the arithmetic mean of the $|\beta_{wt\%}|$ values in the temperature range from $T - T_c$ = −5 to 25°C. The temperature dependence of the $\beta_{wt\%}$ values of **25**, **30** and **36** is represented in the Figure 3.9.

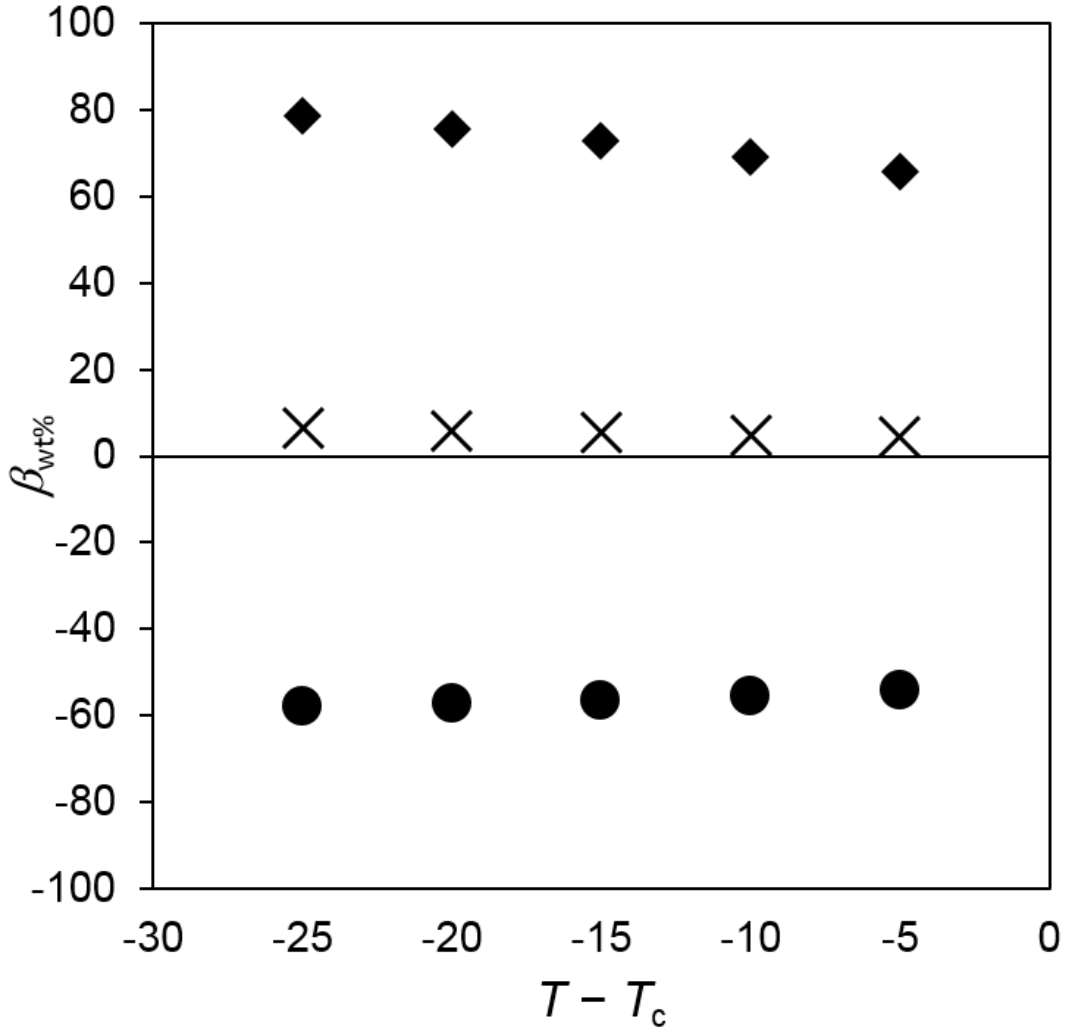

Figure 3.9 The temperature dependence of the $\beta_{wt\%}$ values for **25**, **30** and **36**.

The $\beta_{wt\%}$ at T_c −5 °C and $HTP_{t.d.}$ values, calculated by the equation 2.4, for **25**, **30** and **36** are shown in the Table 2.7.

Table 2.7 The $\beta_{wt\%}$ at T_c−5 °C and $HTP_{t.d.}$ values for **25**, **30** and **36**. The concentration of the chiral dopant was 0.2wt% for **25** and **36**, and 1.0wt% for **30**.

	Linker flexibility	$\beta_{wt\%}$ at T_c−5 °C/μm^{-1}	$HTP_{t.d.}$/%·T^{-1}
30	Flexible	+4.3	1.92
25	Moderate	−54.3	0.33
36	Rigid	+65.8	0.89

Two trends were found as a result of their HTP investigations. First, the N*LC sample, doped with **36** in the host nematics exhibited the highest $\beta_{wt\%}$ value. By contrast, the smallest $\beta_{wt\%}$ value enabled to be found in the sample of **30** in the Figure 3.9. Second, the $HTP_{t.d.}$ value of **36** displayed moderate, although linker flexibility of **36** is rigidity due to the linker, including the strained alkyne.

Consider utilising the surface chirality model for the first trend. The theoretical HTP equation is expressed as follows[13]:

$$\beta = RT\xi Q / 2\pi K_{22} v_m \tag{3.3}$$

where R is the gas constant, T is the temperature, ξ is the orienting strength, which is proportional to the order parameter of the nematic solvent and inversely proportional to temperature,[14] K_{22} is the twist elastic constant of the host nematic solvent, v_m is the molar volume of the solution and Q is the chirality order parameter, which is a scalar quantity of a helicity tensor ($\boldsymbol{Q}_{ii}$), based on molecular helix and an ordering matrix ($\boldsymbol{S}_{ii}$) of the solute. According to the theoretical model, the dihedral angle θ of a binaphthyl-type chiral dopant plays an important role in its induced HTP value. When θ is 45° and 135°, a HTP value reaches to a maximum value, since the chirality parameter Q is also maximum. By contrast, Q leads to approximately 0 at θ = 0°, 90° and 180°, respectively.[15] Moreover, it is difficult for flexible binaphthyl-type chiral dopants, e.g. **30**, to consider Q, since flexible chiral dopants form various conformations in host NLCs due to free rotation of their dihedral angle of two naphthyl plains at C1-C1'. This means that flexible chiral dopants can form both *cisoid* and *transoid* conformations in a NLC by heat and/or arene-arene interactions between chiral dopants and host NLC molecules. Therefore, Q must append the probability of binaphthyl conformers for considering Q of the flexible chiral binaphthyl dopant.[16] Thus, the chirality parameter Q can be rewritten as:

$$Q = \sum_{\chi} p_{\chi} Q_{\chi} \tag{3.4}$$

where χ is the alternative conformations of a flexible binaphthyl-type chiral dopant, p_χ is the probability of its chiral dopant's conformations and Q_χ is the chirality parameter of its chiral dopant's conformations, respectively. According to scanning dihedral angle of **30**, its potential energy was the lowest around $\theta = -95°$ (**Figure 3.4**). Similarly, **30** was crystallised the *transoid* conformation in its crystal (**Figure 3.5**). Further, **30** showed the right-handed helical sense from the evidence of the contact method in the host NLC (**Figure 3.8**). Therefore, the *transoid* conformations of **30** should be energically favour in the host NLC, even after taking account into the arene-arene interactions between chiral dopants and host NLCs. Furthermore, the population of the *transoid* conformation of **30** at $\theta \approx 95°$ might be richer than that of the *cisoid* conformation of **30** in the host nematics, so that the $\beta_{wt\%}$ value of **30** displayed the lowest due to its averaging $Q \approx 0$ (equation 3.4). On the other hand, the bridged binaphathyl-type chiral dopants **25** and **36** exhibited relatively large $\beta_{wt\%}$ values in the host NLC. The $\beta_{wt\%}$ values and dihedral angle θ of **25** and **36** in the gas and crystalline phase are summarised in the Table 2.8.

Table 2.8 The $\beta_{wt\%}$ values and dihedral angle θ of **25** and **36** in the gas and crystalline phase.

	$\beta_{wt\%}/\mu m^{-1}$	θ in gas/°	$\Delta\lvert\theta\rvert$/°	θ in cryst./°	$\Delta\lvert\theta\rvert$/°
25	−54.3	−67.7	22.7	−67.3	22.3
				−75.7	30.7
				−102.0	33.0
36	+65.8	−103.5°	31.5	−105.3	29.7
				−108.0	27.0

where $\Delta|\theta|$ is the absolute value of the variation in the dihedral angle for **25** and **36** against 45° for a *cisoid* conformation and 135° for a *transoid* conformation. The dihedral angle of **25** possessed near 45°, meaning to show maximum Q for a *cisoid*

conformation of a binaphthyl-type chiral dopant, however, its $\beta_{wt\%}$ value was lower than that of **36**. Therefore, it is assumed that a different intermolecular interaction between host NLC molecules and the alkyneyl bridged binaphthyl-type chiral dopant **36** shuold have impact on its HTP value. The possible interaction between them is the CH···π interaction[16–17] between the host NLC molecules' hydrogen atom and π electron cloud of acetylene moiety of **36** (**Figure 3.10**). Therefore, the CH···π interaction between host NLC molecules and the alkynyl moiety of **36** might exert a favourable influence on the HTP value for **36**.

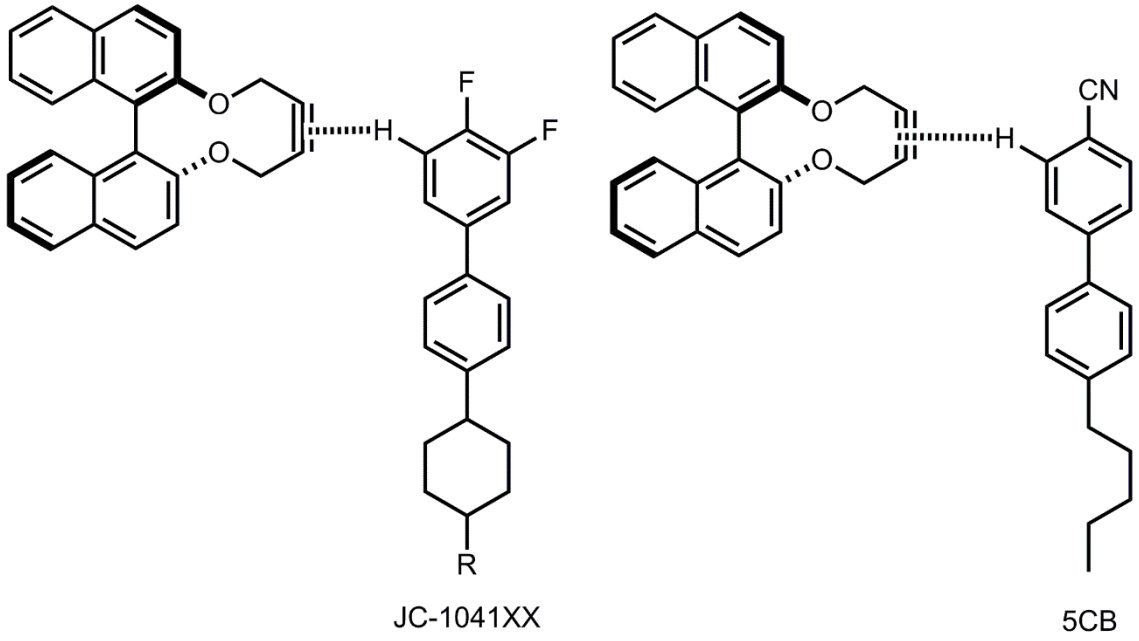

Figure 3.10 The possible interaction model for the CH···π interaction between host NLC molecules and **36**.

The data for next point to be discussed fall in the $HTP_{t.d.}$ values. The $HTP_{t.d.}$ value of **30** observed the largest in the binaphthyl analogues. As mentioned above, **30** formed various kinds of its conformation due to free rotation of its dihedral angle of two binaphthyl plains. Hence, the dihedral angle of **30** can significantly be affected by thermal stimuli. The $HTP_{t.d.}$ value of **30** was, therefore, the largest. The $HTP_{t.d.}$ value of **36** was larger than that of **25**, although **36** was linked the rigid alkynyl linker at the 2,2'

positions. The theoretical IR spectra of **25** and **36** were calculated at 25 °C and 1.0 atom. via B3LYP/6-31G(d) level of DFT (see *Chapter 4*). According to DFT calculation of the theoretical IR spectra for **25** and **36**, vibrations of their dihedral angle theoretically corresponded to 47.3 cm^{-1} for **25** and 34.0 cm^{-1} for **36**, respectively (**Figure 3.11**). Further, the variation in the dihedral angle $\Delta\theta$, caused by their theoretical vibrations was 9.2° for **25** and 13.0° for **36**, respectively.[18] the larger variation in the dihedral angle of **36** is derived from the strong symmetric stretching vibration of the alkyne (**Figure 3.12**). Therefore, the $HTP_{t.d.}$ value of **36** exhibited large, compared with that of **26**, since the strong symmetric stretching vibration of the alkyne for **36** might be vigorous by heat.

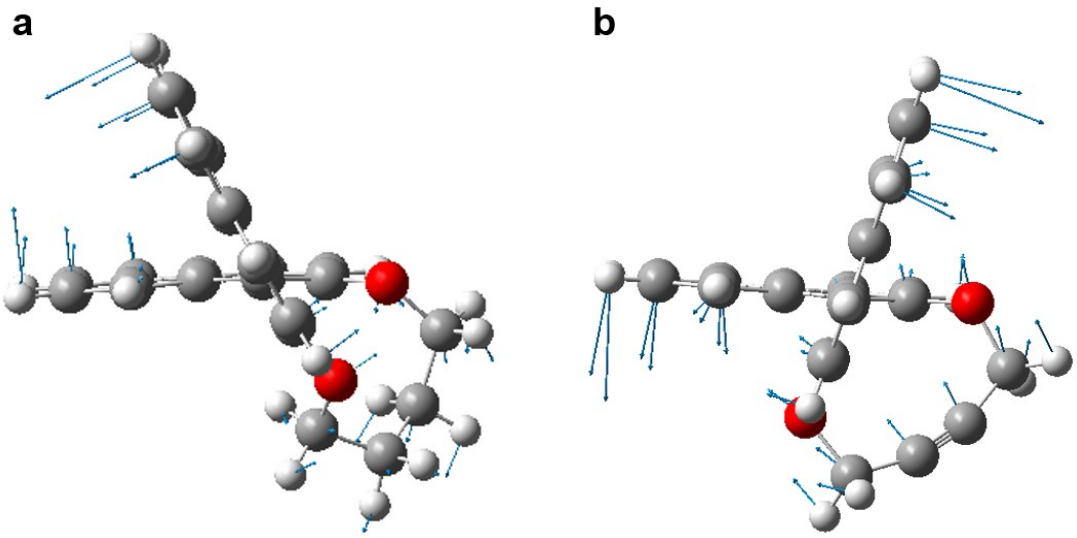

Figure 3.11 The theoretical vibrations of (a) **25** at 47.3 cm^{-1} and (b) **36** at 34.0 cm^{-1}. The vectors denote directions of their atomic vibrations.

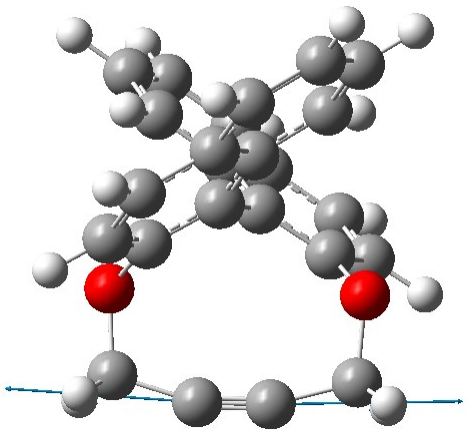

Figure 3.12 The symmetric stretching vibration of the alkynyl moiety in **36**. The vectors denote directions of the carbon atomic vibrations.

3.3 – Conclusions

The effect of linker flexibility of the binaphthyl-type chiral dopants has confirmed that the induced $\beta_{wt\%}$ and $HTP_{t.d.}$ values were significantly affected by the linker structures, such as alkyl, alkynyl bridged and unbridged alkyl chain, at the 2,2' positions. The unbridged chiral dopant did not exhibit excellent helical twisting ability and thermal properties due to its free rotation of two naphthyl plains. By contrast, the alkyl and alkynyl bridged binaphthyl-type chiral dopants possessed better $\beta_{wt\%}$ and $HTP_{t.d.}$ values than that of the unbridged chiral dopant. In particular, the alkynyl bridged binaphthyl-type chiral dopant displayed the relatively large $\beta_{wt\%}$ value. The CH···π interaction between the host NLC molecules' hydrogen atom and π electron cloud of the alkynyl moiety of the alkynyl bridged binaphthyl-type chiral dopant might have a beneficial effect on its $\beta_{wt\%}$ value. Moreover, the $HTP_{t.d.}$ value of the alkynyl bridged binaphthyl-type chiral dopant was larger than that of the alkyl bridged one, although the alkynyl bridged one was linked the rigid linker at the 2,2' positions. The strong symmetrical stretching vibration of the alkyne moiety of the alkynyl bridged chiral dopant can ineffectively affect its $HTP_{t.d.}$ value, since its dihedral angle might be easily alternative by strong thermal vibration of the alkyne moiety.

3.4 – References and Notes

1. N. Abdullah, A. R. A. Talib, A. A. Jaafar, M. A. M. Salleh, W. T. Chong, *Experimental Thermal and Fluid Science* **2010**, *34*, 1089.
2. C. R. Smith, D. R. Sabatino, T. J. Praisner, *Experiments in Fluids* **2001**, *30*, 190.
3. N. Tamaoki, A. V. Parfenov, A. Masaki, H. Matsuda, *Adv. Mater.* **1997**, *9*, 1102.
4. J. Stasieka, A. Stasiek, M. Jewartowski, M.W. Collins, *Optics & Laser Technology* **2006**, *38*, 243.
5. A. M. Chaudhari, T. M. Woudenberg, M. Albin, K. E. Goodson, *J. Microelectromech. Syst*. **1998**, *7*, 345.
6. G. Proni, G. P. Spada, *J. Org. Chem.* **2000**, *65*, 5522.
7. K. Kakisaka, H. Higuchi, Y. Okumura, H. Kikuchi, *Chem. Lett*. **2014**, 43, 624.
8. K. Akagi, S. Guo, T. Mori, M. Goh, G. Piao, M. Kyotani, *J. Am. Chem. Soc*. **2005**, *127*, 14647.
9. The scanning of the dihedral angle of **30** at C8-C1-C1'-C8' did not enable to be carried out, since its structure was distorted during the scanning.
10. Potential energy in the gas phase.
11. Data from **2.2.1 – Effects of Substituents on Dihedral Angle of Synthesised Binaphtyl-type Chiral Dopants**
12. J. C. Jewetta, C. R. Bertozzi, *Chem. Soc. Rev.* **2010**, *39*, 1272.
13. A. Ferrarini, S. Pieraccini, S. Masiero, G. P. Spada, *Beillstein J. Org. Chem*. **2009**, *5*, 50.
14. A. Ferrarini, G. J. Moro, P. L. Nordio, *Mol. Phys*. **1996**, *87*, 485.
15. A. Ferrarini, G. J. Moro, P. L. Nordio, *Phys. Rev. E* **1996**, *53*, 681.
16. M. Majumder, B. K. Mishra, N. Sathyamurthy, *Chem. Phys. Lett*. **2013**, *557*, 59.
17. F. Meyer-Wegner, H.W. Lerner, M. Bolte, *Acta Crystallographica C* **2010**, 66, 182.
18. The variation in the dihedral angle for **25** and **36** was measured by operating manually for vibrations at 47.3 for **25** and 34.0 cm^{-1} for **36**.

Chapter 4
Experimental

4.1 – General

All of reagents and solvents were purchased from Aldrich Chemical Co., Kanto Chemical Co., Inc., Tokyo Chemical Industry Co., Ltd. and Wako Pure Chemical Industries, Ltd. and used without further purification. Analytical thin layer chromatography (TLC) was performed on silica gel layer glass plate Merck 60 F_{254} and visualised by UV irradiation (254 nm). Column chromatography was undertaken on Wako Pure Chemical Industries, Ltd. Wakogel 60N 63–212 μm or Wakogel C-400HG 20–40 μm. ^{1}H- and ^{13}C-NMR spectra were recorded on JEOL JNM-LA 400 and JNM-ECA 600 with the TMS (Trimethylsilane) as an internal standard for ^{1}H and the deuterated solvent for ^{13}C. ^{19}F-NMR spectra were recorded on JEOL ECZ 400 with the Benzotrifluoride as an internal standard. Chemical shift (δ) was expressed in parts-per million (ppm) to relative internal standards. Signal multiplicities were abbreviated by s (singlet), d (doublet), t (triplet), q (quartet), dd (double-doublet), br (broad) and m (multiplet), respectively. High resolution mass spectra were performed on JEOL JNM-700. Elemental analyses were performed at Kyushu University. Polarised optical microscopy was performed on Nikon ECLIPSE E600 POL, equipped with Zeiss AxioCam HRc as a high-resolution camera. The temperature of the samples were controlled, utilising the heating stage Linkam LTS420E with Linkam 10084L controller. The geometry optimisations of all synthesised chiral dopants were calculated, using B3LYP/6-31G(d) for **25–27**, **30** (calculated by scanning dihedral angle C1–C8a–C8a'–C1' in 18 steps 5° each one[1]), **33**, **35** and **36** and B3LYP/Gen basis set for the iodo atom of **34** level of density function theory (DFT) *via* the Gaussian 09.[2] The theoretical IR spectra of **25** and **36** also were calculated, utilising B3LYP/6-31G(d) by means of the Gaussian 09 program.[2] Diffraction data of **25–27**, **30**, **33**, **35** and **36** was collected on Rigaku R-AXIS RAPID. The crystal structures of **25–27**, **30**, **33**, **35** and **36** were solved by direct methods, SIR 2008[3], and refined with full-matrix least-squares procedures,

utilising the program SHELXL2013[4]. All non-hydrogen atoms were refined anisotropically. Hydrogen atoms were refined, using the riding model.

4.2 – Syntheses

The binaphthyl-type chiral dopants were synthesised as shown in the Scheme 4.1 to evaluate substituents effects on the induced HTP values. The detailed synthetic procedures, ^{1}H-, ^{13}C-, ^{19}F-NMR, high resolution mass spectral and elemental analysis data are as follows.

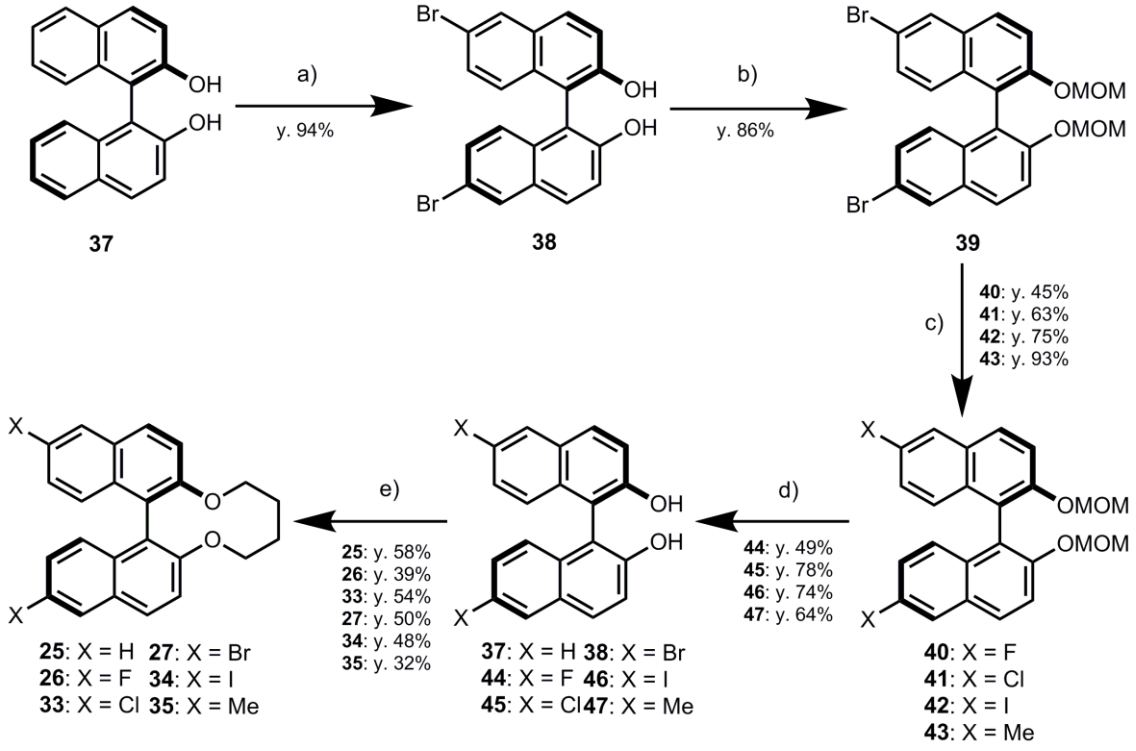

Scheme 4.1 Synthetic route for syntheses of **25**–**27** and **33**–**35**.

Synthesis of (R)-6,6'-dibromo-2,2'-dihydroxy-1,1'-binaphthalene (**38**)

To a solution of **37** (15.2 g, 53.1 mmol) in anhydrous DCM (300 mL), bromine (8.8 mL) was added slowly dropwise under nitrogen atmosphere at −78 °C. The resulting mixture was gradually allowed to warm to room temperature. After stirring for 3 hs, the

reaction mixture was treated with 10% sodium bisulphate aq (375 mL) to destroy excess bromine. The organic layer was separated, washed with brine (ca. 100 mL), dried over $MgSO_4$ and evaporated. The crude residue was purified by recrystallisation from toluene/*n*-heptane to afford **38** (22.2 g, 94%) as a white powder; ^{1}H-NMR (400 MHz, $CDCl_3$) δ 8.05 (d, *J* = 2.0 Hz, 2H), 7.90 (d, *J* = 9.8 Hz, 2H), 7.41–7.36 (m, 4H), 6.96 (d, *J* = 8.8 Hz, 2H), 5.01 (s, 2H); ^{13}C-NMR (100 MHz, $CDCl_3$) δ 152.97, 131.87, 130.86, 130.70, 130.58, 130.44, 125.86, 118.96, 118.02, 110.62.

Synthesis of (R)-6,6'-dibromo-2,2'-di(methoxymethyl)oxy-1,1'-binaphthalene (**39**)

To a suspension of 60% sodium hydride (6.8 g, 170.0 mmol) in anhydrous THF (100 mL), a solution of **38** (15.1 g, 34.0 mmol) in anhydrous THF (200 mL) was added slowly dropwise under nitrogen atmosphere at room temperature. After stirring for 0.5 hrs at room temperature, a solution of chloromethyl methyl ether (6.5 mL, 85.0 mmol) in anhydrous THF (10 mL) was added to the mixture at room temperature. After stirring for 2 hrs at room temperature, the reaction mixture was quenched with MeOH and H_2O. The organic layer was separated, and the water phase was extracted Et_2O. The combined organic layers were washed with water (ca. 100 mL), sat. $NaHCO_3$ aq (ca. 100 mL) and brine (ca. 100 mL), dried over $MgSO_4$ and evaporated. The crude residue was purified by recrystallisation from DCM/*n*-heptane to afford **39** (15.6 g, 86%) as a white crystal; ^{1}H-NMR (400 MHz, $CDCl_3$) δ 8.03 (d, *J* = 2.0 Hz, 2H), 7.86 (d, *J* = 8.8 Hz 2H), 7.59 (d, *J* = 9.8 Hz, 2H), 7.29 (dd, *J* = 6.8 Hz, *J* = 2.0 Hz, 2H), 6.98 (d, *J* = 8.8 Hz 2H), 5.09 (d, *J* = 6.8 Hz, 2H), 4.98 (t, *J* = 3.9 Hz, 2H), 3.16 (s, 6H); ^{13}C-NMR (100 MHz, $CDCl_3$) δ 152.92, 132.38, 130.86, 129.87, 129.70, 128.70, 127.12, 120.69, 118.04, 117.98, 95.01, 55.91.

*General procedure A of **40–43***

To a solution of (*R*)-6,6'-dibromo-2,2'-bis(methoxymethoxy)-1,1'-binaphthalene **39** (1.0 equiv.) in anhydrous THF (ca. 5.3 mL per 1.0 mmol of **39**), *n*-BuLi in hexanes (*ca*. 1.6 M, 3.0 equiv.) was added slowly dropwise under argon atmosphere at −78 °C. After stirring for 0.5 hrs at −78 °C, a solution of the halogenating reagents (**40**: *N*-fluorobenzenesulfonimide, 3.0 equiv.; **41**: hexachloroethane, 1.1 equiv.; **42**: iodine 3.0 equiv.) or methylating reagent (**43**: iodomethane, 3.0 equiv.) in anhydrous THF[5] was added to the mixture at −78 °C and then the reaction mixture was gradually allowed to warm to room temperature. After stirring for over 12 hrs at room temperature, the resulting mixture was quenched or treated with water[6], sat. NH_4Cl aq[7] or 10% sodium bisulphate aq[8] and extracted with EtO_2 (3×50 mL). The ethereal extracts were washed with sat. $NaHCO_3$ aq solution (50 mL), water (50 mL), brine (50 mL), dried over $MgSO_4$ and evaporated. The crude product was purified by silica-gel chromatography (DCM/*n*-heptane) and/or recrystalisation from DCM/*n*-heptane to afford the titled compounds.

(R)-6,6'-difluoro-2,2'-di(methoxymethyl)oxy-1,1'-binaphthalene (**40**): **40** was prepared according to a general procedure A. The crude product was purified by silica-gel chromatography (DCM/*n*-heptane = 1/1, v/v%) to afford **40** (1.4 g, 45%) as an off-white powder; ^{1}H-NMR (400 MHz, $CDCl_3$) δ 7.60 (d, *J* = 9.8 Hz, 2H), 7.49 (dd, *J* = 6.8 Hz, *J* = 2.9 Hz, 2H), 7.13–7.09 (m, 2H), 7.04–6.99 (m, 4H), 5.08 (d, *J* = 6.8 Hz, 2H), 4.96 (d, *J* = 6.8 Hz, 2H), 3.14 (s, 6H); ^{19}F-NMR (376 MHz, $CDCl_3$) δ −118.85–−118.92 (m, 2F).

(R)-6,6'-dichloro-2,2'-di(methoxymethyl)oxy-1,1'-binaphthalene (**41**): **41** was prepared according to a general procedure A. The crude product was purified by silica-gel chromatography (DCM/*n*-heptane = 1/1, v/v%) to afford **41** (2.1 g, 63%) as a white powder; ^{1}H-NMR (400 MHz, $CDCl_3$) δ 7.86 (d, *J* = 9.8 Hz, 4H), 7.60 (d, *J* = 9.8 Hz,

2H), 7.16 (dd, *J* = 6.8 Hz, *J* = 1.9 Hz, 2H), 7.05 (d, *J* = 8.8 Hz, 2H), 5.08 (d, *J* = 6.8 Hz, 2H), 4.97 (d, *J* = 7.8 Hz, 2H), 3.15 (s, 6H); ^{12}C-NMR (100 MHz, $CDCl_3$) δ 152.84, 132.17, 130.37, 129.89, 128.71, 127.25, 127.02, 126.55, 120.78, 118.13, 95.06, 55.89.

(R)-6,6'-diidodo-2,2'-di(methoxymethyl)oxy-1,1'-binaphthalene (**42**): **42** was prepared according to a general procedure A. The crude product was purified by silica-gel chromatography (DCM/*n*-heptane = 6/4, v/v%), followed by recrystallisation from DCM/*n*-heptane to afford **42** (7.0 g, 75%) as an off-white crystal; ^{1}H-NMR (400 MHz, $CDCl_3$) δ 8.25 (d, *J* = 1.9 Hz, 2H), 7.83 (d, *J* = 9.8 Hz 2H), 7.57 (d, *J* = 8.8 Hz, 2H), 7.44 (dd, *J* = 6.8 Hz, *J* = 2.0 Hz, 2H), 6.83 (d, *J* = 8.8 Hz 2H), 5.08 (d, *J* = 6.8 Hz, 2H), 4.97 (d, *J* = 6.8 Hz, 2H), 3.16 (s, 6H); ^{13}C-NMR[9] (100 MHz, $CDCl_3$) δ 153.05, 136.55, 134.83, 132.70, 131.43, 128.57, 127.08, 117.81, 94.98, 89.30, 55.91.

(R)-6,6'-dimethyl-2,2'-di(methoxymethyl)oxy-1,1'-binaphthalene (**43**): **43** was prepared according to a general procedure A. The crude product was purified by silica-gel chromatography (DCM/*n*-heptane = 1/1, v/v%) to afford **43** (5.6 g, 93%) as a white viscous powder; ^{1}H-NMR (400 MHz, $CDCl_3$) δ 7.85 (d, *J* = 8.8 Hz, 2H), 7.63 (br s, 2H), 7.52 (d, *J* = 8.8 Hz, 2H), 7.05 (br s, 4H), 5.04 (d, *J* = 6.8 Hz, 2H), 4.94 (d, *J* = 6.8 Hz, 2H), 3.14 (s, 6H), 2.45 (s, 6H); ^{13}C-NMR[9] (100 MHz, $CDCl_3$) δ 152.08, 133.53, 132.22, 130.15, 128.57, 126.82, 125.48, 121.54, 117.65, 95.46, 55.80, 21.40; HRMS (EI) calcd. for $C_{26}H_{26}O_4$ [M^+] 402.1831, found 402.1831.

*General procedure B of **44–47***

To a solution of **40–43** in anhydrous DCM (5 mL), methanoic acid (3.0 N, 10 mL, 30 mmol) was added dropwise under argon atmosphere at 0 °C. After stirring for 3 hrs at room temperature, the reaction mixture was evaporated and diluted with DCM (50 mL). The organic layer was washed with sat. $NaHCO_3$ *aq* (50 mL), water (50 mL) and brine

(50 mL), dried over $MgSO_4$ and evaporated. The crude product was purified by silica-gel chromatography (DCM/*n*-heptane or EtOAc/*n*-heptane) and/or recrystallisation from DCM/*n*-heptane to afford the titled compounds.

(R)-6,6'-fluoro-2,2'-dihydroxy-1,1'-binaphthalene (**44**): **44** was prepared according to a general procedure B. The crude product was purified by silica-gel chromatography (DCM/*n*-heptane = 1/1, v/v%), followed by recrystallisation from DCM/hexanes to afford **44** (534 mg, 49%) as a white crystal; ^{1}H-NMR (400 MHz, $CDCl_3$) δ 7.92 (d, *J* = 8.8 Hz, 2H), 7.53 (d, *J* = 8.8 Hz, 2H), 7.41 (d, *J* = 8.8 Hz, 2H), 7.10 (dd, *J* = 4.8 Hz, *J* = 2.0 Hz, 4H), 4.96 (s, 2H); ^{19}F-NMR (376 MHz, $CDCl_3$) δ −118.75–−118.81 (m, 2F).

(R)-6,6'-dichloro-2,2'-dihydroxy-1,1'-binaphthalene (**45**): **45** was prepared according to a general procedure B. The crude product was purified by silica-gel chromatography (DCM/*n*-heptane = 1/1, v/v%) to afford **45** (1.25 g, 78%) as a white powder; ^{1}H-NMR (400 MHz, $CDCl_3$) δ 7.93–7.88 (m, 4H), 7.41 (d, *J* = 8.8 Hz, 2H), 7.27–7.23 (m, 2H), 7.03 (d, *J* = 4.8 Hz, 2H), 5.03 (s, 2H); ^{13}C-NMR (100 MHz, $CDCl_3$) δ 152.86, 131.63, 130.70, 130.09, 130.03, 128.37, 127.16, 125.74, 118.99, 110.66.

(R)-6,6'-diiodo-2,2'-dihydroxy-1,1'-binaphthalene (**46**): **46** was prepared according to a general procedure B. The crude product was purified by recrystallisation from DCM/ *n*-heptane to afford **46** (1.18 g, 74%) as a white powder; ; ^{1}H-NMR (400 MHz, $CDCl_3$) δ 8.28 (d, *J* = 2.0 Hz, 2H), 7.87 (d, *J* = 8.8 Hz, 2H), 7.53 (dd, *J* = 8.0 Hz, *J* = 2.0 Hz, 2H), 7.38 (d, *J* = 8.8 Hz, 2H), 6.82 (d, *J* = 8.8 Hz, 2H), 4.96 (s, 2H); ^{13}C-NMR (100 MHz, $CDCl_3$) δ 153.08, 137.03, 136.03, 132.21, 131.12, 130.57, 125.83, 118.74, 110.52, 89.13.

(R)-6,6'-dimethyl-2,2'-dihydroxy-1,1'-binaphthalene (**47**): **47** was prepared according to a general procedure B. The crude product was purified by silica-gel chromatography (EtOAc/*n*-heptane = 2/8, v/v%), followed by recrystallisation from DCM/*n*-heptane to afford **47** (2.8 g, 64%) as a white crystal; ^{1}H-NMR (400 MHz, $CDCl_3$) δ 7.88 (d, *J* = 9.8 Hz, 2H), 7.66 (br s, 2H), 7.34 (d, *J* = 8.8 Hz, 2H), 7.14 (dd, *J* = 2.0 Hz, *J* = 2.0 Hz, 2H), 7.05 (d, *J* = 8.8 Hz, 2H), 4.96 (s, 2H), 2.46 (s, 6H); ^{13}C-NMR (100 MHz, $CDCl_3$) δ 152.02, 133.56, 131.51, 130.64, 129.65, 129.64, 127.47, 124.13, 117.70, 110.85, 21.31; HRMS (EI) calcd. for $C_{22}H_{18}O_2$ [M^+] 314.1307, found 314.1308.

*General procedure C of (R)-Closed binaphthyl type chiral dopants (**25**–**27** and **33**–**35**)*

A solution of **37**–**38** and **44**–**47** (1 equiv.), 18-crown-6 (catalytical quantity), and K_2CO_3 (2.2 equiv.) in acetone (100 mL per 1 mmol of **37**–**38** and **44**–**47**) was refluxed under argon atmosphere at 60 °C. After refluxing for 2 hrs at 60 °C, a solution of 1,4-dibromobutane (1.1 equiv.) in acetone (15.5 mL per 1 mmol of 1,4-dibromobutane) was slowly added to the refluxing solution for over 8hrs by using syringe pump and then the resulting mixture was refluxed for 120 hrs at 60 °C. After cooling, the reaction mixture was filtered out and evaporated. The residue was diluted with water and extracted with Et_2O (2×50 mL). The ethereal extracts were washed with water (50 mL) and brine (50 mL), dried over $MgSO_4$ and evaporated. The crude product was purified by silica-gel chromatography (DCM/hexanes) and then recrystallisation from EtOH or DCM/hexanes to afford the titled compounds.

25: **25** was prepared according to a general procedure C. The crude product was purified by silica-gel chromatography (DCM/hexanes = 3/7, v/v%), followed by recrystallization from DCM/hexanes to afford **25** (587 mg, 58%) as a white crystal; ^{1}H-NMR (400 MHz, $CDCl_3$) δ 7.95 (d, *J* = 8.8 Hz, 2H), 7.86 (d, *J* = 8.8 Hz, 2H), 7.49 (d, *J* = 8.8 Hz, 2H), 7.32 (t, *J* = 7.8 Hz, *J* = 6.8 Hz, 2H), 7.19 (t, *J* = 8.8 Hz, *J* = 6.8 Hz, 2H), 7.09 (d, *J* = 8.8

Hz, 2H), 4.55-4.51 (m, 2H), 4.11 (t, *J* = 9.8 Hz, *J* = 10.8 Hz, 2H), 1.88–1.71 (m, 4H); ^{13}C-NMR (100 MHz, $CDCl_3$) δ 153.30, 134.12, 129.83, 129.36, 127.95, 126.37, 125.81, 123.97, 122.39, 117.41, 70.36, 25.31; Elemental anal. calcd. for $C_{24}H_{20}O_2$ C 84.68, H 5.92, found C 84.65, H 5.96; HRMS (EI) calcd. for $C_{24}H_{20}O_2$ [M^+] 340.1463, found 340.1463.

26: **26** was prepared according to a general procedure C. The crude product was purified by silica-gel chromatography (DCM/hexanes = 2/8, v/v%), followed by recrystallization from EtOH to afford **26** (234 mg, 41%) as a white crystal; ^{1}H-NMR (400 MHz, $CDCl_3$) δ 7.88 (d, *J* = 9.8 Hz, 2H), 7.51 (d, *J* = 8.8 Hz, 2H), 7.48 (dd, *J* = 9.7 Hz, *J* = 2.9 Hz, 2H), 7.05-6.96 (m, 4H), 4.50 (d, *J* = 11.7 Hz, 2H), 4.12 (t, *J* = 10.8 Hz, *J* = 11.7 Hz, 2H), 1.86–1.71 (m, 4H); ^{13}C-NMR (150 MHz, $CDCl_3$) δ 180.34 (d, *J* = 303.4 Hz), 171.73, 144.44, 143.74 (d, *J* = 10.8 Hz), 141.67 (d, *J* = 5.4 Hz), 140.77 (d, *J* = 10.8 Hz), 133.80, 129.12, 126.64 (d, *J* = 30.5 Hz), 119.51 (d, *J* = 25.1 Hz), 68.90, 12.29; ^{19}F-NMR (376 MHz, $CDCl_3$) −119.09–−119.16 (m, 2F); Elemental anal. calcd. for $C_{24}H_{18}F_2O_2$ C 76.58, H 4.82, found C 76.91, H 4.86; HRMS (EI) calcd. for $C_{24}H_{18}F_2O_2$ [M^+] 376.1275, found 376.1275.

33: **33** was prepared according to a general procedure C. The crude product was purified by silica-gel chromatography (DCM/hexanes = 3/7, v/v%), followed by recrystallization from EtOH to afford **33** (666 mg, 54%) as a white crystal; ^{1}H-NMR (400 MHz, $CDCl_3$) δ 7.87 (d, *J* = 8.8 Hz, 2H), 7.84 (d, *J* = 2.0 Hz, 2H), 7.51 (d, *J* = 8.8 Hz, 2H), 7.14 (dd, *J* = 2.0 Hz, *J* = 6.8 Hz, *J* = 3.0 Hz, 2H), 6.99 (d, *J* = 8.8 Hz, 2H), 4.50 (d, *J* = 11.6 Hz, 2H), 4.13 (t, *J* = 10.1 Hz, 2H), 1.86–1.73 (m, 4H); ^{13}C-NMR (100 MHz, $CDCl_3$) δ 153.69, 132.24, 130.39, 129.87, 128.72, 127.33, 127.26, 126.68, 121.96, 118.52, 70.51, 25.39; Elemental anal. calcd. for $C_{24}H_{18}Cl_2O_2$ C 70.43, H 4.43, found C 70.47, H 4.43; HRMS (EI) calcd. for $C_{24}H_{18}Cl_2O_2$ [M^+] 408.0684, found 408.0684.

27: **27** was prepared according to a general procedure C. The crude product was purified by silica-gel chromatography (DCM/hexanes = 3/7, v/v%), followed by twice recrystallization from EtOH to afford **27** (410 mg, 28%) as a white crystal; ^{1}H-NMR (400 MHz, $CDCl_3$) δ 8.02 (d, *J* = 2.0 Hz, 2H), 7.86 (d, *J* = 9.8 Hz, 2H), 7.50 (d, *J* = 9.8 Hz, 2H), 7.26 (dd, *J* = 2.0 Hz, *J* = 7.8 Hz, 2H), 6.92 (d, *J* = 9.8 Hz, 2H), 4.50 (d, *J* = 10.8 Hz, 2H), 4.13 (t, *J* = 8.8 Hz, *J* = 10.7 Hz, 2H), 1.87–1.73 (m, 4H); ^{13}C-NMR (100 MHz, $CDCl_3$) δ 153.79, 132.44, 130.87, 129.98, 129.79, 128.71, 127.37, 121.91, 118.45, 117.98, 70.49, 25.40; Elemental anal. calcd. for $C_{24}H_{18}Br_2O_2$ C 57.86, H 3.64, found C 57.77, H 3.59; HRMS (EI) calcd. for $C_{24}H_{18}Br_2O_2$ [M^+] 495.9674, found 495.9673.

34: **34** was prepared according to a general procedure C. The crude product was purified by silica-gel chromatography (DCM/hexanes = 3/7, v/v%), followed by recrystallization from DCM/hexanes to afford **34** (306 mg, 48%) as a white powder; ^{1}H-NMR (400 MHz, $CDCl_3$) δ 8.24 (d, *J* = 1.9 Hz, 2H), 7.83 (d, *J* = 8.8 Hz, 2H), 7.48 (d, *J* = 9.8 Hz, 2H), 7.41 (dd, *J* = 2.0 Hz, *J* = 6.8 Hz, 2H), 6.78 (d, *J* = 8.8 Hz, 2H), 4.50 (d, *J* = 11.7 Hz, 2H), 4.12 (t, *J* = 8.8 Hz, *J* = 10.8 Hz, 2H), 1.85–1.71 (m, 4H); ^{13}C-NMR (100 MHz, $CDCl_3$) δ 153.93, 136.65, 134.93, 132.76, 131.743 128.57, 127.34, 121.83, 118.21, 89.27, 70.46, 25.43; Elemental anal. calcd. for $C_{24}H_{18}I_2O_2$ C 48.68, H 3.06, found C 48.74, H 2.99; HRMS (EI) calcd. for $C_{24}H_{18}I_2O_2$ [M^+] 591.9396, found 591.9395.

35: **35** was prepared according to a general procedure C. The crude product was purified by silica-gel chromatography (DCM/hexanes = 1/1, v/v%), followed by recrystallization from EtOH to afford **35** (382 mg, 35%) as a colourless crystal; ^{1}H-NMR (400 MHz, $CDCl_3$) δ 7.84 (d, *J* = 8.8 Hz, 2H), 7.62 (s, 2H), 7.44 (d, *J* = 9.8 Hz, 2H), 7.01 (q, *J* = 8.8 Hz, *J* = 7.8 Hz, 2H), 4.49 (d, *J* = 11.7 Hz, 2H), 4.08 (t, *J* = 9.8 Hz, *J* = 11.7 Hz, 2H), 2.43 (s, 6H), 1.86–1.82 (m, 2H), 1.74–1.68 (m, 2H); ^{13}C-NMR (100 MHz, $CDCl_3$) δ 152.56, 133.40, 132.33, 130.03, 128.62, 128.57, 126.90, 125.67, 122.57, 117.55, 70.33,

25.18, 21.35; Elemental anal. calcd. for $C_{26}H_{24}O_2$ C 84.75, H 6.57, found C 84.83, H 6.53; HRMS (EI) calcd. for $C_{26}H_{24}O_2$ [M^+] 368.1776, found 368.1778.

The binaphthyl-type chiral dopants were synthesised as shown in the Scheme 4.2 and 4.3 to evaluate molecular shape effects on the induced HTP values. The detailed synthetic procedures, ^{1}H-, ^{13}C-NMR, high resolution mass spectral and elemental analysis data are as follows.

Synthesis of (R)-2,2'-diethoxy-1,1'-binaphthalene (30)

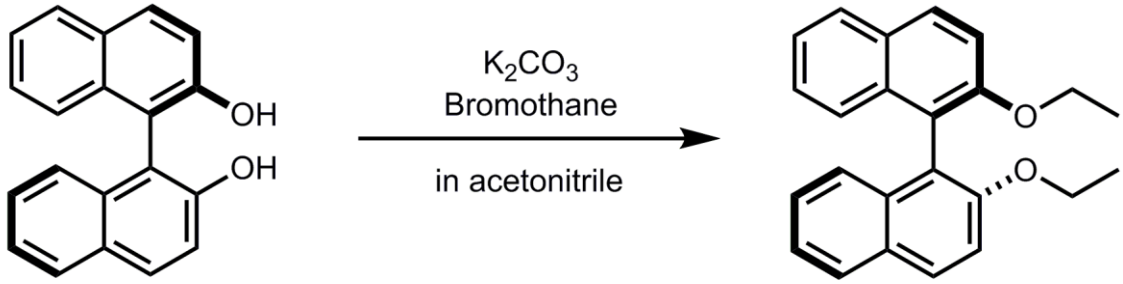

Scheme 4.2 Synthesis of **30**.

A solution of **37** (1.2 g, 4.2 mmol), bromoethane (1.6 mL, 21.0 mmol) and K_2CO_3 (21.0 mmol) in acetonitrile (20 mL) was refluxed for 20 hs at 85 °C. After cooling, the reaction mixture was evaporated. The residue was dissolved in Et_2O (100 mL) and then the ethereal layer was with water (50 mL) and brine (50 mL), dried over $MgSO_4$ and evaporated. The crude product was purified by silica-gel chromatography (DCM/hexanes = 1/1, v/v%) and then recrystallisation from EtOH to afford **30** (1.13 g, 79%) as a colourless single crystal; ^{1}H-NMR (400 MHz, $CDCl_3$) δ 7.93 (d, *J* = 8.8 Hz, 2H), 7.85 (d, *J* = 8.7 Hz, 2H), 7.42 (d, *J* = 8.8 Hz, 2H), 7.32–7.28 (m, 2H), 7.22–7.18 (m, 2H), 7.13 (d, *J* = 7.8 Hz, 2H), 4.07–4.01 (m, 4H), 1.05 (t, *J* = 7.8 Hz, *J* = 6.8 Hz, 6H); ^{13}C-NMR (100 MHz, $CDCl_3$) δ 154.34, 134.19, 129.27, 129.06, 127.77, 126.03, 125.51, 123.41, 120.71, 115.91, 65.22, 14.99; Elemental anal. calcd. for $C_{24}H_{22}O_2$ C

84.18, H 6.48, found C 84.01, H 6.45; HRMS (EI) calcd. for $C_{24}H_{22}O_2$ [M^+] 342.1620, found 342.1620.

Synthesis of ***36***

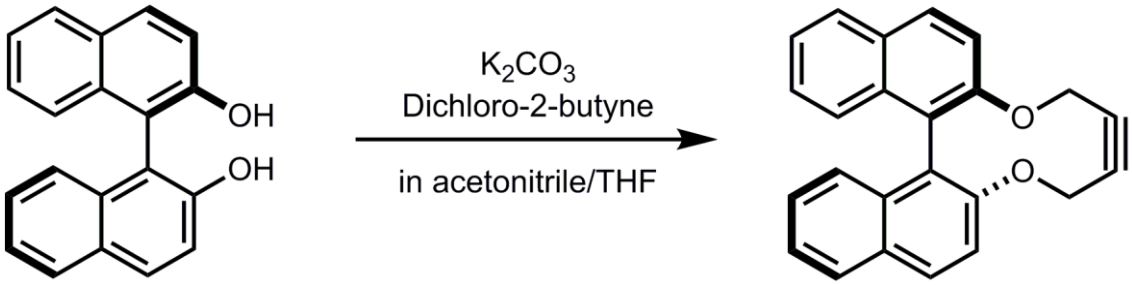

Scheme 4.3 Synthesis of **36**.

A solution of **37** (930 mg, 3.3 mmol), and K_2CO_3 (3.7 g, 26.4 mmol) in acetonitrile (2.5 L) and THF (250 mL) was refluxed under argon atmosphere at 80 °C. After refluxing for 1 hr at 80 °C, a solution of 1,4-dichloro-2-butyne (500 mg, 4.1 mmol) in acetonitrile (250 mL) was slowly added to the refluxing solution for over 15 hrs by using syringe pump. After addition, the resulting mixture was refluxed for 24 hrs at 80 °C. After cooling, the reaction mixture was filtered out and evaporated. The residue was diluted with water and Et_2O (100 mL). The ethereal extract was washed with water (100 mL) and brine (100 mL), dried over $MgSO_4$ and evaporated. The crude product was purified by silica-gel chromatography (DCM/hexanes = 1/1, v/v%) and then recrystallisation from DCM/ethanol to afford **36** (200 mg, 18%) as a colourless single crystal; ^{1}H-NMR (400 MHz, DMSO-d_6) δ 8.10 (d, J = 9.8 Hz, 2H), 7.99 (d, J = 7.8 Hz, 2H), 7.61 (d, J = 8.8 Hz, 2H), 7.44 (t, J = 6.8 Hz, J = 7.8 Hz, 2H), 7.32–7.28 (m, 2H), 7.07 (d, J = 8.8 Hz, 2H), 4.67–4.51 (m, 4H); (400 MHz, $CDCl_3$) δ 8.01 (d, J = 9.8 Hz, 2H), 7.90 (d, J = 7.8 Hz, 2H), 7.44–7.40 (m, 4H), 7.31 (d, J = 3.9 Hz, 4H), 4.58–4.43 (m, 4H); ^{13}C-NMR (100 MHz, $CDCl_3$) δ 152.50, 133.77, 131.17, 130.27, 128.01, 127.86, 126.57, 126.17, 125.19, 121.12, 88.04, 62.29; Elemental anal. calcd. for $C_{24}H_{16}O_2$ C 85.69, H 4.79,

found C 85.43, H 4.75; HRMS (EI) calcd. for $C_{24}H_{16}O_2$ [M^+] 336.1150, found 336.1150.

4.3 – Measurement of synthesised chiral dopants' helical twisting power

Helical twisting power (HTP) values was evaluated by the Grandjean–Cano method (**Figure 4.1**).[10] The synthesised chiral dopants were dissolved in host NLCs. JC-1041XX, which is a fluorinated nematic mixture supplied by JNC Co., *N*-(4-methoxybenzylidene)-4-butylaniline (MBBA) and the mixture of JC-1041XX and 5CB (= 1/1, wt/wt%), were used as 0.2, 0.5 or 1.0wt% sample solutions. Prepared solutions were stirred at their isotropic phase temperature for three hours, and were injected in a Grandjean–Cano wedge-shaped cell (E. H. C. Co., KCRK-03, $\tan\theta$ = 0.0079 ± 10% or KCRK-11, $\tan\theta$ = 0.0288 ± 5%). After cooling to a N* phase, the interval distances of the striped defect lines that appeared in the cell were measured at temperatures well below the clearing point (T_c), T_c −5°C, −10°C, −15°C, −20°C, and −25°C, in host nematics by means of a polarising optical microscope. Measurements were repeated more than twice, and their given HTP values were averaged.

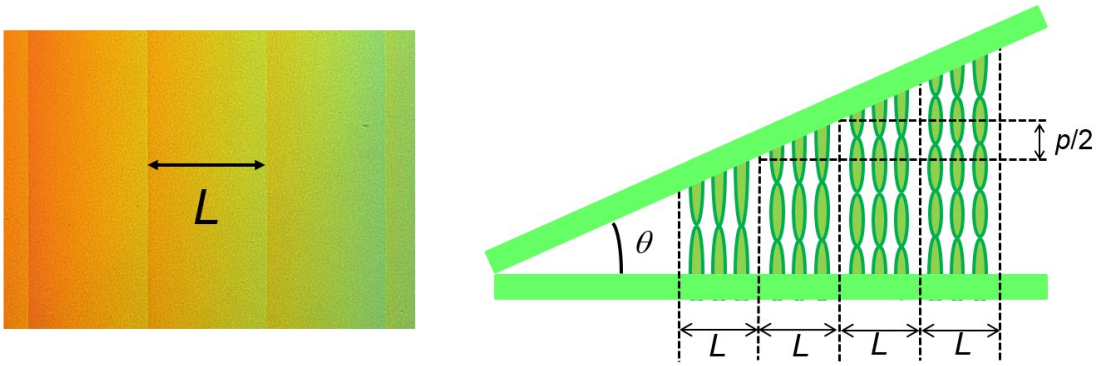

Figure 4.1 Schematic illustration of the Grandjean–Cano method.

The equation of a HTP value is described, using the Grandjean–Cano method as follow:

$$p = 2L\tan\theta \tag{4.1}$$

Then,

$$\beta_{wt\%} = (pc_w)^{-1} \tag{4.2}$$

where p is the helical pitch of the chiral nematic (N*) phase, L is the distance between defect lines, θ is the wedge angle, $\beta_{wt\%}$ is the HTP and c_w is the concentration of the chiral dopant in weight percentage.

4.4 – Identification of the helical sense of the synthesised chiral dopants

The helical sense of the synthesised chiral dopants was determined by a contact method using cholesteryl oleyl carbonate (COC), possessing *M* helicity, as a reference material. The 0.2, 0.5 or 1.0wt% samples doped with synthesised chiral dopants were injected from one side of the Grandjean–Cano wedge-shaped cell (E. H. C. Co., KCRK-03, $\tan\theta$ = 0.0079 ± 10%), and the COC was injected from the other side of its cell. After being in static for several hours, the helical sense was determined by polarising optical microscopy.

4.5 – Determination of Crystal Structures of Synthesised Chiral Dopants

The single crystals of **25**–**27**, **33** and **35** was obtained by the slow evaporation method. The recrystallised method and solvents have been finalised in the Table 4.1.

Table 4.1 The recrystallisation method and solvents for **25**–**27** and **33**–**35**.

Entry	Single crystal	method	solvents
25	○	Slow evaporation	Ethyl acetate
26	○	Slow evaporation	Ethanol
33	○	Slow evaporation	Ethanol
27	○	Slow evaporation	Ethanol
34	×	Slow evaporation	Ethanol
35	○	Slow evaporation	Ethanol

The single crystal of **30** and **36** was obtained by conventional recrystallisation.

The crystalline sample was mounted on a fibre loop in a viscous oil.

ORTEP [Mercury] representation of **25**–**27**, **30**, **33**, **35** and **36** is represented in the Figures 4.2–4.8.

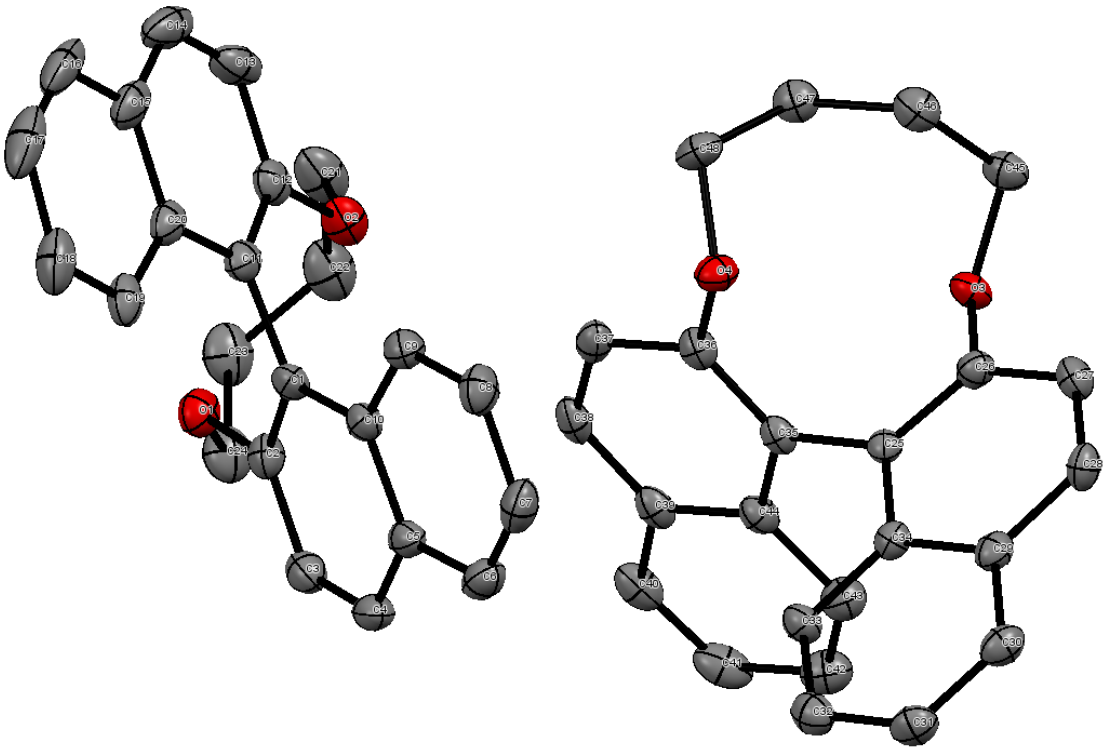

Figure 4.2 ORTEP [Mercury] representation of **25** at 123 K. Hydrogen atoms have been omitted for clarity. Thermal ellipsoids are displayed at the 50% probability level.

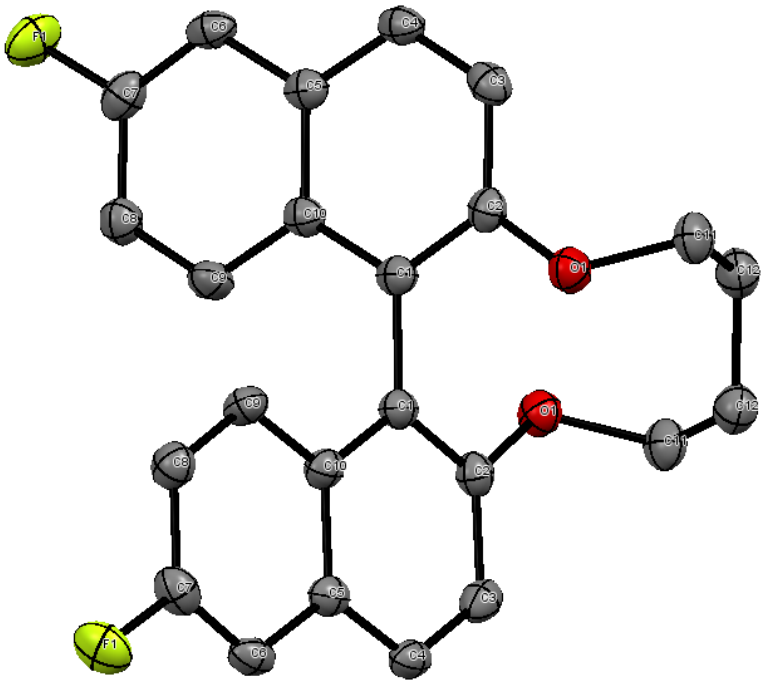

Figure 4.3 ORTEP [Mercury] representation of **26** at 123 K. Hydrogen atoms have been omitted for clarity. Thermal ellipsoids are displayed at the 50% probability level.

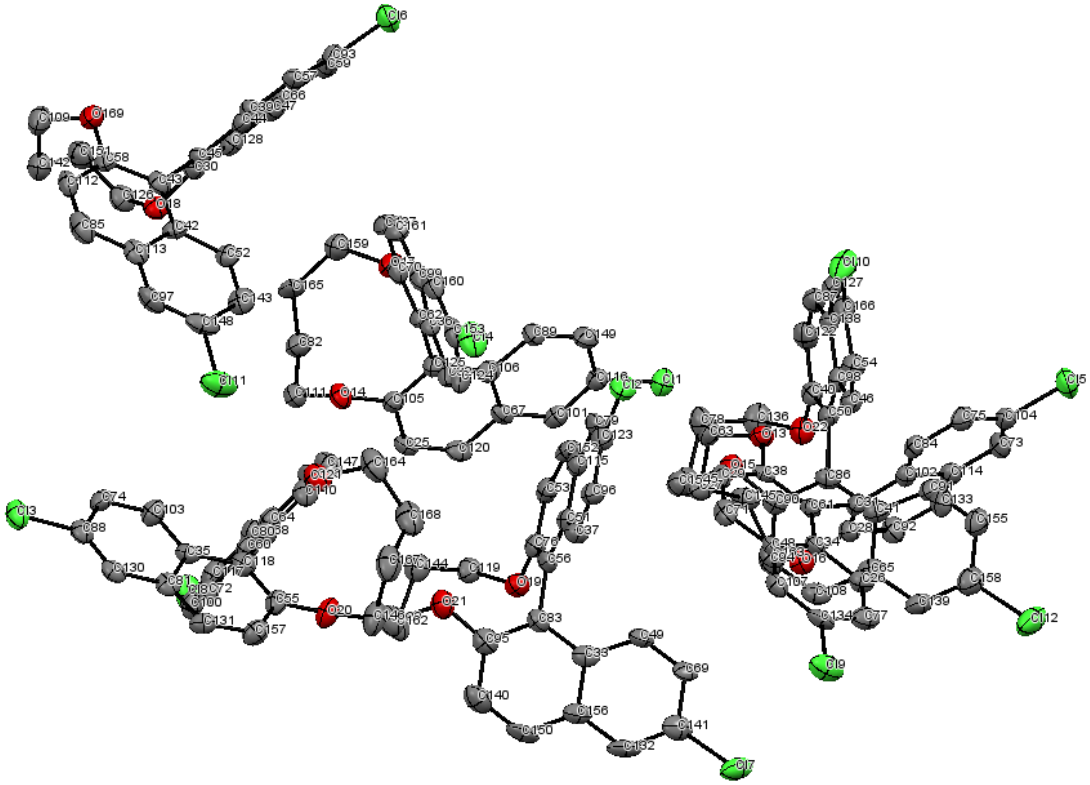

Figure 4.4 ORTEP [Mercury] representation of **33** at 123 K. Hydrogen atoms have been omitted for clarity. Thermal ellipsoids are displayed at the 50% probability level.

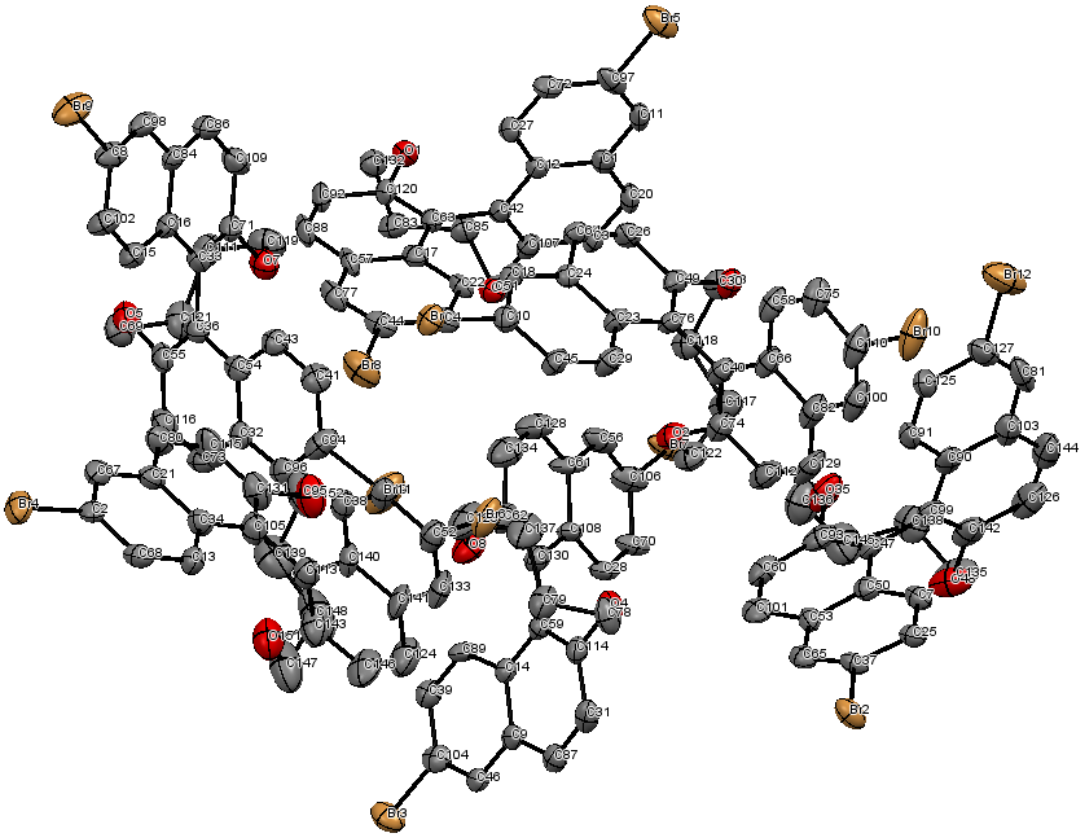

Figure 4.5 ORTEP [Mercury] representation of **27** at 123 K. Hydrogen atoms have been omitted for clarity. Thermal ellipsoids are displayed at the 50% probability level.

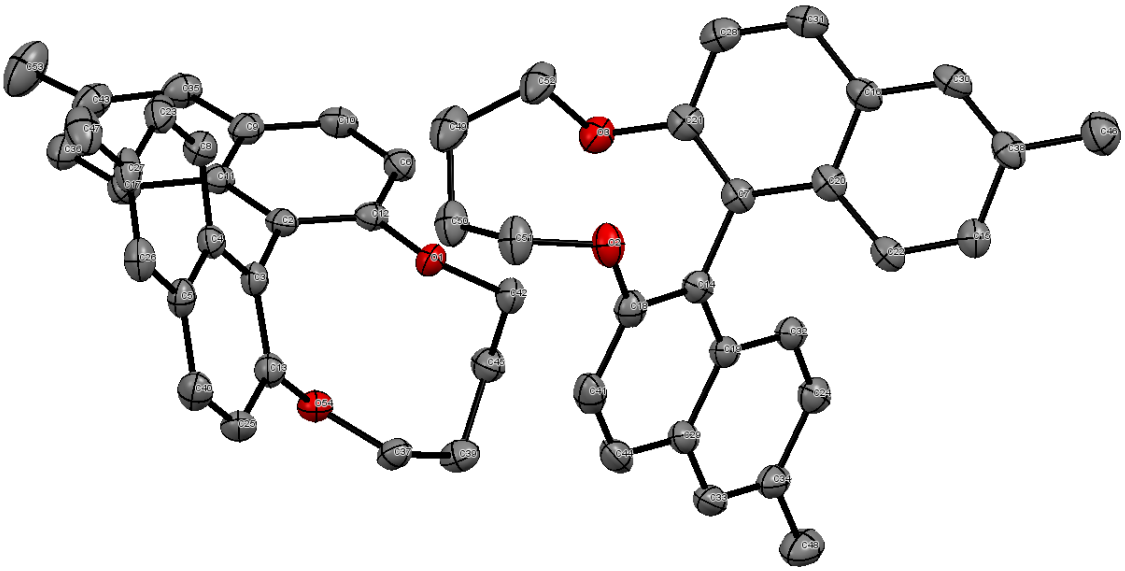

Figure 4.6 ORTEP [Mercury] representation of **35** at 123 K. Hydrogen atoms have been omitted for clarity. Thermal ellipsoids are displayed at the 50% probability level.

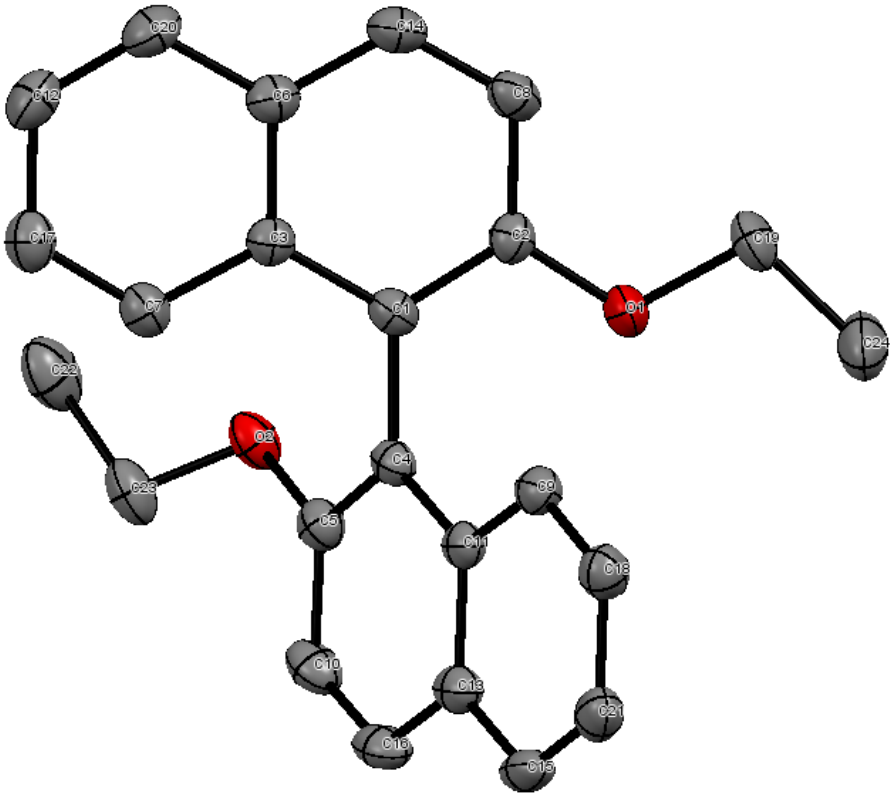

Figure 4.7 ORTEP [Mercury] representation of **30** at 123 K. Hydrogen atoms have been omitted for clarity. Thermal ellipsoids are displayed at the 50% probability level.

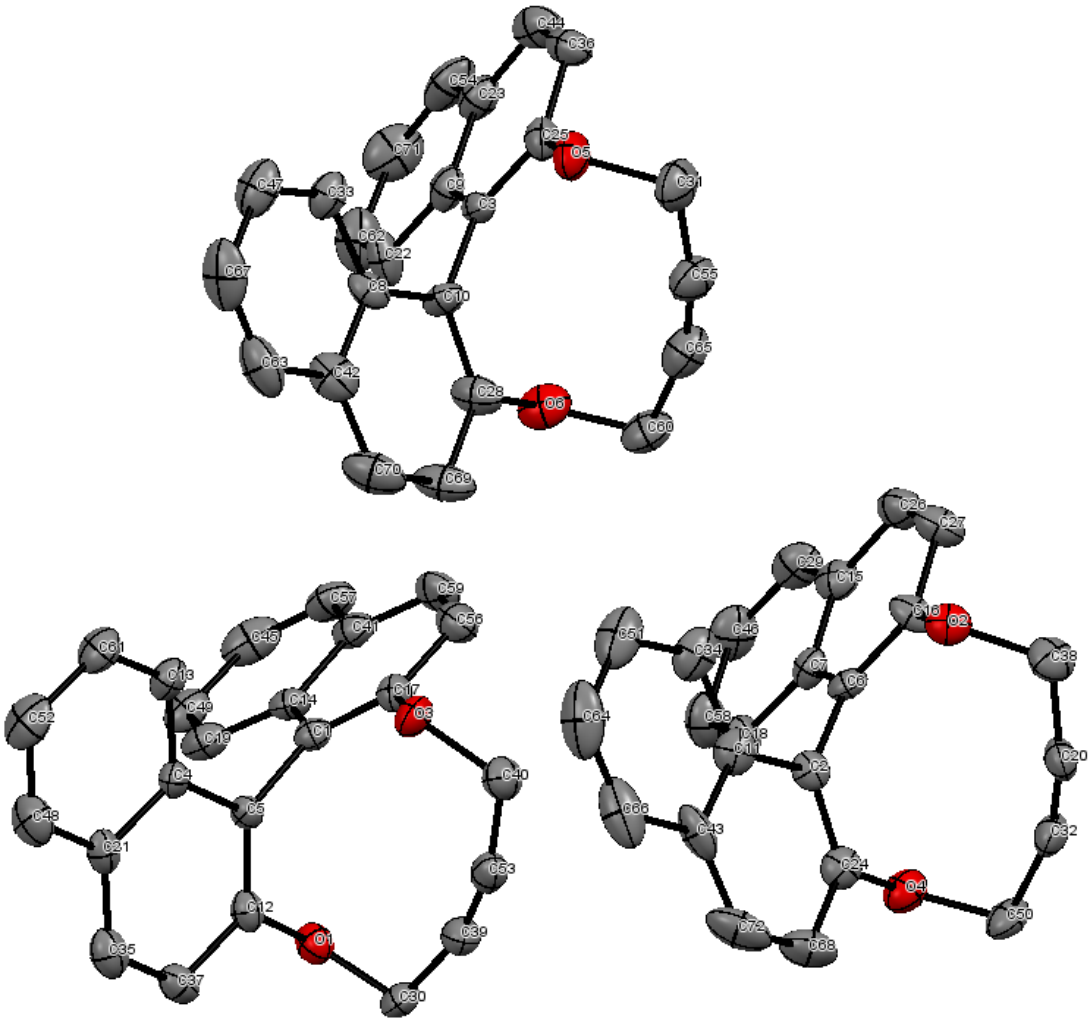

Figure 4.8 ORTEP [Mercury] representation of **36** at 123 K. Hydrogen atoms have been omitted for clarity. Thermal ellipsoids are displayed at the 50% probability level.

Their crystallographic data are presented in the Table 4.2.

Table 4.2 Summary of crystallographic data for **25**–**27**, **30**, **33**, **35** and **36**

Crystallographic Data		
	25	**26**
Empirical Formula	$C_{24}H_{20}O_2$	$C_{24}H_{18}F_2O_2$
Formula Weight	340.42	376.40
T/K	123	123
Crystal Colour, Habit	Colourless, prism	Colourless, prism
Crystal System	monoclinic	tetragonal
Lattice Type	Primitive	I-centred
a/Å	8.8125(3)	11.5685(7)
b/Å	14.2451(4)	11.5685(7)
c/Å	14.3071(4)	13.7819(5)
α/°	90.0000	90.0000
β/°	105.868(8)	90.0000
γ/°	90.0000	90.0000
V/Å^3	1727.60(11)	1844.43(17)
Space Group	$P2_1$ (#4)	$I4_1$ (#80)
Z value	4	4
D_{calc}/g/cm^3	1.309	1.355
F(0 0 0)	720.00	784.00
Total Reflections	12300	5059
Unique Reflections	5612	1484
R_{int}	0.0453	0.0360
R_1	0.0456	0.0343
wR_2	0.1001	0.0882

Flack Parameter	–0.06(15)	–0.02(9)
Goodness of Fit	1.084	1.047

Crystallographic Data

	33	**27**
Empirical Formula	$C_{24}H_{18}Cl_2O_2$	$C_{24}H_{18}Br_2O_2$
Formula Weight	409.31	498.21
T/K	123	123
Crystal Colour, Habit	Colourless, prism	Colourless, prism
Crystal System	monoclinic	monoclinic
Lattice Type	Primitive	Primitive
a/Å	14.2406(3)	14.6701(3)
b/Å	21.7973(4)	21.8668(4)
c/Å	18.8854(4)	18.8653(3)
α/°	90.0000	90.0000
β/°	91.200(6)	91.086(6)
γ/°	90.0000	90.0000
V/Å^3	5860.87(19)	6050.69(19)
Space Group	$P2_1$ (#4)	$P2_1$ (#4)
Z value	12	12
D_{calc}/g/cm^3	1.392	1.641
F(0 0 0)	2544.00	2976.00
Total Reflections	61421	71931
Unique Reflections	19844	21539
R_{int}	0.0719	0.0421
R_1	0.0645	0.0518
wR_2	0.1707	0.1381
Flack Parameter	0.059(6)	0.014(5)

Goodness of Fit	1.030	0.937
Crystallographic Data		
	35	**30**
Empirical Formula	$C_{26}H_{24}O_2$	$C_{24}H_{22}O_2$
Formula Weight	368.47	342.44
T/K	123	123
Crystal Colour, Habit	Colourless, block	Colourless, platelet
Crystal System	monoclinic	orthorhombic
Lattice Type	Primitive	Primitive
a/Å	11.1056(4)	7.41893(19)
b/Å	12.6168(4)	11.4130(3)
c/Å	14.0082(5)	21.3510(5)
α/°	90.0000	90.0000
β/°	99.803(7)	90.0000
γ/°	90.0000	90.0000
V/Å^3	1934.12(12)	1807.85(8)
Space Group	$P2_1$ (#4)	$P2_12_12_1$ (#19)
Z value	4	4
D_{calc}/g/cm^3	1.265	1.258
F(0 0 0)	784.00	728.00
Total Reflections	21484	12438
Unique Reflections	6936	3280
R_{int}	0.0443	0.0423
R_1	0.0537	0.0399
wR_2	0.1357	0.0827
Flack Parameter	0.22(10)	–0.11(13)
Goodness of Fit	1.070	1.046

Crystallographic Data	
	36
Empirical Formula	$C_{24}H_{16}O_2$
Formula Weight	336.39
T/K	123
Crystal Colour, Habit	Colourless, platelet
Crystal System	hexagonal
Lattice Type	Primitive
a/Å	13.5204(6)
b/Å	13.5204(6)
c/Å	48.3201(10)
α/°	90.0000
β/°	90.0000
γ/°	120.0000
V/Å^3	7649.6(5)
Space Group	$P6_1$ (#169)
Z value	18
D_{calc}/g/cm^3	1.314
F(0 0 0)	3168.00
Total Reflections	65516
Unique Reflections	9320
R_{int}	0.0956
R_1	0.0742
wR_2	0.1556
Flack Parameter	0.27(17)
Goodness of Fit	1.018

4.6 – Measurement of Thermal Stability of the Strained Alkynyl Bridged Binaphthyl-type Chiral Dopant

A 0.2wt% solution of **36** in DMSO-d_6 was warmed at 60, 70, 80 and 90 °C for 3 hs in air. After cooling, the resulting samples were measured ^{1}H-NMR spectra to confirm the presence of several impurities by its thermal decomposition at room temperature.

4.7 – References and Notes

1. The scanning of the dihedral angle of **30** was carried out from −45° to −135°.
2. a) Gaussian 09, Revision D.01, M. J. Frisch, G. W. Trucks, H. B. Schlegel, G. E. Scuseria, M. A. Robb, J. R. Cheeseman, G. Scalmani, V. Barone, B. Mennucci, G. A. Petersson, H. Nakatsuji, M. Caricato, X. Li, H. P. Hratchian, A. F. Izmaylov, J. Bloino, G. Zheng, J. L. Sonnenberg, M. Hada, M. Ehara, K. Toyota, R. Fukuda, J. Hasegawa, M. Ishida, T. Nakajima, Y. Honda, O. Kitao, H. Nakai, T. Vreven, J. A. Montgomery, Jr., J. E. Peralta, F. Ogliaro, M. Bearpark, J. J. Heyd, E. Brothers, K. N. Kudin, V. N. Staroverov, T. Keith, R. Kobayashi, J. Normand, K. Raghavachari, A. Rendell, J. C. Burant, S. S. Iyengar, J. Tomasi, M. Cossi, N. Rega, J. M. Millam, M. Klene, J. E. Knox, J. B. Cross, V. Bakken, C. Adamo, J. Jaramillo, R. Gomperts, R. E. Stratmann, O. Yazyev, A. J. Austin, R. Cammi, C. Pomelli, J. W. Ochterski, R. L. Martin, K. Morokuma, V. G. Zakrzewski, G. A. Voth, P. Salvador, J. J. Dannenberg, S. Dapprich, A. D. Daniels, O. Farkas, J. B. Foresman, J. V. Ortiz, J. Cioslowski, and D. J. Fox, Gaussian, Inc., Wallingford CT, **2009**.
3. M. C. Burla, R. Caliandro, M. Camalli, B. Carrozzini, G. L. Cascarano, L. De Caro, C. Giacovazzo, G. Polidori, D. Siliqi, R Spagna, *J. Appl. Cryst*. **2007**, *40*, 609.
4. G. M. Sheldrick, *Acta Cryst. A* **2008**, *64*, 112.
5. Their reagents had completely been dissolved in anhydrous THF
6. To destroy excess the fluorinating reagent.
7. For treatment of the reaction mixture.
8. To destroy excess iodine.

9. One ^{13}C signal derived from its naphthyl ring could not be observed.

10. *Textures of Liquid crystals*, ed. by I. Dierking, John Wiley & Sons, **2003**. DOI: 10.1002/3527602054.fmatter.

Chapter 5
General Conclusions

In Chapter 1, chemical and physical aspects of liquid crystal science, review of cholesteric inducer, that is the so-call 'chiral dopants', and objectives of my Ph. D thesis have been elucidated.

In Chapter 2, the 6,6'-substituents' effects of the synthesised binaphthyl-type chiral dopants on the dopant-induced chiral nematic phase have been described the research results and discussion. the bridged binaphthyl-type chiral dopant with the least steric hindrance and a largest substituent polarisability, the 6,6'-chlorinated chiral dopant, exhibited large helical twisting power (HTP) values in two host NLCs, namely JC-1041XX as the host fluorinated nematic liquid crystals (NLCs) and MBBA as the host azomethyne-type NLC. Moreover, the aromatic polarity of the chiral dopants and host NLC molecules exerted a beneficial impact on the induced HTP values. The temperature dependence HTP ($HTP_{t.d.}$) values depended upon the structural similarity of a solute-solvent interaction between chiral solutes and host nematic solvents. In addition, the $HTP_{t.d.}$ values were affected by the steric and polarisability substituent parameters.

In Chapter 3, the induced HTP and $HTP_{t.d.}$ values were significantly affected by linker flexibility, such as alkyl, alkynyl bridged and unbridged alkyl chain, at the 2,2' positions of the synthesised binaphthyl-type chiral dopants. The alkynyl bridged binaphthy-type chiral dopant possessed larger HTP value in the host NLC under the influence of the CH···π interaction between host NLC molecules' hydrogen and the chiral dopant's alkynyl moiety than those of different linker flexibility of the synthesised chiral dopants. However, the alkynyl bridged chiral dopant unlikely exhibited large $HTP_{t.d.}$ values, compared with the conventional alkyl bridged binaphthyl-type chiral dopant due to strong symmetrical stretching vibration of the alkyne moiety in the alkyl bridged one. I believe that my PhD research results presented herein significantly advance the design of novel, binaphthyl-type chiral dopants with larger HTP and adequate $HTP_{t.d.}$ values.

In Chapter 4, synthetic procedures, spectral data, experimental procedures of HTP measurement and the contact method and crystallographic data have been described.